MASTER'S THESIS

Thermal Analysis of Hard Ceramics

Latifa Melk

Master of Science in Engineering Technology
Materials Technology (EEIGM)

Luleå University of Technology
Department of Engineering Sciences and Mathematics

LULEÅ UNIVERSITY OF TECHNOLOGY

Abstract

Titanium carbonitrides (TiC_xN_{1-x}) are known by their excellent properties. They are widely used in cutting tools and in the preparation of advanced engineering ceramic-based composites.

It has been found that $TiC_{0.3}N_{0.7}$ is a precursor of carbon nitride (C_3N_4) which has a structure similar to that of Si_3N_4 and a hardness comparable to diamond. Due to the exciting potential of C_3N_4, a large effort has been put into synthesizing it. However to date, the synthesis of C_3N_4 as a crystalline material has not been achieved. This thesis work aims to crystallize C_3N_4 on SiC and Si_3N_4 substrates.

Four different mixtures were studied in this project: $TiC_{0.3}N_{0.7}/Si_3N_4$ and $TiC_{0.7}N_{0.3}$/SiC with different molar ratios (2:1) and (1:1). Differential scanning calorimetry (DSC) and Thermogravimetry (TG) were first used in both nitrogen and argon gas in order to study the thermal behaviour of the mixtures and X-ray diffraction (XRD) was used afterwards to determine the composition of the new phases.

DSC/TG results show that in argon atmosphere, the mixtures $TiC_{0.3}N_{0.7}$: Si_3N_4 (2:1) and $TiC_{0.7}N_{0.3}$: SiC (2:1) decompose at 1300 °C. While they decompose at 1450 °C in nitrogen atmosphere.

XRD results indicate that at 1450 °C, $TiC_{0.3}N_{0.7}$: Si_3N_4 with molar ratios (2:1) and (1:1) decompose to SiC and TiN. Besides that, $TiC_{0.7}N_{0.3}$: SiC with molar ratio (2:1) decomposes to Si_3N_4 and Ti_2N.

The thermal analysis results show that $TiC_{0.3}N_{0.7}/Si_3N_4$ and $TiC_{0.7}N_{0.3}$/SiC might be interesting precursors for C_3N_4.

Acknowledgements

This work would not have been succeeded without the expert guidance of my supervisor, Marta-Lena Antti. Her supervision and advices helped me to develop my research skills.

This Master thesis research would not be also accomplished without the invaluable support of Professor Ragnar Tegman throughout the project. His kind attitude and patience have made this research a thoroughly enjoyable experience.

I am also indebted to Andreas Engström a PhD student, for his help and useful ideas.

I would like to thank Mr. Jesper Alkebro from the company Element Six for his valuable suggestions during our meeting.

I would also to express my gratitude to the technicians of the division of Material Science: Mr. Johnny Grahn and Mr. Lars Frisk for their help and support during the laboratory work.

Finally, I would like thank my parents, my sister, my brothers and all my friends for their unconditional love and support.

Table of contents

List of figures

1. Introduction

TiC_xN_{1-x} can be synthesized by direct element reaction of titanium, carbon, nitrogen or ammonia, by carbothermal reduction, or by pyrolysis of titanium tetrachloride and nitrogen polymer (1). $TiC_{0.3}N_{0.7}$ is used as a precursor of carbon nitride (C_3N_4). Recently, Jian et al. (2) has used a selective chloride etching of commercially available $TiC_{0.3}N_{0.7}$ to synthesize C_3N_4. Only C and N in amorphous phase have been found in the final product. A reason for the amorphous C_3N_4 could be a lack of crystalline substrate particles adhered to the $TiC_{0.3}N_{0.7}$ during etching. Therefore, using substrates such as SiC or Si_3N_4 together with $TiC_{0.3}N_{0.7}$ in the form of $TiC_{0.3}N_{0.7}/Si_3N_4$ and $TiC_{0.7}N_{0.3}$/SiC mixtures could lead to the formation of crystalline C_3N_4.

2. Background and Theory

2.1 Boron nitride

2.1.1 History and properties of boron nitride

Boron nitride (BN) is the hardest material in the world after diamond. Boron nitride is a synthetic product. In 1957 Wentorf et al. (3) has tried the synthesis of cubic boron nitride (c-BN) using high pressure high temperature (HPHT). In 1969 boron nitride became commercially available. Its main crystallographic structures are c-BN, hexagonal boron nitride (h-BN), and wurtzitic boron nitride (w-BN) see figure 1. The c-BN is the stable phase at standard temperature and pressure (3).

Cubic boron nitride is called “Borazon” as a trade name by the General Electric Corporation. It is also called z-BN due to its zinc-blende lattice structure. Boron nitride has a similar structure to diamond. Boron and nitrogen have sp^3 hybridization and every boron atom is surrounded by four nitrogen atoms. Due to this short bonding length, BN exhibits a high hardness. Cubic boron nitride has also a high thermal conductivity, good chemical resistance and a low reactivity with iron and its alloys. It has been used as a suited material for machining ferrous metals due to its abrasive resistance with these alloys. However, ferrous materials attack diamonds chemically at

the hot cutting edge because diamonds do not have good chemical stability as boron nitride. (3) (4) Table 1 shows different mechanical properties of c-BN and natural diamond.

Table 1: Mechanical properties of natural diamond, and c-BN (5)

Property	Diamond	c-BN
Density (g/cm^3)	3.50	3.48
Fracture toughness($MPa*m^{0.5}$)	3.4	5.0
Knoop hardness (GPa)	57-104	43-46
Young´s Modulus (GPa)	1141	600-800
Thermal expansion (10^{-6} k^{-1})	1.5-4.8	4.9
Thermal conductivity 20° C(Wm^{-1} k^{-1})	500-2000	150-700

Hexagonal BN, is named also g-BN (graphitic BN), or α-BN. It has a layered structure similar to graphite. B and N form (0001) planes and build hexagonal rings. The rings are very strong (covalent bonding) while the bonding between atomic planes are very weak (Van der Waals bonding). Hexagonal BN is an electrical insulator and has a white color. Boron nitride can also be found in wurtzite-type at high pressure. It has a polycrystalline structure that provides superior cutting properties and sharpens itself during cutting. (3)

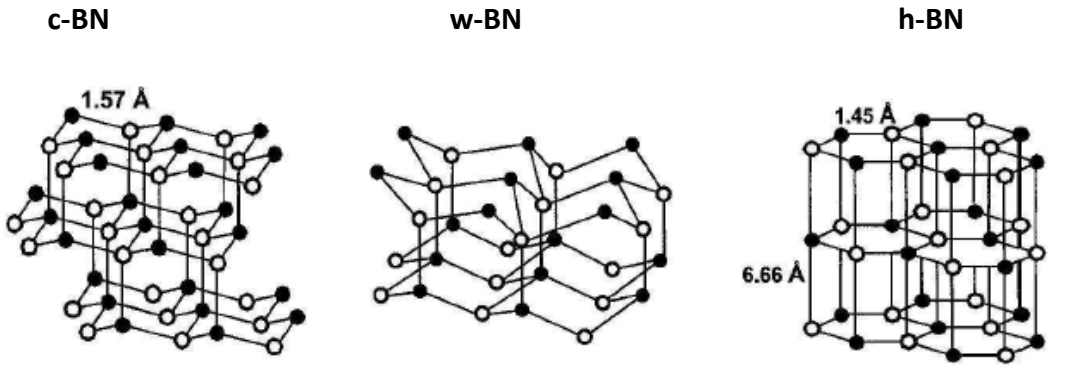

Figure 1: Crystal structure of c-BN, w-BN and h-B (3)

2.1.2 Synthesis of cubic Boron nitride

Cubic boron nitride is synthesized industrially from the conversion of h-BN to c-BN at a high pressure (4.4-7.5 GPa) and high temperature (1200-2000 °C) with the presence of a solvent as catalyst (6). Nakano et al. (7), have carried out the synthesis of c-BN by decomposition of Mg_3BN_3 under high pressure (4 GPa) and high temperature. Cubic boron nitride is also obtained by pyrolizing $Ca_3B_2N_4$ at high temperature (1800°C) and high pressure (4-6.5 GPa) (7). However, there have been many studies concerning the synthesis of c-BN under low pressure and low temperature (below 1000 °C). Hao et al. (6) has successfully produced BN nanocrystals at 480 °C and ambient pressure using BBr_3 and Li_3N as reactants. The c-BN was the dominant phase.

The transition from c-BN into h-BN has also been studied. Sachdev et al. (8) has investigated the c-BN /h-BN phase transformation at normal pressure. The phase transition of c-BN to h-BN is performed between 1000 °C and 1800 °C, under the influence of two factors especially the grain size of c-BN and the presence of boron oxide in the starting material.

Scanning Electron Microscopy (SEM) results indicate that the phase transformation is performed either by a gas phase or by a solid bulk material (8). Another study carried out by Fukunang et al. (9), shows that the ratio of the intensity of c-BN to h-BN is 4 after heating at 1200 °C for 48h and it decreases to 0.3 after heating at 1250 °C for 48h. These results demonstrate that the phase transition from c-BN to h-BN occurs at lower temperatures.

2.1.3 Polycrystalline c-BN

Polycrystalline cubic boron nitride (pcBN) has a high hardness and less reactivity with ferrous metals compared to diamonds. For this reason, it has a wide range of applications in cutting tools and in the production of automotive parts (10).

Polycrystalline c-BN is produced by sintering of c-BN composites using binders at a pressure of 4-6 GPa and at temperatures of 1200-1500 °C. During sintering, chemical reactions take place between the binder and the c-BN particles (grains), leading to strong covalent bonds. Increasing the surface area between both c-BN and binder phase particles promotes the increasing of chemical reaction rate (11).

The sintering process of c-BN composite materials at high pressure and high temperature induces deformation and shrinkage of the composite. The composite constituents have different deformation and shrinkage rate. Therefore, different residual stress field occurs around each particle. Equiaxed or spherical particles tend to reduce localized regions of high stress. However, fine particles obtained by crushing the equiaxed grains promote homogeneous stress distribution around each particle (11).

The properties of pcBN products are determined by the final microstructure and the phases formed during sintering. Table 2 shows the properties of the main phases. It has been found that increasing the grain size of c-BN results in decreasing the strength of pcBN composite materials. However, ultra-fine particles can agglomerate in the matrix. Therefore, agglomeration is considered as a defect in the microstructure. For this reason, it is important to achieve a good homogeneity of phases in c-BN composite (12).

Table 2: The main phases appearing during sintering of pcBN (10)

	cBN	**AlN**	**TiB_2**	**TiN**	**TiC**	**Al_2O_3**
Crystal structure	Cubic	Hexagonal	Hexagonal	Cubic	Cubic	Hexagonal
Density [g cm^{-3}]	3.48	3.26	4.52	5.22-5.44	4.92	3.96
Melting point [°C]	2700	2300	3197	2930	3065	2050
Knoop hardness [GPa]	47	12	26.5	19	28-35	23
Young modulus [GPa]	700-800	318	434-540	370	450	427
Thermal expansion coefficient [10^{-6} K^{-1}]	3.2	3.9	8.1	8	8.6	8.1
Thermal conductivity [$W.m^{-1}$ K^{-1}]	150-700	200	80	25	33-43	14

The presence of porosity in c-BN composites decreases the strength because pores behave as crack initiating sites. Pores can be the result of a poor sintering. Therefore, in order to eliminate

porosity, it is important to optimize the sintering conditions. It appears that using high pressure and high temperature for sintering lead to a good bonding between phases (12).

Large grains in the microstructure of c-BN composites are potential defects that lead to crack formation. Hence, it is important that c-BN composites contain narrow particle size in in order to improve toughness (13).

2.1.4 Cubic-BN reinforced composite materials

During sintering of pure c-BN, it is difficult to obtain fully dense material because it requires a very high pressure (around 7 GPa). Due to this difficulty, some research has been done to develop the c-BN composite material such as cBN –TiN (14), cBN-WC-Co (15), cBN-AlN (16), cBN-TiN , cBN-TiC (17), cBN-TiN-Al (15) . In the study carried out by Benko et al. (17) the transition metals from group IV and group VI from the periodic table are used as a binding phase. In that work, the phase equilibrium and the morphology in cBN–TiN and cBN-TiC systems were studied. The microstructure of c-BN with TiN was found compact with a uniform volume distribution of TiN. The microanalysis of chemical composition showed the formation of thin layers formed by TiB_2. A similar microstructure has been found in c-BN sintered with TiC with the presence of TiB_2 grains in cBN –TiC interface and $TiC_{0.8}N_{0.2}$. TiB_2 and $TiC_{0.8}N_{0.2}$ have been located in a sequence: BN/TiB_2/TiN in BN/TiN composites and in a sequence BN/TiB_2/ $TiC_{0.8}N_{0.2}$/TiC in BN/TiC composites (18). An XPS study of the c-BN-TiC system has been also reported by Benko et al. (19). In this study they confirmed the formation of TiB_2 at the BN-TiC interface. Analysis of the electron diffraction showed that fine crystallites of TiB_2 were formed at the boundary and the larger grains were formed inside TiC. Klimczyk et al. (20) reported the theoretical and the experimental studies of cBN-Ti/TiN under high pressure and high temperature. TEM results showed that the composites cBN-Ti and cBN-TiN have similar compact structure. In the cBN-TiN sample, TiB_2 phase has been identified and the contribution of this phase does not depend on the annealing temperature. In the cBN-Ti composite, TiB_2 and TiN were formed in large amounts and they were uniformly distributed. The phase TiB_2 in cBN-Ti/TiN composites is a determining factor for obtaining high micro-hardness.

2.1.5 Organic binders

The organic binders or organic additives help ceramic particles to adhere to each other. The commonly used binders are plasticizers, lubricants and liquefiers. The strength and plasticity of the green body can be affected depending on the choice and amount of binder. The additives should be removed from the green body during sintering. A thermal removal is a technique usually used for this purpose. The temperature of the green body is raised to the temperature of polymer degradation leading to a volatilization of binders from the green body. However, firing of the green body under a high heating rate can result in volatizing large amount of additives, which result in microstructural defects and cracks (21) (22).

In case of non-oxidative conditions, especially during firing, there is a high amount of carbon left in the compact which prevents the volatilization of the binder. Though, it is important that the selection of organic additives should be based on the heating conditions and awareness of the interaction of binder with other substances in the green body (23).

2.1.5.1 Polyethylene glycol (PEG)

Polyethylene glycol is used as lubricant in ceramic industry and its chemical structure is $HO(CH_2CH_2O)nH$. It has been found by Grassie et al. (24) that PEG that has a molecular weight of 1000 and 1500 starts to degrade at 280-290°C in nitrogen atmosphere while it degrades before that in vacuum. In that work, they did not find any volatile products at 410 °C, except some negligible residues at 450 °C. TG curves for both samples are shown in figure 2.

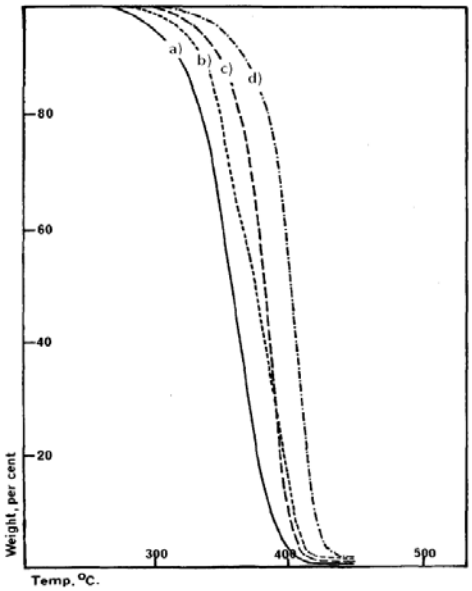

Figure 2: TG traces from the study of Grassie et al. [24] for PEG with molecular weights of 1000 and 1500. PEG 1000 a) in vacuum and b) in nitrogen. PEG 1500 c) in vacuum and d) in nitrogen (24).

During decomposition, first methane, ethane and carbon monoxide were observed, followed by acetaldehyde and finally aldehydes, ethylene glycol and water.

Decomposition of pure PEG in air has been studied by Eusterbrock et al. (21), and in accordance to Grassie, it was observed that pure PEG ends at 450 °C. Fares et al. (25) has found that degradation of pure PEG with a high molecular weight of 900,000 and 400,000 take place between 225-255 °C.

2.1.6 Application of polycrystalline BN

As mentioned in section 2.1.3, polycrystalline boron nitride (pcBN) has high hardness comparable to the diamond hardness and it is harder than Al_2O_3, SiC. Polycrystalline boron nitride is widely used in cutting tools and machining ferrous metals due to its stable chemical reactivity. It is resistant to chemical attack up to 1500-1600 °C. For cutting tools application, c-BN should be in sintered form. For this reason, it is very important to avoid conversion of c-BN into h-BN during sintering. Therefore, sintering process should be performed in the stability region of c-BN. Cubic boron nitride is also used in electronics especially in semiconductors due to its high thermal conductivity. In this kind of application c-BN is coated with aluminium alloys

by chemical vapour deposition or with gold by sputtering. BN is also used to get n-type or p-type semiconductors when it is doped with silicon or beryllium. Mishima et al. (26) described a method to grow semiconducting c-BN crystals. These doped c-BN crystals can be used as n-p junction diodes at high temperatures.

2.2 TiC_xN_{1-x}/Si_3N_4 and TiC_xN_{1-x}/SiC as a precursor of C_3N_4

2.2.1 Carbides and titanium carbide

The transition metal carbides have high hardness and high melting point. For this purpose they are used as hard components in cutting tools. The carbides WC, TiC and TaC are the most used ones. The preparation of these cemented carbides can be done using powder metallurgical techniques. Pure graphite can reduce transition metal oxides at about 2000 °C, while chemical vapour deposition is used to obtain non-abrasive coatings (10). The most important transition metal carbide is WC. As all the carbides embedded in a binder matrix, WC has a metallic binder phase of Co and or Cr, Fe, Ni. Some addition carbides can also be added such as: TiC, TaC, NbC in order to determine the corrosion resistance. The oxidation rate of WC increased at 800 °C because tungsten oxides WO_2 and WO_3 started to form at 500 °C and WO_3 evaporated at 800 °C. Hydrothermally corrosion treatment of WC- 6% Ni has been studied and showed less corrosion rate below 500 °C, whereas the corrosion rates increased after 500 °C and WC grains of the surface were dissolved in supercritical fluid. Ni grains are not influenced by these conditions and Ni grain boundary phase protects the material from corrosion forming a diffusion barrier. X-ray diffraction analysis of the sample after heat treatment at 400-500 °C showed the presence of WC, Ni and WO_3. At 700 °C, WO_3 interacted with nickel oxide and formed $NiWO_4$ (10) (27).

The system Ti-C, see figure 3, represents two eutectic reactions and one peritectoid reaction at 1646, 2776 and 920 °C respectively. The system consists of solids α-Ti and β-Ti in addition to a refractory monocarbide TiC (1).

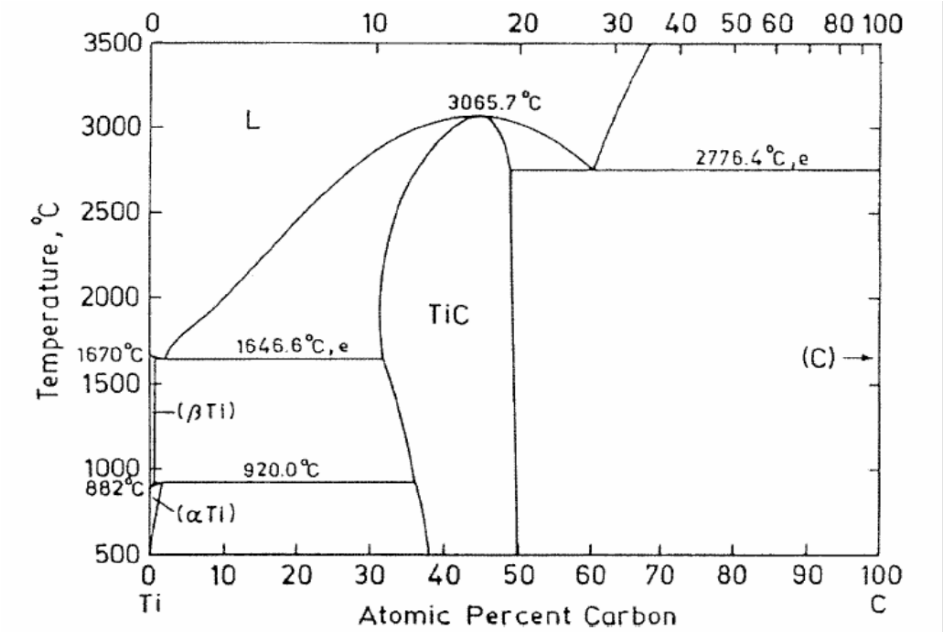

Figure 3: Ti-C phase diagram (1)

2.2.2 Nitrides and titanium nitride

Transition metal nitrides are hard materials used for surface coatings. Titanium nitrides can be obtained by reduction of titanium dioxide: $2TiO_2+N_2+4C \rightarrow 2TiN+4CO$.

Chemical vapour deposition techniques are used for surface coatings of titanium nitride: $2TiCl_4+H_2+2NH_3 \longrightarrow 2TiN+8HCl$. Mononitrides and nitrides have large homogeneity, for example, NaCl type titanium nitride can be found with different stoichiometry: $TiN_{0.1}$ and $TiN_{0.5}$. Nitrogen atom in TiN can be replaced by carbon or oxygen atoms resulting in the component Ti (C, N, and O). The phase diagram of the system titanium-nitrogen contains three nitrides, which are stable at temperature below 1300 °C, see figure 4. The oxidation of TiN (powders, thin films, dense bodies) has been studied. It starts from room temperature and increases following a parabolic law at 500 °C. TiN and TiC are both used as ceramic matrix in order to improve electrical conductivity and mechanical properties (10).

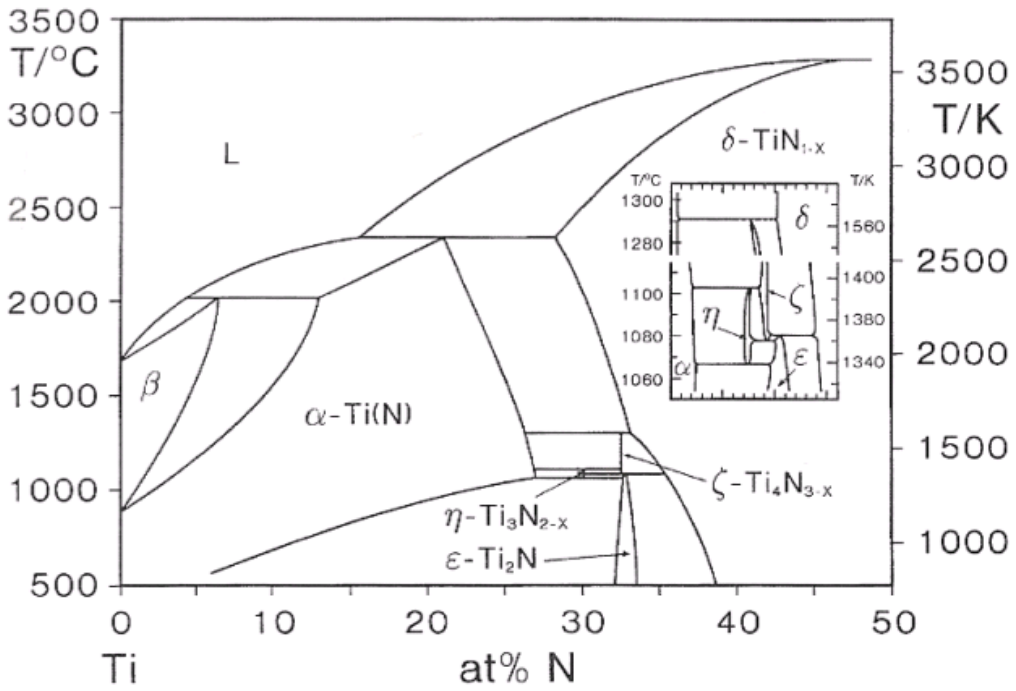

Figure 4: Phase diagram of Ti-N (28)

2.2.3 Titanium carbon nitride

Titanium carbon nitride Ti(C, N) is an excellent monoxide ceramic. It has high thermal conductivity and chemical stability, high melting point, high hardness and high temperature strength. Due to these outstanding properties, Ti(C,N) has been used widely in cutting tools, in wear resistant materials, in fabricating advanced engineering ceramic-based composites, and electrical or automatic refractory devices (29) (30) (31).

In the Ti(C, N) structure, there is a wide homogeneity distribution of atoms. The carbon and nitrogen atoms occupy randomly all the octahedral interstitial lattice sites. Therefore, there is a large variation of composition can be possible for the preparation of carbonitrides, see figure 5 (10).

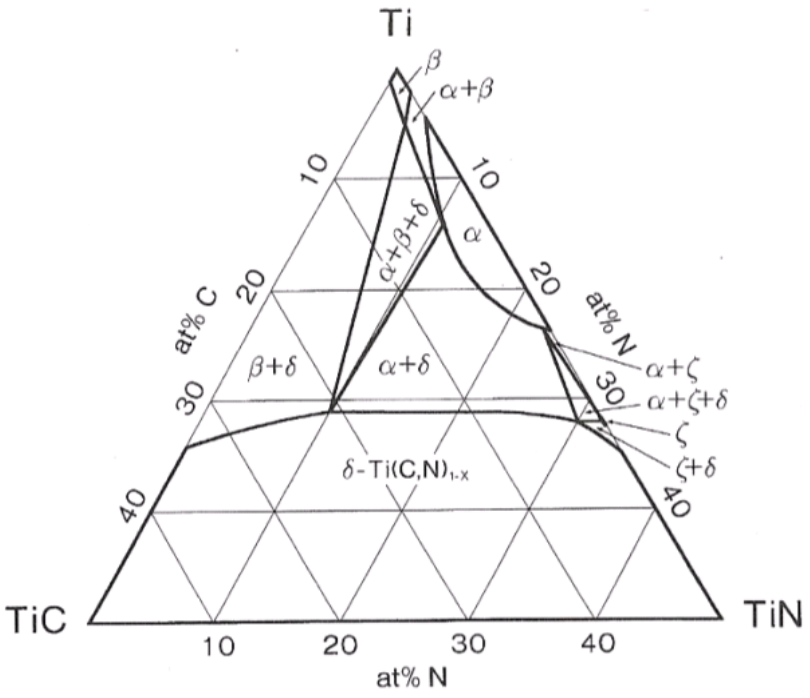

Figure 5: Ternary phase diagram of Ti-C-N at 1200°C (10)

2.2.3.1 Synthesis of Ti(C, N)

Ti(C, N) can be synthesized by direct chemical reduction of titanium oxide, titanium chloride, or titanium hybrid by carbon, nitrogen and ammonia or by a carbothermal reduction. The carbothermal reduction is considered as a low-cost method for synthesis of carbides and nitrides of transition metals. Yongdi et al. (1) developed a method for formation of TiC_xN_{1-x} nanopowders. In this study a synthesis of TiC_xN_{1-x} is developed using coked precursors. Dehydrogenation of alkanes was used as carbon source. After an annealing treatment of refluxing-derived precursor, TiC_xN_{1-x} was easily obtained.

Xin et al. (30) has successfully prepared TiCN nanocrystallites by a direct reaction of $TiCl_4$, CCl_4, and NaN_3 at low temperature (420 ^oC) (21). Guozhen et al. (31) also reported synthesis of TiCN by direct reaction of $TiCl_4$ and $C_3N_3Cl_3$ at 600 ^oC.

Feng-shi et al. (29) synthesized Ti(C, N) using high-energy ball milling of elemental powders of Ti and C in nitrogen atmosphere with Ti/C atomic ratio less than 0.25. The formation of titanium

carbonitride phase undergoes an abrupt reaction, which indicates that this reaction is a self – propagating high temperature synthesis (SHS) process.

Lichtenberger et al. (32) reported the synthesis of titanium carbonitride at pyrolysis temperatures via a polymer to ceramic transformation of a titanium carbodiimide polymer. Pyrolysis at 800 ^{o}C results in a mixture of amorphous carbon and titanium nitride in form of crystalline particles of about 4 nm in size, whereas pyrolysis at 1100 ^{o}C leads to nanocrystalline particles of 20-30 nm in size.

Other physical and chemical methods have been used to synthesis Ti(C, N) nanocrystallites such as chemical and physical deposition and ion implantation process (30).

2.2.4 Carbon nitride (C_3N_4)

In 1989 Liu and Cohen (33) predicted the existence of C_3N_4 by using "ab initio" calculations based on the density functional theory (DFT) within the local density approximation (LDA). These calculations showed that carbon nitride has a bulk-modulus (B=430GPa) close to that of diamond (B=442GPa).

Teter and Hemley (34) proposed five different structures for C_3N_4, see figure 6:

- Two forms α-C_3N_4 and β-C_3N_4 are derived from the corresponding β and α varieties observed for Si_3N_4.
- A "pseudo-cubic" form, usually called defect-zinc blende structure (bl-C_3N_4) with carbon vacancies.
- A two-dimensional structure derived from the graphitic structure (g- C_3N_4) with carbon vacancies.
- An isostructural cubic variety (c-C_3N_4) of the high form of zinc silicates: Zn_2SiO_4.

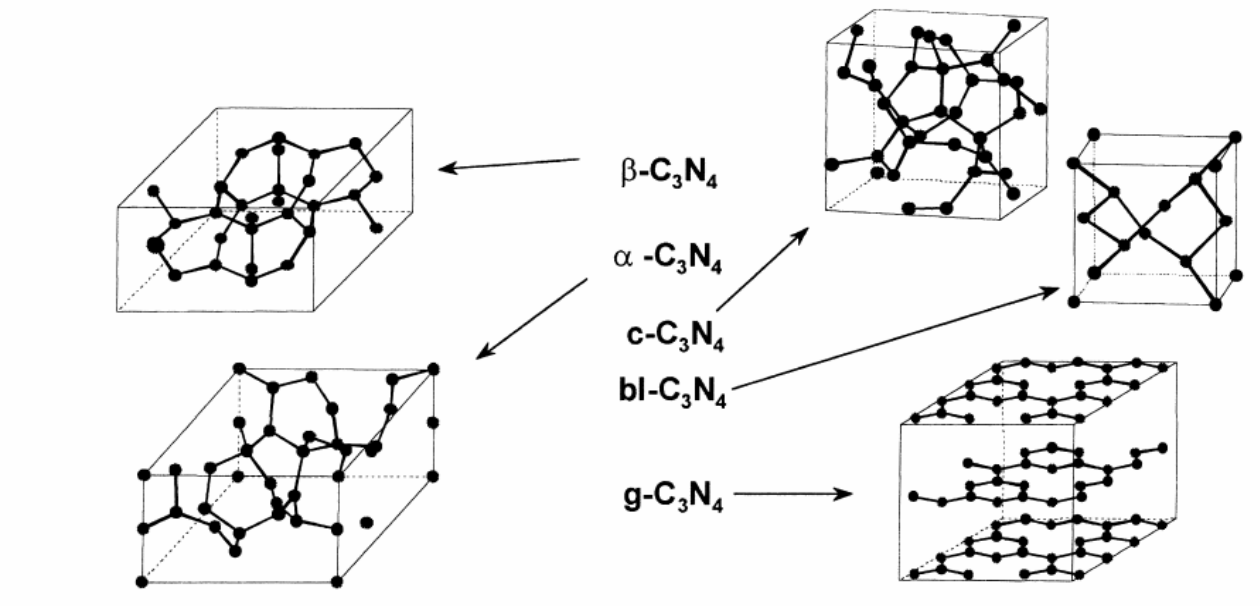

Figure 6: Different structures for C_3N_4 (34)

2.2.4.1 Synthesis of C_3N_4

Since 1990 when Cohen and Lieu (35) predicted high bulk modulus of β-C_3N_4 comparable to that of diamond, no synthesis of crystals has been done. Therefore, no physical and chemical properties have been discovered. Initial studies about synthesis of β-C_3N_4 lead to amorphous carbon-nitrogen films. Small fractions of crystalline C_3N_4 have been also synthesized in C-N films by using sputtering deposition and pulsed laser deposition. Physical vapour deposition (PVD) and chemical vapour deposition (CVD) techniques have been used to synthesis C_3N_4. However, C-N films showed bad surface morphology (34).

Yan et al. (36), reported successful synthesis of crystalline β- and α-C_3N_4 films via hot filament chemical vapour deposition (HFCVD) using a mixture of nitrogen and methane on silicon. The attempts have been turned to produce macroscopic samples of C_3N_4. The pressures needed for phase transformation from g-C_3N_4 and α -C_3N_4 to cubic C_3N_4 are 12 and 68 GPa respectively.

Therefore, Ha Ma et al. (37) suggested that the application of high pressure high temperature (HPHT) may be an effective method for synthesizing C_3N_4. In this study, g-C_3N_4 was synthesized by studying high pressure pyrolysis behaviour of melamine. HPHT (5 GPa and 650 °C) method provides a new route to synthesis superhard cubic nitride.

Montigaud et al. (34) prepared g-C_3N_4 using a solvothermal process which is the pyrolysis of melamine in presence of a nitriding solvent (NH_2NH_2) at high pressure conditions (P=3 GPa, 800≤T≥850 °C). Two years later, Montigaud et al. (35), carried out two synthesis attempts of graphite form of C_3N_4. The first route is based on the condensation of melamine and cyanuric chloride under pressure of about 130 MPa and temperature of 250 °C with presence of triethylamine as a solvent. The second route consists of the pyrolysis of melamine at high pressure condition (P=2.5 GPa. T=800 °C) in presence of hydrazine.

Recently, Jian et al. (38) reported synthesis of carbon nitride using a novel chlorination method based on extracting titanium from single inorganic precursor $TiC_{0.3}N_{0.7}$. The crystalline structure of $TiC_{0.3}N_{0.7}$ was used as a template; the atomic distance between C and N atoms was small which lead to rearrangement and rebounding. However, titanium is removed in the form of titanium chloride $TiCl_4$. So, only C and N remain in the final product as an amorphous phase.

2.2.5 Silicon nitride

Silicon nitride (Si_3N_4) has been studied for more than 40 years. It has two different crystallographic forms: β, see figure 7 and α, see figure 8. Both forms have hexagonal crystal structure. The c-axis dimension of the unit cell of α phase is twice that of β phase. Alpha phase is characterized by a (Be_2SiO_4) structure, where Be is replaced by Si and O by N. The β-Si_3N_4 has a Si_6N_8 structure (39).

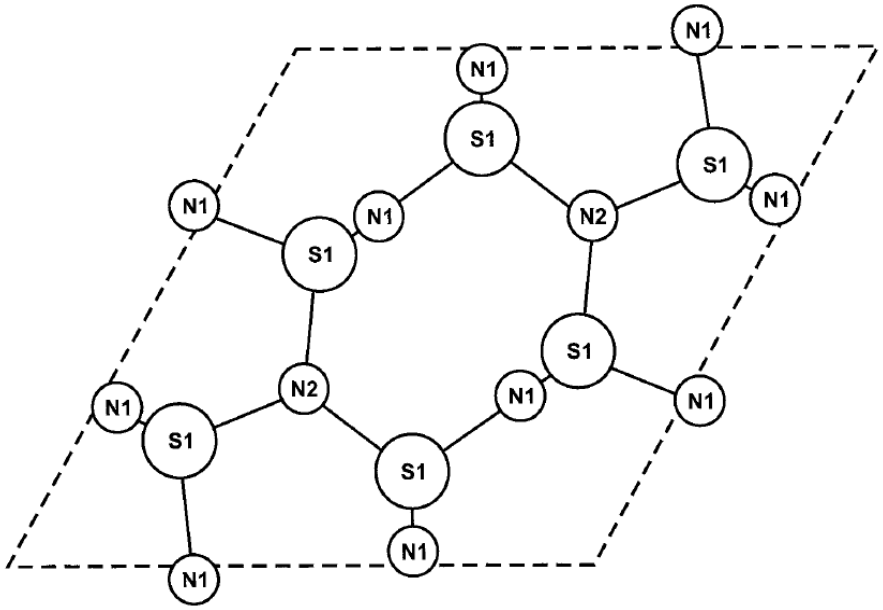

Figure 7: β -Si_3N_4 unit cell (39)

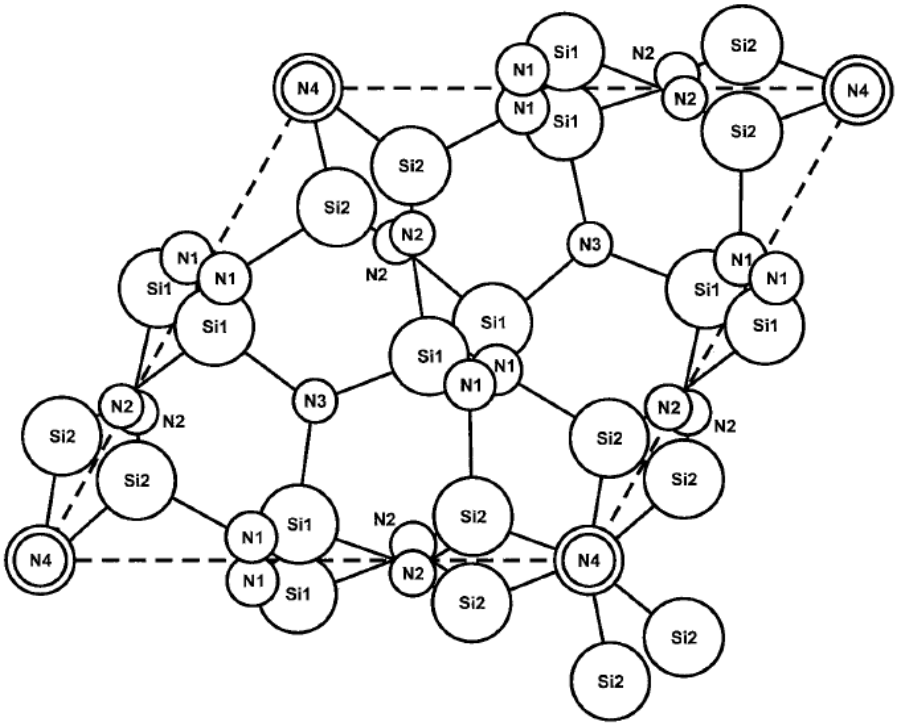

Figure 8: α -Si_3N_4 unit cell (39)

The conversion of α-Si_3N_4 to β-Si_3N_4 has been found to occur in presence of liquid phase through a reconstructive transformation. The difference between Gibbs function of formation of beta and alpha is small but the activation energy is high. Due to this reason the transformation can only be possible in presence of liquids that lower the transformation activation energy. However, transformation from beta to alpha has never been observed. It was expected that it is too slow to be detected at temperatures below 1400 °C.

Early research about sintering silicon nitride has not been managed to increase density or strength. The reason was explained by the low lattice mobility of silicon and nitrogen atoms at high temperature in addition to the volatility of silicon nitride. Some attempts consist of using specific standard liquid additives developed for hot pressing, even though only small density increase was achieved. In 1975 Terwiliger and Lange (40) claim a sintered Si_3N_4 powder without applying a mechanical pressure. Using graphite die "hot pressing" and MgO-doped Si_3N_4 powder at high temperature without pressure leads to shrinkage of the Si_3N_4 powder cylinder. Giachello (41) showed that Si_3N_4 powder containing sintering additives (MgO for example) can be sintered without using high nitrogen pressure. Si_3N_4 powder with MgO was immersed in a bed of loosely packed Si_3N_4 powder, in such a way that the equilibrium vapour pressures of nitrogen and silicon were established over the component to suppress the outward fluxes of silicon and nitrogen gas, which results in evaporation and grain growth (39).

2.2.6 Silicon carbide

Silicon carbide (SiC) has more than 70 crystalline forms. The most used one is α-SiC. It has hexagonal crystal structure and it is formed at temperatures above 2000 °C. Beta form or β-SiC has a zinc blende crystal structure and it is formed below 2000 °C. Recently β-SiC is used as a support for heterogeneous catalysts due to its high surface area compared to α-SiC. Silicon carbide does not melt under any pressure. It is inert chemically and its high sublimation temperature is about 2700 °C. It is used as a semiconductor material in electronics due to its high thermal conductivity and high electric conductivity (42).

The system Si-C is characterized by one peritectic reaction at 2545 °C and one eutectic reaction at 1404 °C, see figure 9 (42).

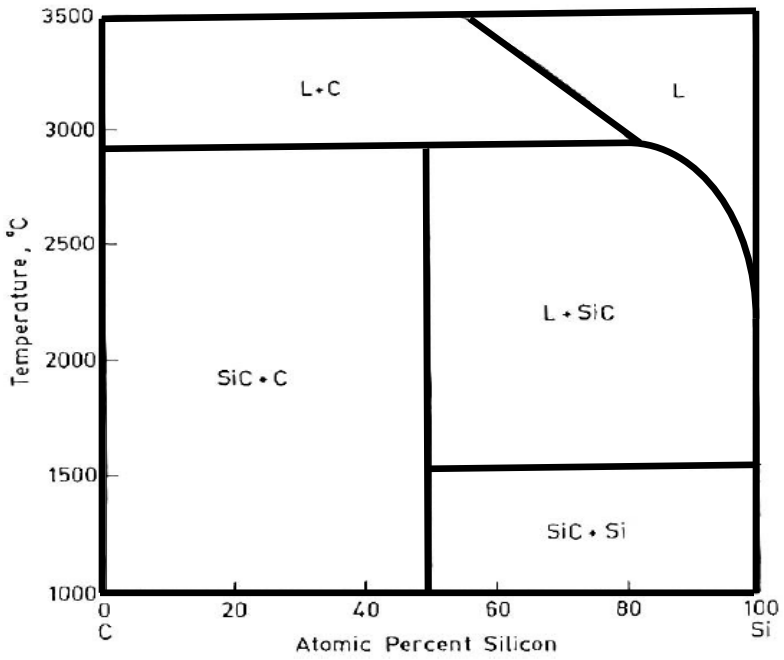

Figure 9: Si-C phase diagram (43)

2.2.7 Ti-Si-C system

The Ti-Si-C system is considered as an important system due to its importance for joining SiC with Ti. However, there are few studies and no experimental measurement information about the ternary phase diagram Ti-Si-C. Bruk et al. (44) has done the first measurement of this system and he succeeded to determine the isothermal section at 1200 °C by using XRD techniques. Wakelkamp et al. (45) used XRD and EPMA methods and they measured the sections at 1250 °C. Later on and based on Brukl measurements Seifert and Zimmermann (46) determined isothermal sections from 700 °C to 1200 °C and at 1400°C. Recently, Yong et al. (47) provided new experimental phase diagram in the ternary Ti-Si-C system. Isothermal sections have been determined in the Ti-Si-C system based on thermodynamics modelling. In this study, Yong et al. (47) developed a set of thermodynamic functions for the Ti-Si-C system. The calculated isothermal sections at 1400 °C and 1800 °C are represented in figures 10 and 11. The liquidus projection and reaction scheme for the whole ternary system is constructed. The work of Yong et al. (47) showed that limited experiments can be combined with thermodynamic modelling in order to know phase relation in the Ti-Si-C at any temperature and composition.

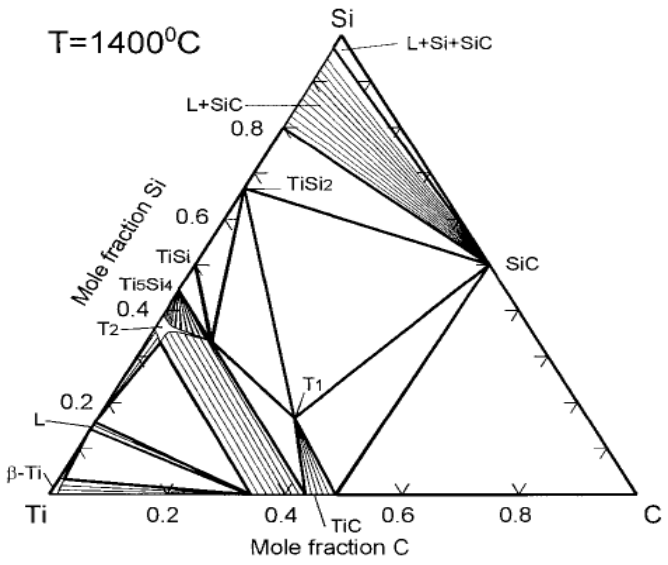

Figure 10: Calculated 1400°C isothermal section according to the present modelling. (b-Ti is bcc-(Ti), T_1 is Ti_3SiC_2, and T_2 is $Ti_5Si_3C_x$.) (47)

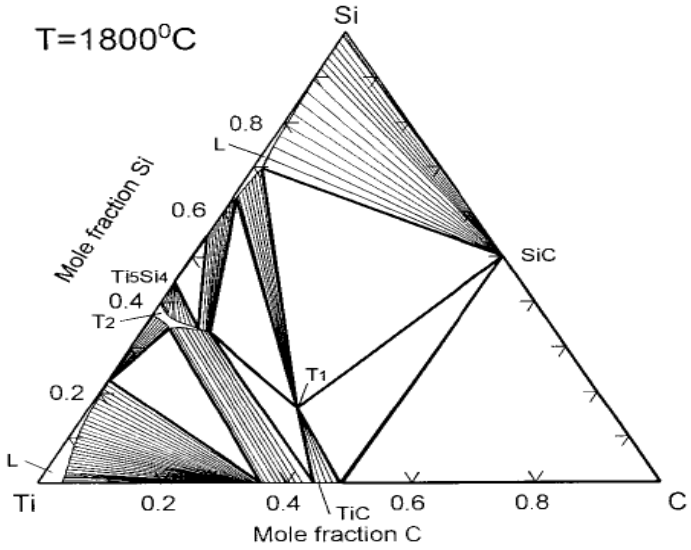

Figure 11: Calculated 1800°C isothermal section according to the present modelling. (T_1 is Ti_3SiC_2 and T_2 is $Ti_5Si_3C_x$.). (47)

2.2.8 Ti-Si-C-N

The mechanical properties of Ti-Si-C-N ceramics and electrical conductivity are relatively low and their poor properties limit the use of such ceramics. Guan Duan et al. (48) investigated the combination of Si_3N_4, SiC and TiC_xN_{1-x} in one composite due to its excellent mechanical and thermal properties. A novel ceramic sintering technique, pulse electric current sintering (PECS) was used for this purpose. PECS technique consists of consolidating powders to near theoretical density by rapid heating pressure under high electric pulsed current (up to 5000 A) at a frequency of about 30 Hz. Therefore, a ceramic composite of nano-sized Si_3N_4/SiC/TiC_xN_{1-x} has been successfully prepared using this approach and for the first time by Guan Duan et al.

A representation of different reaction paths in the system Ti-Si-C-N is represented in figure 12. Two tie triangles within 4 areas are defined at 1923 K: (1) and (3) represent $TiC_{0.3}4N_{0.66}$+SiC+C and $TiC_{0.13}N_{0.87}$+SiC+Si_3N_4 respectively. Whereas, (2) TiC_xN_{1-x}+SiC (0.13<x<0.34) and (4) TiC_xN_{1-x}+Si_3N_4 (0<x<0.13) define two solid phases that are in equilibrium with nitrogen gas. Field (4) is not treated yet. The arrows show reaction paths. Arrows which are pointed far from nitrogen corner indicates that a N_2 gas release during the reaction between Si_3N_4 and TiC. Those oriented towards N_2 corner informs nitrogen consumption. At point **A** localised in the tie triangle (1) no nitrogen is released or consumed from the atmosphere. This result indicates that at specific physico-chemical conditions, titaniumcarbonitride compositions, reaction paths and phase equilibrium depend on the Si_3N_4: TiC ratio (49).

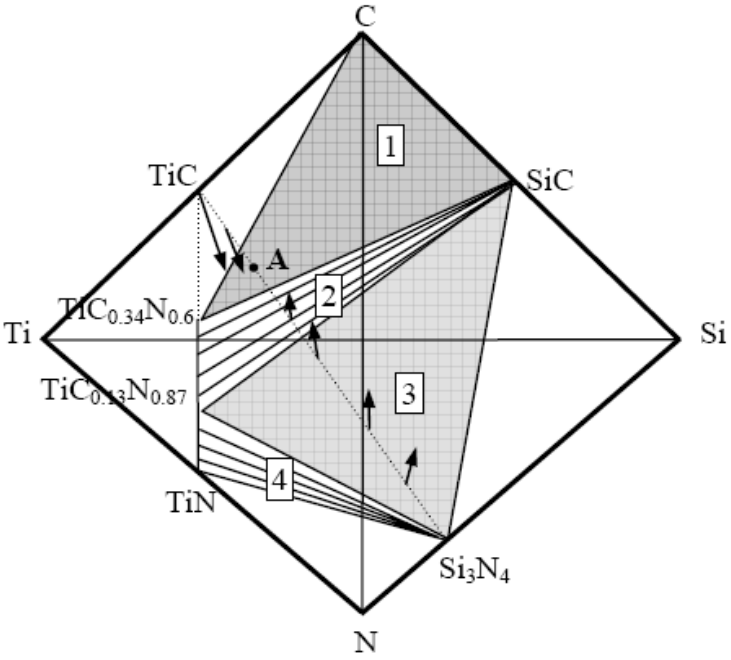

Figure 12: Phase compatibilities with reaction paths for Si_3N_4-TiC mixtures at 1923 K. (49)

2.3 The in-situ synthesis of a TiC_xN_{1-x}/SiC composite using polycarbomethylsilane (PCS) as a precursor for SiC.

2.3.1 Polycarbomethylsilane (PCS)

Polycarbomethylsilane (PCS) has the molecular formula $(C_2H_6Si)n$. Its average molecular weight is 800 g/mol and its softening point is80 °C. It has high ceramic yields of more than 55 wt%. Therefore PCS is widely used as a polymeric precursor of SiC. Its chemical formula is showed in figure 13 (50).

- R_1: hydrogen
- R_2: alkyl (CxHy)
- R_3: aryl
- R_4: silyl group or halogen (H_3Si-)

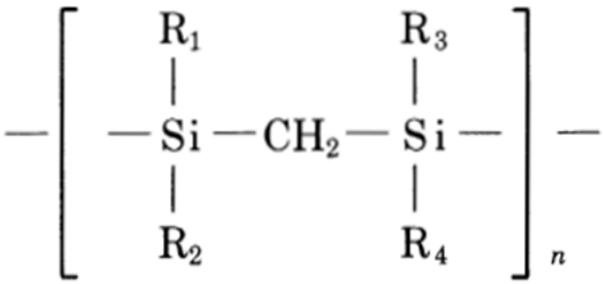

***Figure 13: Chemical formula of PCS* (50)**

2.3.2 Pyrolysis

Pyrolysis is defined as a chemical decomposition induced in organic materials by heat in the absence of oxygen. Pyrolysis is the transformation from solid material into gaseous components small quantities of liquid, and a solid residue containing carbon and ash. It occurs under pressure and at operating temperatures above 430 °C (51).

2.3.3 Pyrolysis of polycarbomethylsilane

Bouillon et al. (52) have studied the conversion of PCS to SiC. This study explains the fundamental steps that induce the conversion of PCS to SiC. These steps are:

- 20 °C < T < 550°C: no change in the structure on the polymer. However, in this temperature range, a large weight loss occurred due to the evolution of heavy gaseous products.
- 550 °C < T < 800 °C: Most part of the Si-H and C-H bonds are broken.
- 800 °C < T < 1000 °C: The material is mineral and it contains some hydrogen, which is important during the ceramization process.
- 1000 °C < T < 1200 °C: The number of SiC nuclei increases and the nucleation of the SiC starts in the whole material.
- 1200 °C < T < 1400 °C: A low continuous crystallization of SiC is observed with an average grain size of about 10nm. The percentage of silica or Si (C, O) decreases slowly.
- 1400 °C < T < 1600 °C: grain coarsening of SiC starts reaching an average grain size of 50nm. In addition to a rapid decrease of amorphous silica contents and a probable evolution of silicon and carbon monoxide.

3. Characterization methods

Thermal analysis (TA) is usually defined as a group of techniques in which a physical property of a substance and/or its reaction products are measured as a function of temperature/time while the substance is subjected to a controlled temperature program. A new definition of TA has been decided by the international confederation for thermal analysis and calorimetry (ICTAC): TA means the analysis of a change in a property of a sample, which is related to an imposed temperature alteration (53).

3.1 Dilatometery

Dilatometry (DIL), see figure 14, is a thermo-analytical technique for measuring expansion or shrinkage of a material under controlled temperature and time program. DIL has many areas of applications: linear thermal expansion, coefficient of thermal expansion, sintering temperature and shrinkage steps, volumetric expansion, density change, glass transition temperature, softening points, phase transitions, influence of additives and raw materials, optimizing of firing processes, kinetics studies and rate controlled sintering (RCS) (54).

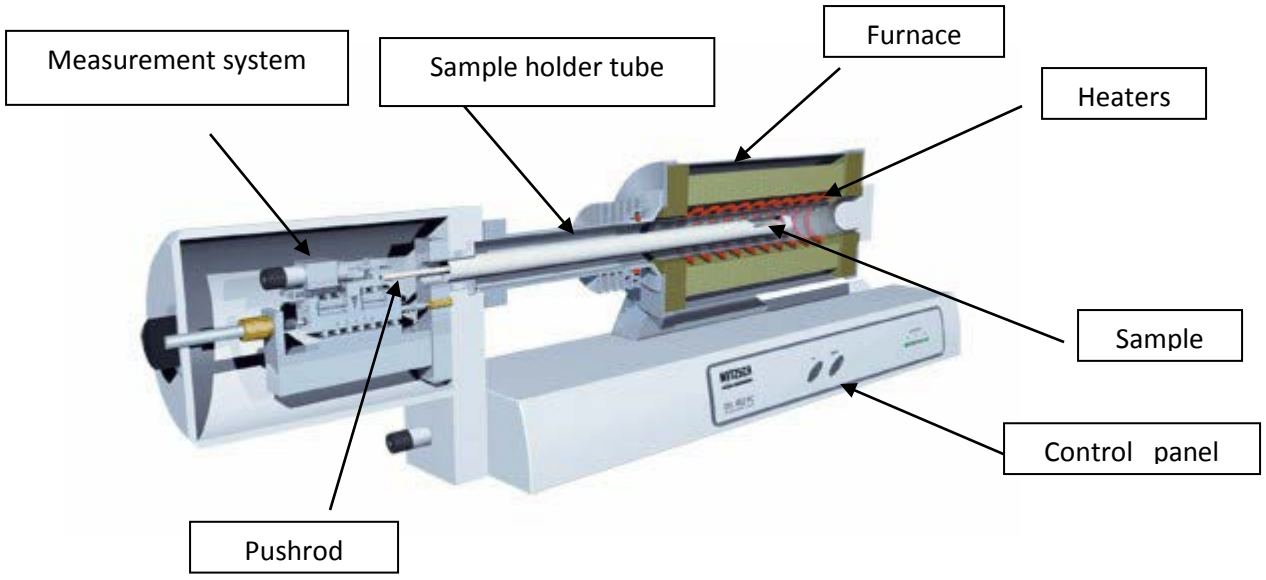

Figure 14: Sketch of the Netzch DIL 402C Dilatometer (54)

3.2 Differential Scanning Calometry (DSC)

3.2.1 Introduction

Differential scanning calometry is the most used thermal technique. It provides quick analysis and measures the basic properties of the material. DSC has been used in many applications: polymers, plastics, glasses and ceramics, proteins and life science materials (55).

3.2.2 Definition

DSC measures the energy changes when the sample is heated, cooled or held isothermally, together with the temperature at which these changes occur. The change in energy helps the user to measure the transitions that occur in the sample at different temperatures and then to characterize a material: such us measuring glass transition, and melting processes. The measurement with DSC is easily made because the sample do not required any preparation (55).

3.2.3 Heat flow measurements

Heat flow measurements are the main property measured by DSC. The value of heat flow measured depends on the effect of the reference. The flow of energy into or out of the sample is represented on y-axis as a function of temperature or time and it is shown in units of mW. There are two kinds of heat flow curves: one show endotherms in the downward direction since the endothermic transitions result in a negative temperature, whilst exothermic transitions are upward (55).

3.2.4 Specific heat (C_p)

The specific heat capacity (Cp) is obtained at constant pressure. The value of Cp can be determined using DSC by subtracting a base line from the heat flow curve. However, any drift error can occur in the fact that the procedure is based on a subtraction technique between measurements made at different temperatures. For this reason, DSC should very stable and it is

preferable to avoid using an instrument at the extremes of its temperature range. The standard should be in sapphire and the mass used should be similar to the sample (55).

3.2.5 Enthalpy

The enthalpy of a material represents the energy required to heat the material to a given temperature. It is obtained by integrating the heat capacity curve. The enthalpy curves help to understand the different transitions taking place during heat treatment of a material (55).

3.2.6 Derivative curves

Derivative curves can help in the interpretation of data, especially where there is an overlapping of peaks. The first derivative curve helps for example to determine the glass transition temperature while the second derivative is useful for analysing the melting processes. A high noise is generated with high derivative level, that is why a good quality data are required for higher derivative studies (55).

3.2.7 DSC Design

DSC has two small identical crucibles, one for the sample and the other one for the reference. The reference is an empty pan. See fig 15 below. They are both heated to a certain heating (or cooling) rate. Finally, DSC sketches the difference between the energy flowing into the sample furnace and the one flowing to the inert reference DSC measures the flow of energy in mW or J/s. The fundamental equation of DSC is the following:

DSC signal (W/g) = Heat Capacity (J/ (Kg))* Scanning Rate (k/s)$\Longrightarrow$ dH/dt= dH/dT*dT/dt. (55)

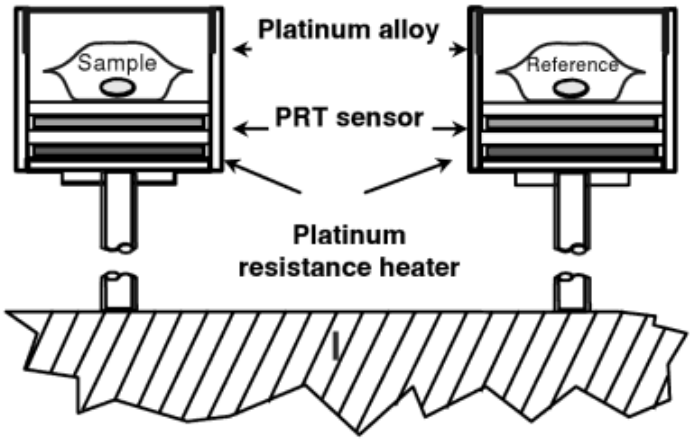

Figure 15: Sketch of DSC system (55).

3.3 X-Ray Diffraction

3.3.1 Introduction

Almost all solid materials (95 %) are described as crystalline substances. In 1919 A.W.Hull (56) claims in his paper "A new Method of Chemical Analysis" that every crystalline substance gives a pattern; the same substance always gives the same pattern; and in a mixture of substances each produces its pattern independently of others.

The X-ray diffraction pattern is therefore a good method to characterize and identify a crystalline substance. It is considered as a fingerprint of the substance.

3.3.2 Definition

X-rays are located between the ϒ-rays and ultraviolet (UV) radiation in the electromagnetic spectrum. They are high energy electromagnetic radiation and their energies are ranging from 200eV to 1 Mev (57).

3.3.3 Theory of X-ray diffraction

Amorphous materials are defined by regular planes of atoms that form a crystal lattice. When X-ray beam interacts with these planes, one part of beam is absorbed by the sample, one part is

transmitted, and third part is refracted and diffracted. In the case of a crystalline material, the diffraction of an X-ray beam is similar to diffraction of light by droplets of water.

X-rays are generated within a sealed tube under vacuum. A current is applied to heat the filament within the tube. The current produces number of electrons and the high voltage accelerate them until they hit the target (copper). When the electrons hit the target, then X-rays are generated and directed into the sample. And, when it is diffracted, then it is possible to measure the distance between the planes of atoms by applying the Bragg´s law. Bragg´s law relation is $n \lambda = 2 d \sin \theta$, where d is the distance between adjacent beam, θ is the angle of incidence of the X-ray beam, see figure 16, λ is the wavelength of the incident beam, and n is the order of the diffracted beam (56).

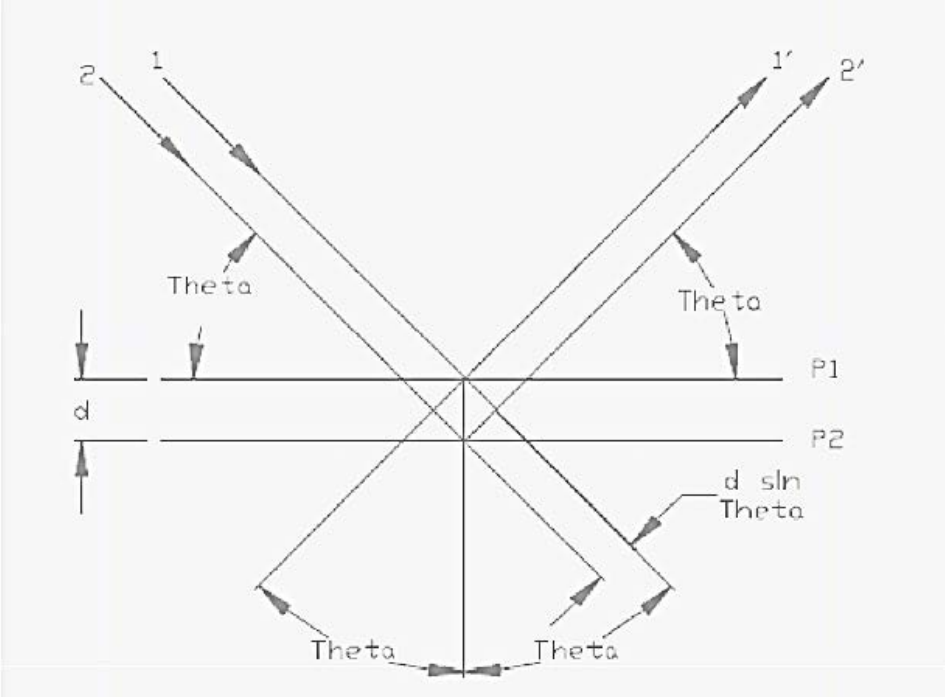

Figure 16: Bragg´s law schematic (56)

4. Experimental procedure

In this chapter, materials, apparatus and procedures will be described.

4.1 Materials investigated

The starting materials used for this work were silicon carbide (average particle size 2µm, purity 99.8%, Alfa Aesar), silicon nitride (average particle size 2µm, H.C. Starck), titanium carbon nitride $TiC_{0.3}N_{0.7}$ and $TiC_{0.7}N_{0.3}$ (average size 2 µm, Element Six).

4.2 Experimental apparatus

4.2.1 Ultrasonic bath

Ultrasonic bath was used to facilitate the wet mixing of the powders in glass tubes using acetone as a solvent. Therefore, a bath made of stainless steel was used. It has a large transducer areas and tanks that produce a high-powered ultrasonic intensity throughout the entire oscillating tank. This step was necessary to avoid agglomeration of the powder, see figure 17.

Figure 17: Ultrasonic bath

4.2.2 Vacuum pump

The vacuum pump used in this project is TRIVAC B. It is an oil-sealed rotary vane pump. The oil injected into the pump chamber is used for sealing and lubrication. It was used for sucking water vapour and humidity from powders using a low gas pressure 10^{-3} atm, see figure 18.

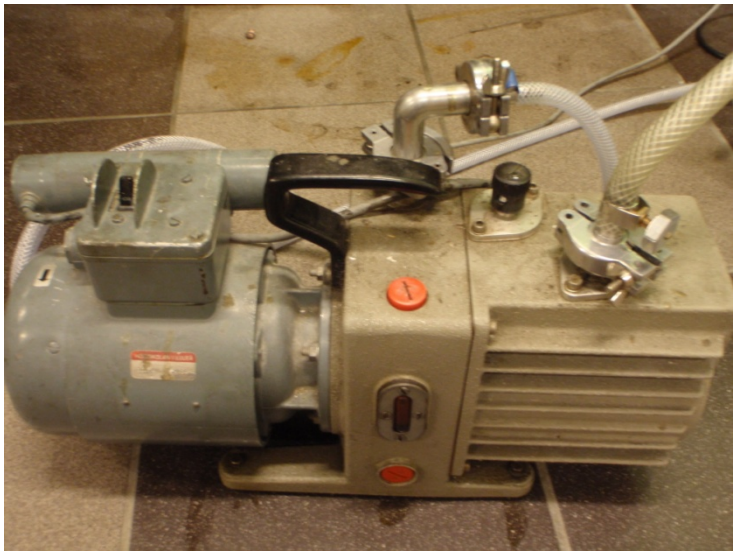

Figure 18: vacuum pump

4.3 Powder processing

4.3.1 Preparation of powder mixtures

Initially, powders were evacuated from water vapour and humidity using vacuum pumping. Then, some silicon nitride powder was added to titanium carbon nitride $TiC_{0.3}N_{0.7}$ in two different molar ratios. ($TiC_{0.3}N_{0.7}$:Si_3N_4) (2:1) and ($TiC_{0.3}N_{0.7}$: Si_3N_4) (1:1). Silicon carbide was also added to $TiC_{0.7}N_{0.3}$. ($TiC_{0.7}N_{0.3}$: SiC) (2:1) and ($TiC_{0.7}N_{0.3}$: SiC) (1:1), see table 3.

Table3: Powder mixtures

Powder mixtures	Molar ratio
$TiC_{0.3}N_{0.7}$: Si_3N_4	2:1
$TiC_{0.3}N_{0.7}$: Si_3N_4	1:1
$TiC_{0.7}N_{0.3}$: SiC	2:1
$TiC_{0.7}N_{0.3}$: SiC	1:1

4.4 Analysis of the samples

The samples were analysed using thermal analysis in order to study the thermal behaviour of the powders in range of temperatures 40-1450 °C. Differential scanning calorimetry DSC was used to observe at what temperatures reactions take place. X-Ray Diffraction (XRD) analysis was also used at room temperature to figure out the different components present in the powders.

4.1.1 DSC/TG mass spectrometer

DSC/TG and mass spectrometer were run both in pure argon and nitrogen atmosphere to obtain global curves and their gas emission. When the sample is heated, DSC analyser measures the energy changes. The energy changes helps to find and measure the transitions that occur in the sample.

The powders were treated thermally from 40 °C up to 1450 °C with a heating rate of 20 °C/min in argon atmosphere, and then cooled down with a cooling rate of 100 °C/min. The same conditions were used for nitrogen atmosphere.

DSC/TG experiments were carried out by Netzsch (STA 449C and QMS 403C) (see figure 19). The instrument contains two alumina crucibles of 159 mg used as sample holder and reference. A calibration of the equipment is necessary to ensure that the scan rate of use is calibrated.

The temperature measurement was calibrated with Indium, Bismuth, Zinc, Aluminium, Silver and Gold that have melting points of 156.66, 271.11, 418.33, 660, 960, 1062.77 °C respectively. A heating rate of 10 °C was used for calibration. In order to avoid the buoyancy effects, it we run an empty pan over the temperature range of interest, under the same conditions and subtract that from the sample.

Figure 19: DSC equipment

4.4.2 XRD analysis

XRD analysis was used to determine the different compositions and phases of the samples. In this project, the samples were scanned using two different XRD equipment. Firstly, samples were scanned with Philips XRD equipment, see figure 20 (a), but this equipment was broken. For this reason, some samples were also scanned with Siemens D5000, see figure 20 (b), at the Chemical Engineering Department. The settings and sample preparation used to scan the samples depend on the XRD equipment used, see table 5.

Table4: Setting of XRD equipment used

	Philips XRD	**Siemens D5000 XRD**
X-Ray source	CuKα (40kV and 45mA)	CuKα (40kV and 40mA)
primary slit	slit of ½°	slit of 6mm
secondary slit	slit of ½°	slit of 6mm
Scan time	2θ=10-120°	2 θ =10-120°
Step width	0.01° and 5s/step	0.02° and 1.5 s/step

Figure 20: a) Philips XRD equipment b) Siemens D5000 equipment

4.4.3 Sample preparation

Samples were crushed with a ceramic mortar. The crushed powder was placed into a polymeric holder and put in the XRD equipment. The sample powders heat treated by DSC/TG were also crushed using the same mortar. However, the sample amount was very small. Therefore, methanol was used to the powder sample and it was placed on glass plate to dry.

5. Results and discussion

5.1 Influence of gas atmosphere and molar ratios

In order to study the thermal behaviour of powders, a study of the influence of atmosphere was studied up to 1450 °C using a heating rate of 20 °C/min under argon and nitrogen atmosphere.

5.1.1 $TiC_{0.3}N_{0.7}$

DSC results

Thermogravimetric (TG) curve of $TiC_{0.3}N_{0.7}$ in nitrogen atmosphere presents a mass loss of about 0.07% from 40 °C up to 500 °C (stage 1), which is confirmed by the release of C_xH_y and N_2 as it is observed on their mass spectrometer curves (see Appendix 1). After that, a mass-gain of 3.71 % started at 500 °C up to 1450 °C (stage 2) with the release of N_2O, CO, and C_3H_8. (See appendix 1). DSC curve is relatively smooth in stage 1 and it descended gradually with increasing temperature, see figure 21.

In argon atmosphere, $TiC_{0.3}N_{0.7}$ presents in stage 1 a mass-gain of 0.14 % between 300 °C and 400 °C because of the release of residual organics and argon gas. (See Appendix 1). However, a mass-gain of 1.21% is observed in stage 2. DSC curve decreased slowly until a peak valley of 790 °C appeared and followed by another peak at 1010 °C, see figure 22.

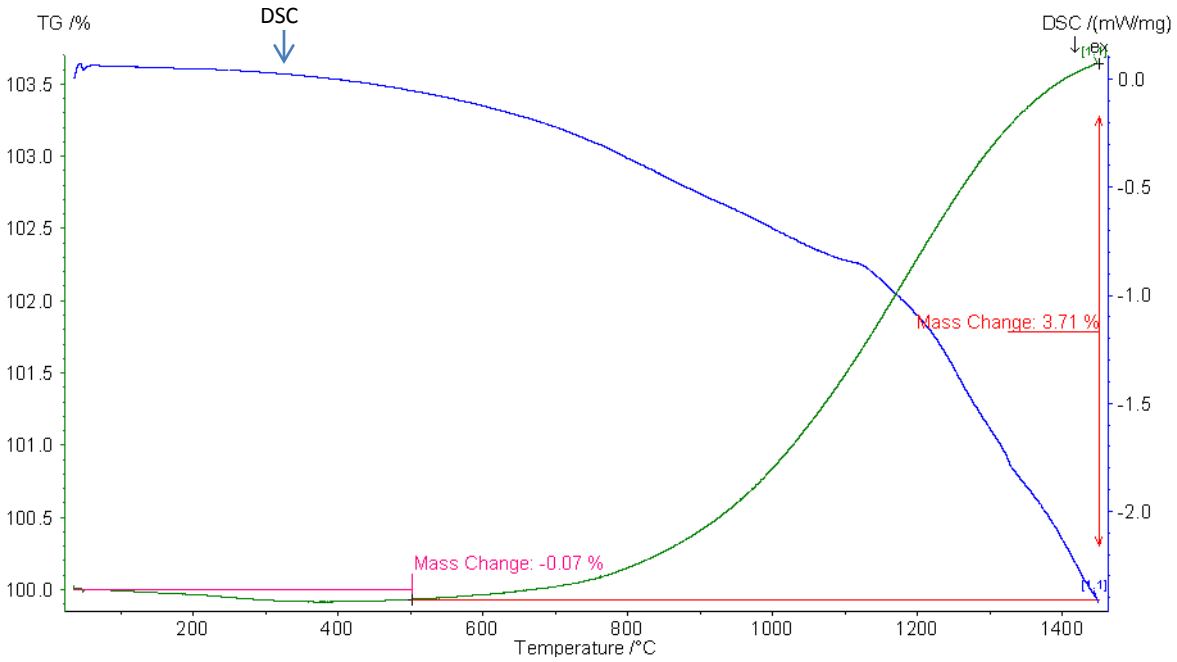

Figure 21: TG/DSC of $TiC_{0.3}N_{0.7}$ in nitrogen atmosphere

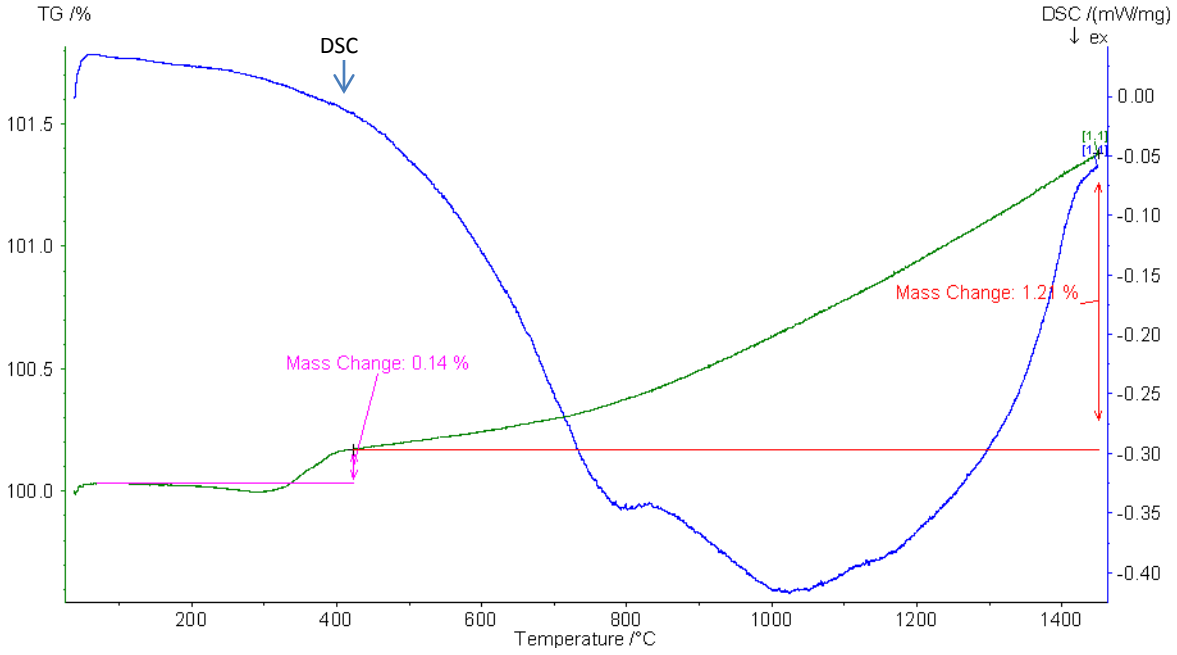

Figure 22: TG/DSC of $TiC_{0.3}N_{0.7}$ in argon atmosphere

XRD results

XRD spectrum of $TiC_{0.3}N_{0.7}$ raw powder is shown in the figure 23. The raw powder spectrum shows that the raw powder contains mainly $TiC_{0.3}N_{0.7}$. There are some minor unidentified peaks possibly belonging to carbon.

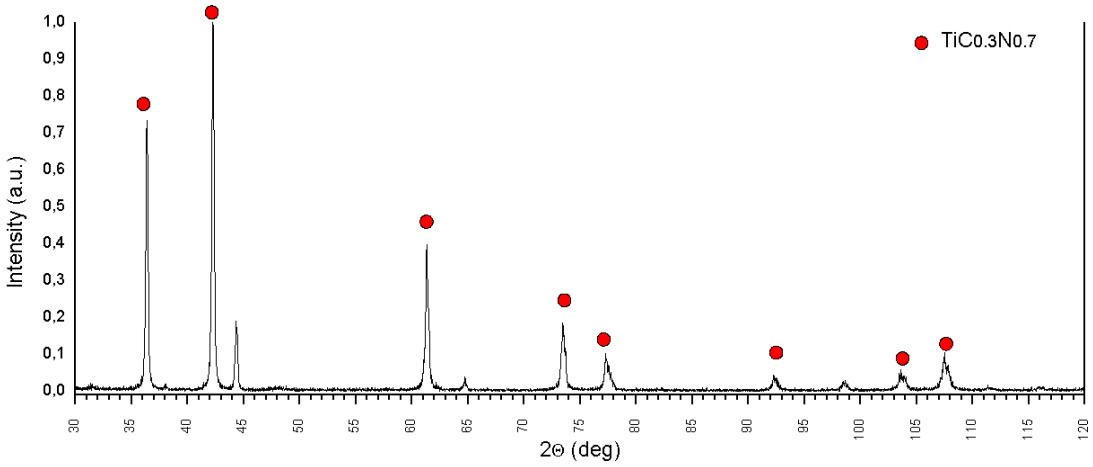

Figure 23: XRD graph of $TiC_{0.3}N_{0.7}$

5.1.2 $TiC_{0.7}N_{0.3}$

DSC results

TG curve of $TiC_{0.7}N_{0.3}$ in nitrogen atmosphere presents a small mass loss of 0.17 % in the range of 40-500 °C (stage 1), which is confirmed by the release of CO_2, C_3H_8 and N_2O (see Appendix 2). After 700 °C (stage 2), a mass-gain of 3.65% is observed, which manifests that a chemical reaction has occurred at this temperature. DSC curve descended smoothly with increasing temperature, see figure 24.

However, in argon atmosphere, a loss of weight of 0.15% is observed between 100 and 400 °C. The mass loss is due to the release of argon and C_xH_y as it is seen in their mass spectrometer curves (see Appendix 2). In stage 2, TG curve increased due to a mass-gain of 0.68%. DSC curve in stage 2 shows an exothermic peak at 1200 °C, see figure 25.

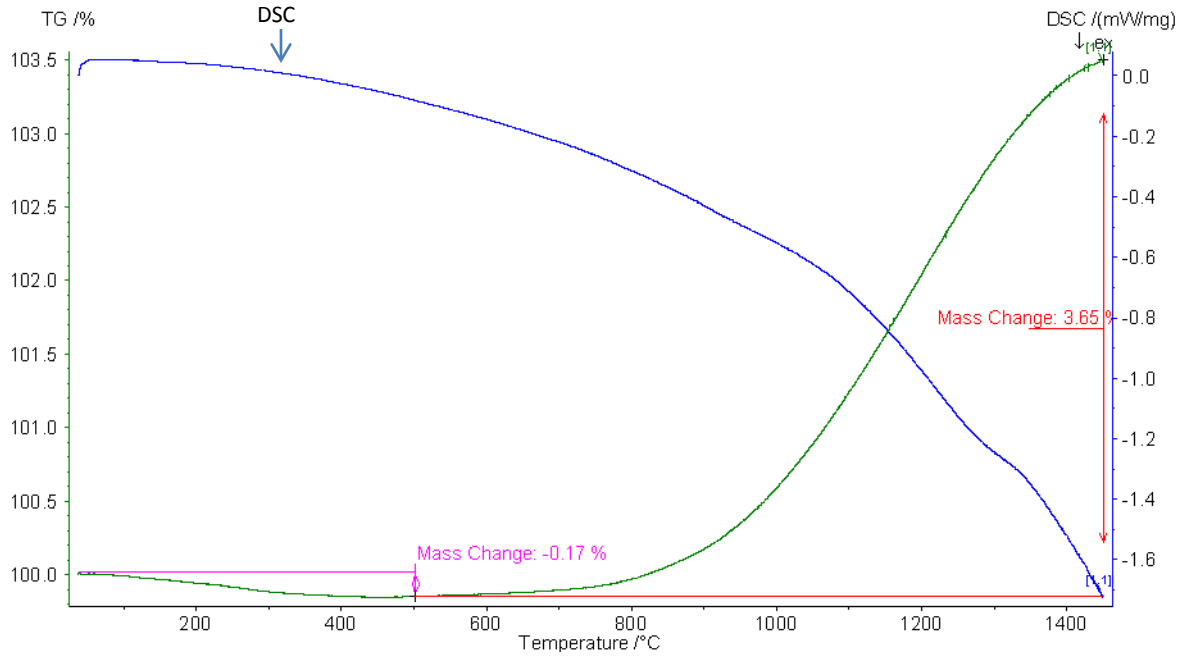

Figure 24: TG/DSC of $TiC_{0.7}N_{0.3}$ in nitrogen atmosphere

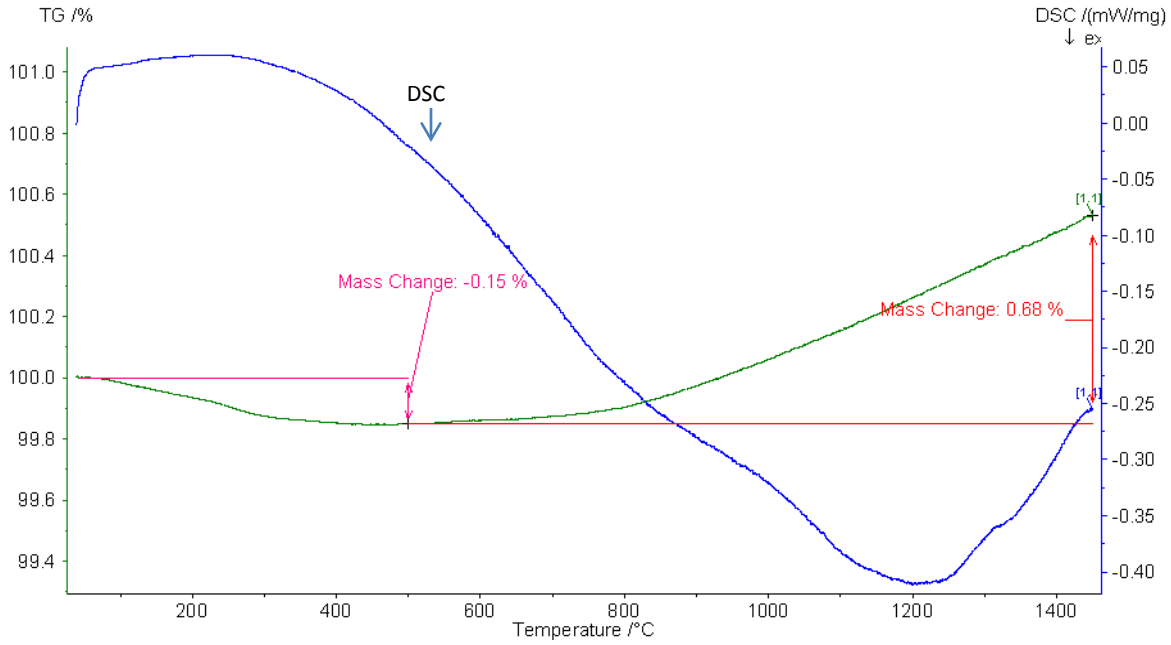

Figure 25: TG/DSC of $TiC_{0.7}N_{0.3}$ in argon atmosphere

XRD results

XRD spectrum below shows that $TiC_{0.7}N_{0.3}$ is the main constituent in the $TiC_{0.7}N_{0.3}$ raw powder. The same unidentified peaks possibly refer to carbon as $TiC_{0.3}N_{0.7}$, see figure 26.

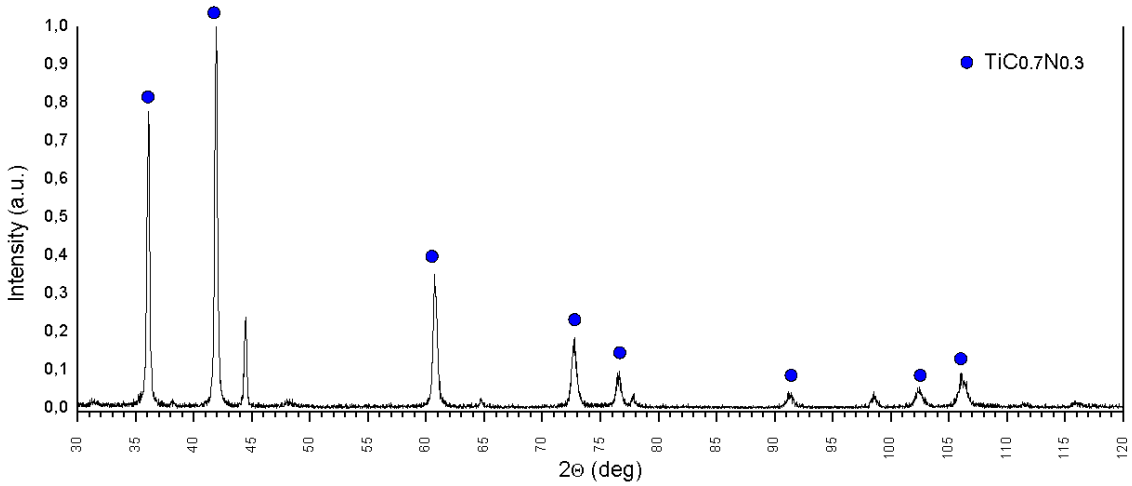

Figure 26: XRD graph of $TiC_{0.7}N_{0.3}$

Discussion of results

In nitrogen atmosphere, for both $TiC_{0.7}N_{0.3}$ and $TiC_{0.3}N_{0.7}$, DSC curve descended gradually with increasing reaction temperature which manifests that the weight losses are small and the reaction rate is low. TG curves present a mass loss of 0.07-0.17% in the first stage (40-500 °C), and a mass-gain from 500 °C up to 1450 °C in the second stage. The first stage corresponds to the drying of the sample, which is confirmed by the release of organics CxHy, while the gain mass in second stage indicates that titanium carbon nitride possesses vacancies in its crystal lattice, therefore, it can accept more nitrogen atoms.

In argon atmosphere, TG curves of $TiC_{0.7}N_{0.3}$ and $TiC_{0.3}N_{0.7}$ have approximately the same thermal behaviour. They present the same behaviour in the second stage (600-1450 °C). However, in the first stage (40-500 °C); $TiC_{0.7}N_{0.3}$ manifests a mass-gain which can be explained by the fact that $TiC_{0.3}N_{0.7}$ picked up some carbon atoms; this can be due to contamination of the crucible and the tubes of DSC/TG instrument. While $TiC_{0.3}N_{0.7}$ presents a mass loss, which is due

to the drying of the sample. DSC curves of both $TiC_{0.7}N_{0.3}$ and $TiC_{0.3}N_{0.7}$ decrease slowly until exothermic peaks appear. Two exothermic peaks are observed in $TiC_{0.7}N_{0.3}$ whereas just one peak is observed in DSC curve of $TiC_{0.3}N_{0.7}$. This suggested that heat emitting reaction occurred, see figure 25.

5.1.3 Si_3N_4

DSC results

TG curve of silicon nitride, in nitrogen atmosphere, presents only a mass loss of around 0.19% up to 1450°C. Whereas, DSC curve is relatively smooth, this may indicate that mass losses are small, while DSC curve falls in the range of 1000-1450 °C, see figure 27.

However, in argon atmosphere, TG curve of Si_3N_4 presents a loss of weight of 0.58% between 40 °C and 1450 °C, which is explained by the release of SiO(g) (see Appendix 3). DSC curve decreases slowly but no reacting peak belonging to this stage emerged, see figure 28.

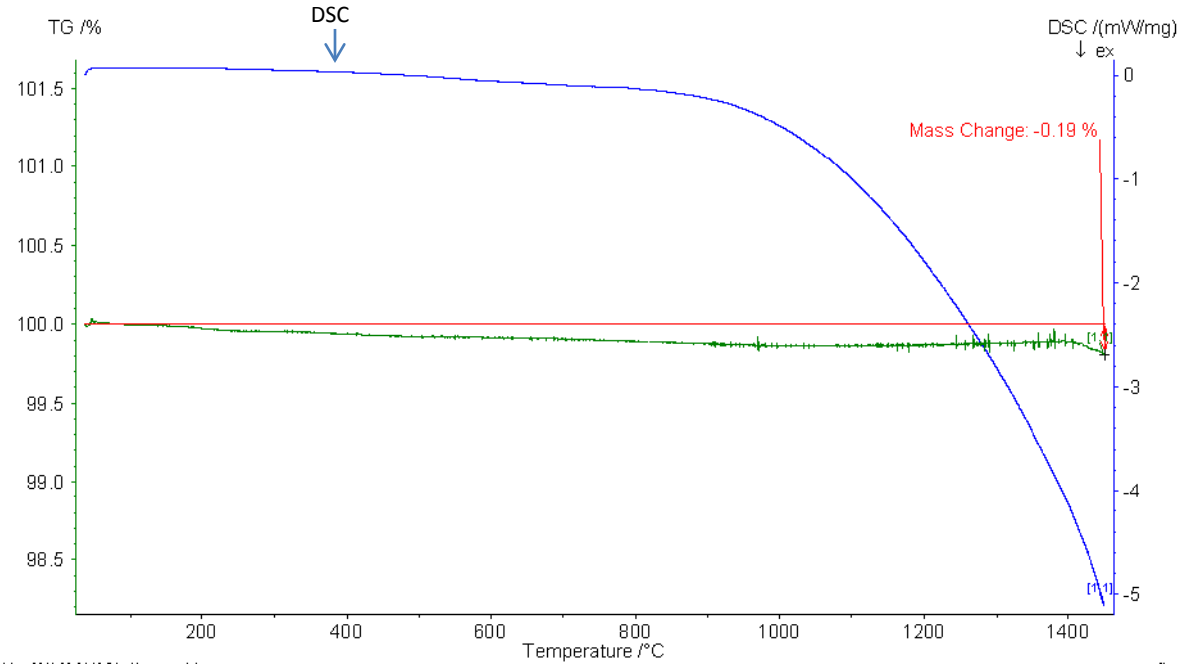

Figure 27: TG/DSC of Si_3N_4 in nitrogen atmosphere

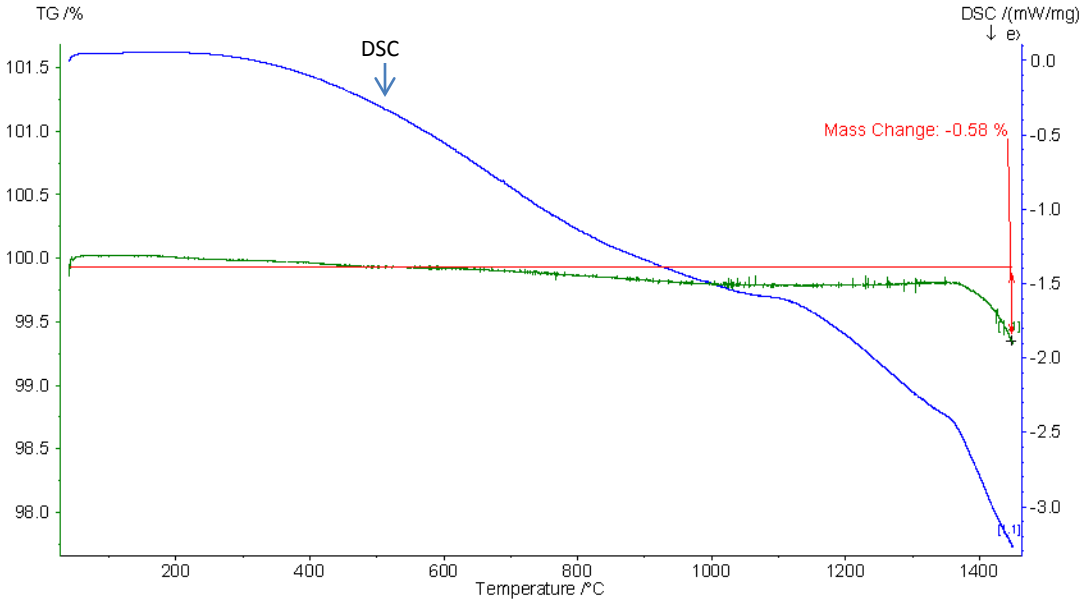

Figure 28: TG/DSC of Si_3N_4 in argon atmosphere

XRD results

As it is seen in figure 29 below, XRD analysis of Si_3N_4 showed that it is composed only of Si_3N_4 phase.

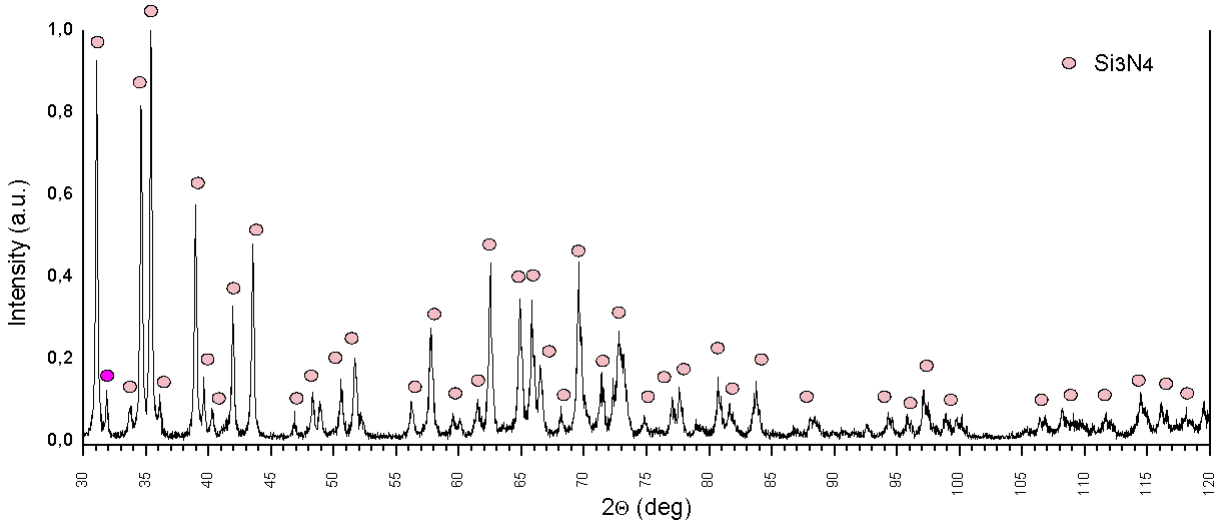

Figure 29: XRD graph of Si_3N_4

Discussion of results

DSC/TG curves indicated that no mass change has been occurred in this range of temperature (40-1450 °C) in nitrogen atmosphere, which is due to the fact that Si_3N_4 is stable in nitrogen atmosphere. As it is seen in section 2.2.5, the phase transformation of Si_3N_4 is too slow to be detected at temperatures below 1400 °C due to its high activation energy. However, in argon atmosphere, Si_3N_4 decomposes to silicon monoxide SiO (g) and N_2 (g) at high temperature (1375 °C). This can be explained by the fact that Si_3N_4 starting powder contains oxygen.

5.1.4 SiC

DSC results

TG curve of silicon carbide presents a small mass loss in nitrogen atmosphere, which is confirmed by the release of NO_2 and organics C_xH_y (see Appendix 4). DSC curve decreases gradually until a weak peak appeared at 1133.8 °C, see figure 30. However, in argon atmosphere, no obvious peak appeared in DSC curve. TG curve presents a mass loss of 0.18 % at high temperature 1400 °C, see figure 31.

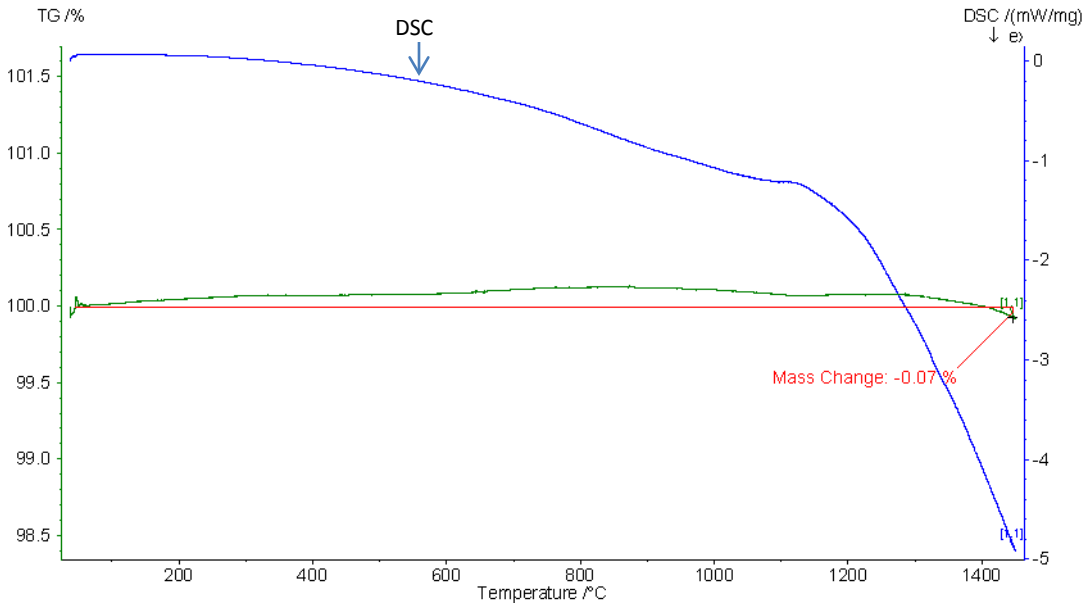

Figure 30: TG/DSC of SiC in nitrogen atmosphere

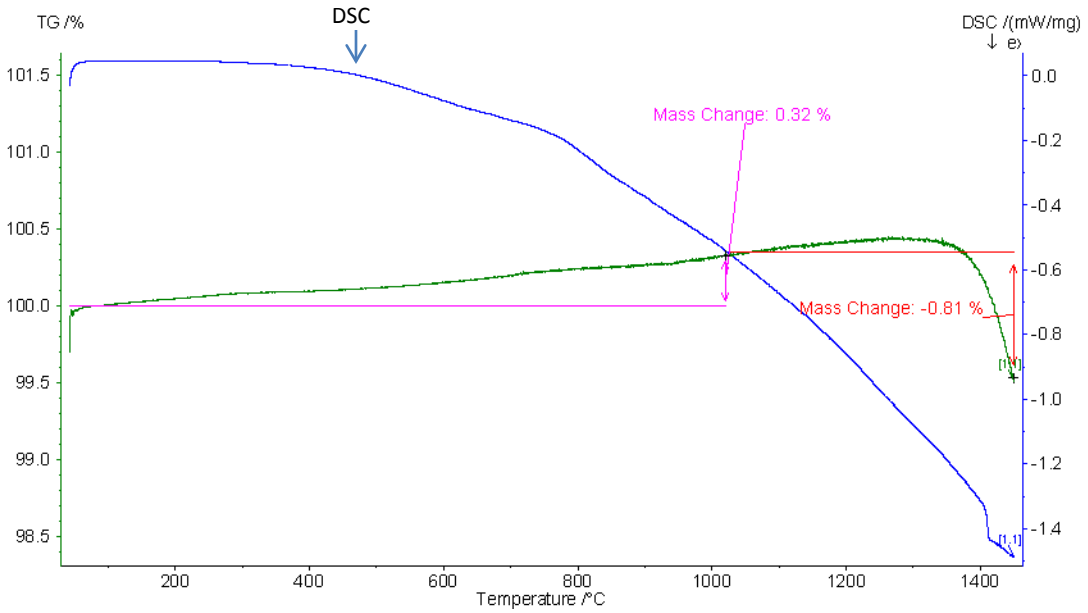

Figure 31: TG/DSC of SiC in argon atmosphere

XRD results

XRD spectrum of SiC raw powder shows that it consists of both cubic and hexagonal silicon carbide, see figure 32.

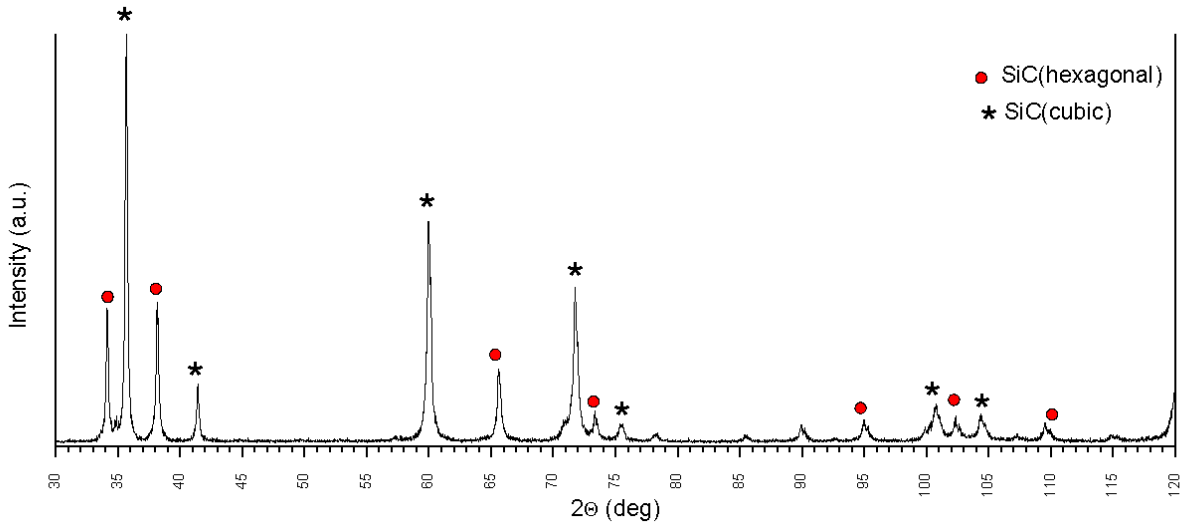

Figure 32: XRD graph of SiC

Discussion of results

Figure 30 shows that SiC presents only a mass loss of 0.07 % in nitrogen, which means that no phase transition of SiC has been occurred from 40 °C to 1450 °C in nitrogen atmosphere. As it was indicated ion section 2.2.6 SiC has a high sublimation temperature of about 2700 °C, which in accordance with our results. However, in argon atmosphere, SiC presents a mass loss of 0.81% at high temperature, which is due to the decomposition of SiC to SiO (g) and CO. This indicates that the starting powder of silicon carbide contained oxygen.

5.1.5 $TiC_{0.3}N_{0.7}/Si_3N_4$ (2:1)

DSC results

In order to study the thermal behaviour of $TiC_{0.3}N_{0.7}$ / Si_3N_4, DSC analysis of two batches of $TiC_{0.3}N_{0.7}$ / Si_3N_4 with different molar ratios $TiC_{0.3}N_{0.7}$ / Si_3N_4 (2:1) and $TiC_{0.3}N_{0.7}$ / Si_3N_4 (1:1) were carried out from room temperature up to 1450°C under nitrogen and argon atmosphere.

DSC curve of $TiC_{0.3}N_{0.7}$ / Si_3N_4 (2:1) in nitrogen atmosphere is relatively smooth and descended gradually with increasing temperature. TG curve presents a loss of weight of 0.24 % up to 800 °C. This loss of mass is due to the evaporation of water (see Appendix 5). After that, a mass-gain of 1.97 % is observed between 900 °C and 1450 °C, see figure 33.

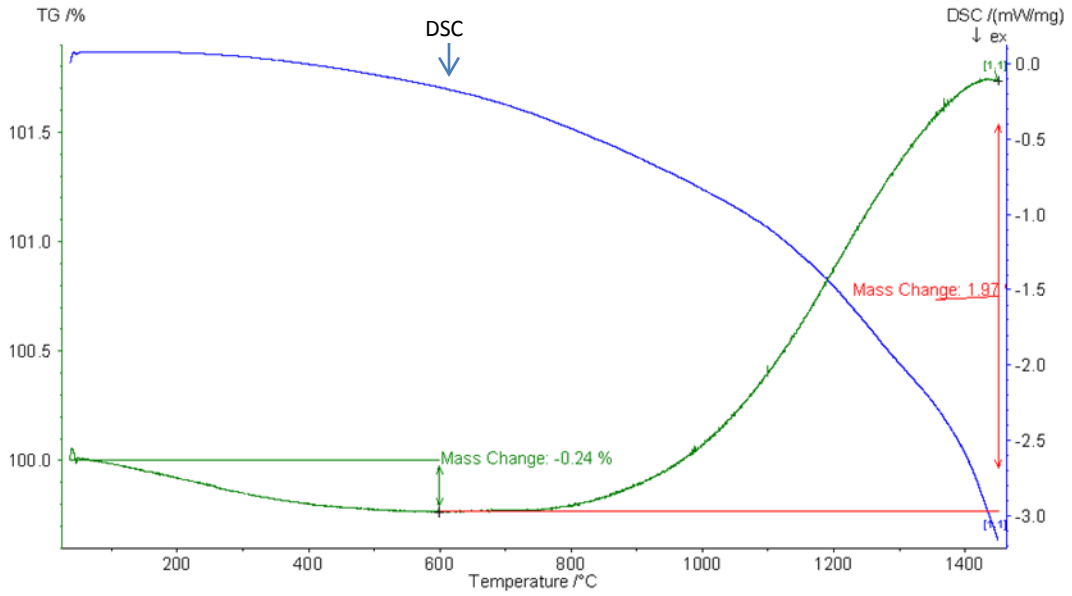

Figure 33: TG/DSC of $TiC_{0.3}N_{0.7}$:Si_3N_4 (2:1) in nitrogen

On the other hand, TG curve of $TiC_{0.3}N_{0.7}$ / Si_3N_4 (2:1) in argon atmosphere is relatively stable between 100 °C and 600°C (stage 1). Therefore only a mass loss of 0.08 % is observed in this range of temperature, see figure 34. This small loss of weight is confirmed by the release of ammonia and evaporation of water, see Appendix 5. However, TG started to increase from 600 °C up to 1300 °C (stage 2), followed by a decomposition (stage 3) that started from 1300 °C.

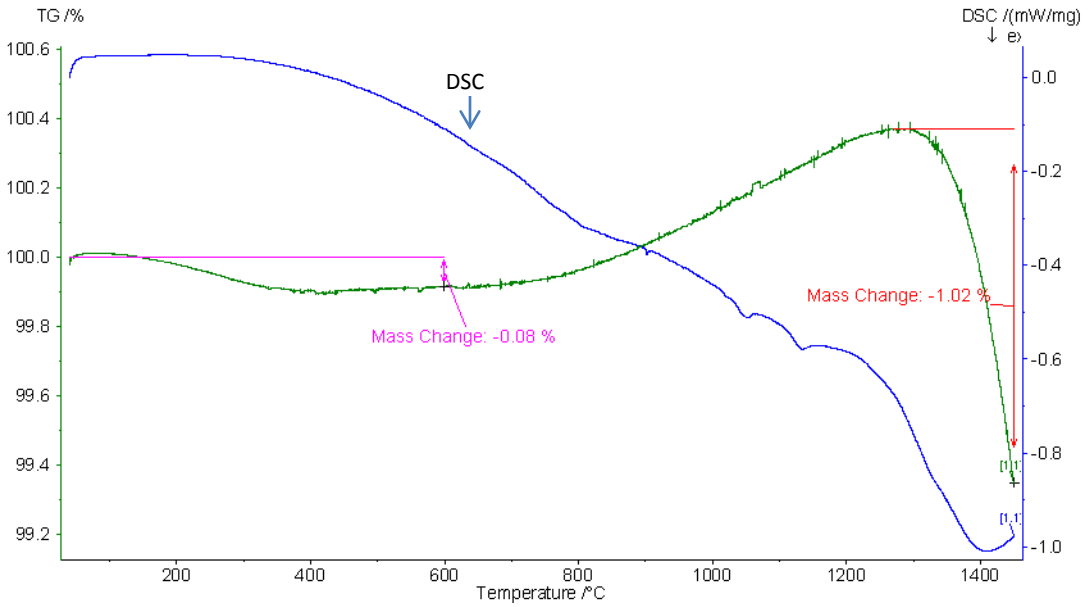

Figure 34: TG/DSC of $TiC_{0.3}N_{0.7}$:Si_3N_4 (2:1) in argon atmosphere

XRD results

XRD analysis of $TiC_{0.3}N_{0.7}$ / Si_3N_4raw powder shows that only $TiC_{0.3}N_{0.7}$ and Si_3N_4 are present in the raw powder. However, after DSC run up to 1450 °C with a heating rate of 5 °C/min in nitrogen atmosphere, XRD analysis of $TiC_{0.3}N_{0.7}$ /Si_3N_4 (2:1) manifests the formation of TiN and SiC (hexagonal), see figures 35 and 36.

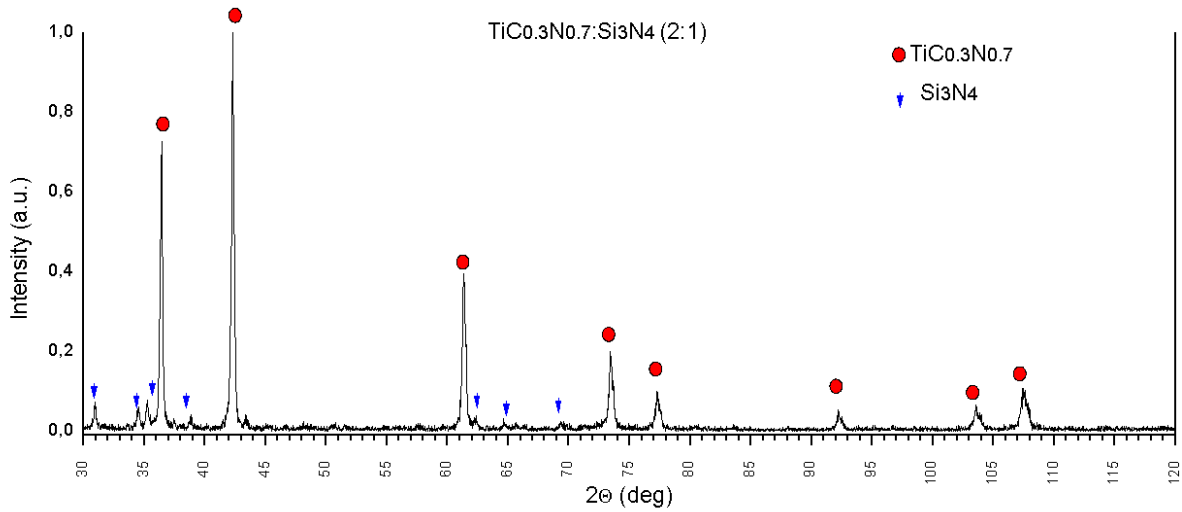

Figure 35: XRD graph of $TiC_{0.3}N_{0.7}$:Si_3N_4 (2:1)

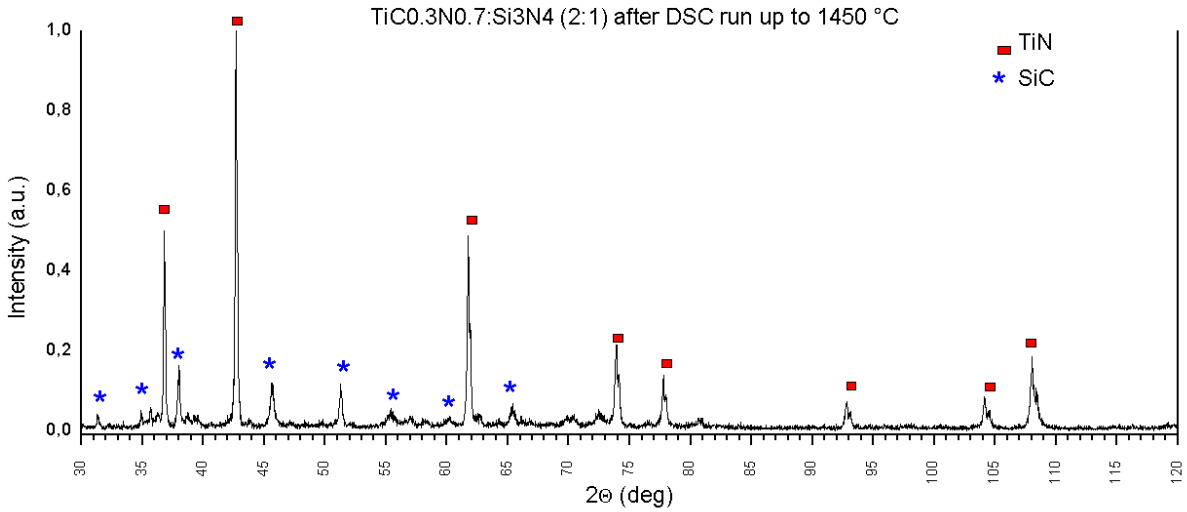

Figure 36: XRD graph of $TiC_{0.3}N_{0.7}$:Si_3N_4 (2:1) after DSC

5.1.6

DSC results

As it is observed in the figure 35, in nitrogen atmosphere, TG curves of $TiC_{0.3}N_{0.7}$: Si_3N_4 (1:1) presents the same behaviour as $TiC_{0.3}N_{0.7}$: Si_3N_4 (2:1). However, there is an early mass loss of 0.3 % at around 200 °C (stage 1). This loss of weight is explained by the release of N_2, C_xH_y and mainly NH_3 (see Appendix 6). Besides that, mass-gain of 2.10 % is observed in the range of 800-

1450 °C (stage 2). Whereas DSC curves decreased smoothly until it falls at about 800 °C. The same behaviour is observed in DSC curve of Si_3N_4. However, no obvious peak is observed, see figure 37.

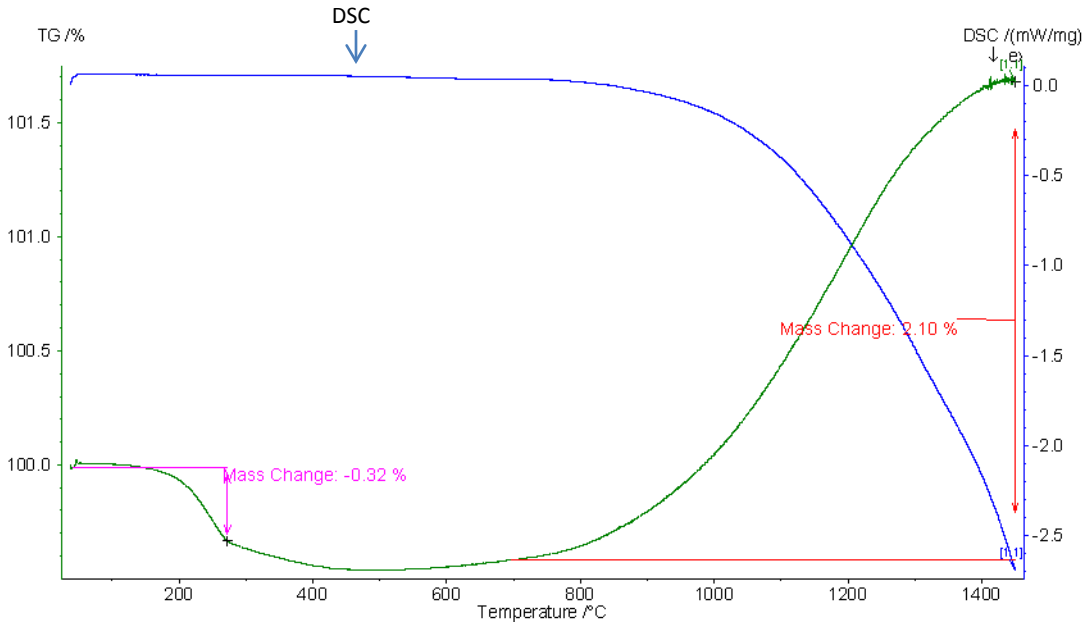

Figure 37: TG/DSC of $TiC_{0.3}N_{0.7}$:Si_3N_4 (1:1) in nitrogen atmosphere

In argon atmosphere, $TiC_{0.3}N_{0.7}$: Si_3N_4 (1:1) presents also the same behaviour as $TiC_{0.3}N_{0.7}$: Si_3N_4 (2:1). In stage 2, the release of C_3H_8 and evaporation of water in addition to the release of argon induce a mass loss of 0.32 % (see Appendix 6). While there is an increase in mass from 800 °C up to 1300 °C in stage 2. Finally, it is followed by decomposition of the reaction products, see figure 38.

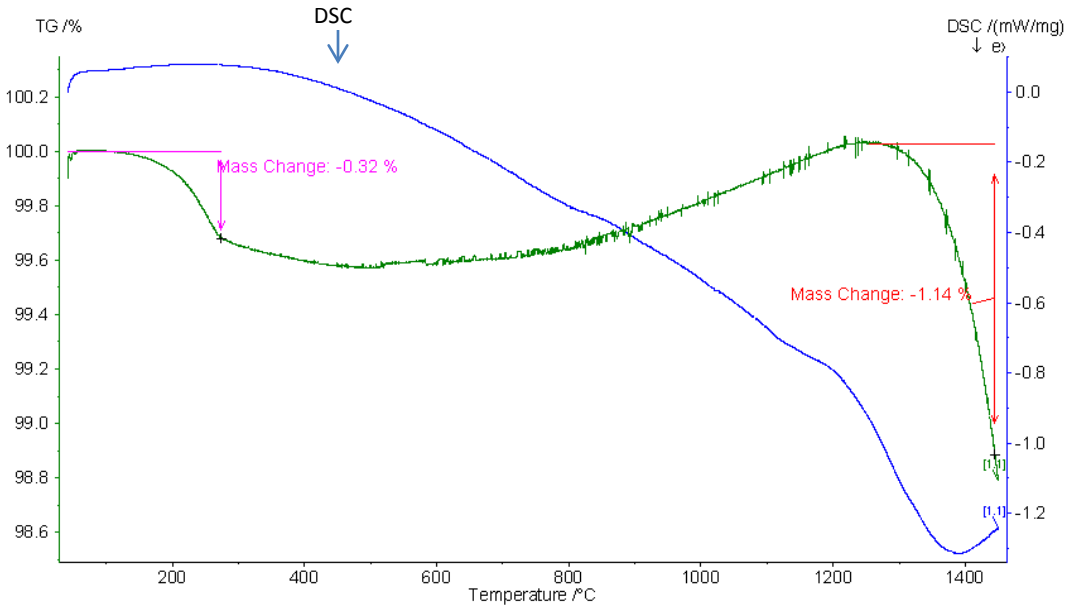

Figure 38: TG/DSC of $TiC_{0.3}N_{0.7}$:Si_3N_4 (1:1) in argon atmosphere

XRD results

XRD analysis of $TiC_{0.3}N_{0.7}$: Si_3N_4 (1:1) raw powder indicates that only $TiC_{0.3}N_{0.7}$ and $Si_3N_4$are present in the raw powder as it is expected. However, after DSC analysis of raw powder in nitrogen atmosphere up to 1450 °C with a heating rate of 5 °C/min, it is observed the formation of α-SiC (hexagonal, rhombo-hedral) and TiN as new components in addition to $TiC_{0.3}N_{0.7}$ and Si_3N_4, see figures 39 and 40.

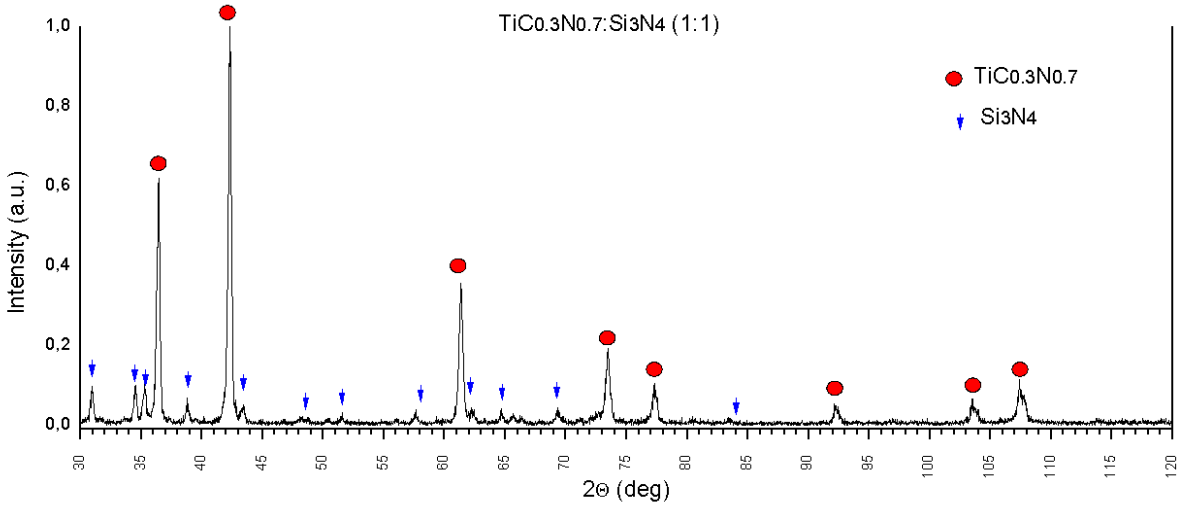

Figure 39: XRD graph of $TiC_{0.3}N_{0.7}$:Si_3N_4 (1:1)

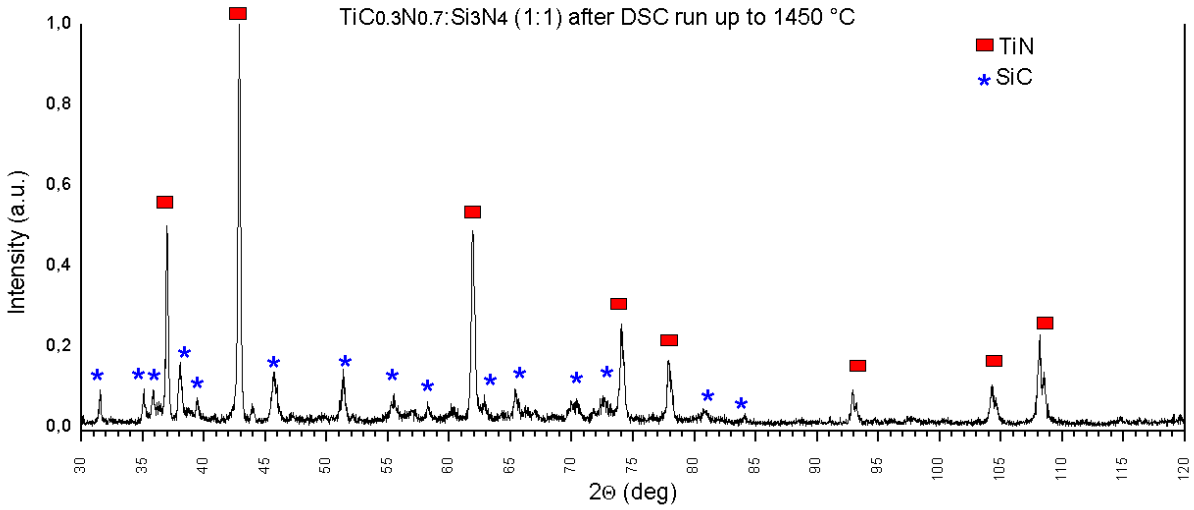

Figure 40: XRD graph of $TiC_{0.3}N_{0.7}$:Si_3N_4 (1:1) after DSC

Discussion of results

The thermal analysis of $TiC_{0.3}N_{0.7}$: Si_3N_4 (1:1) and $TiC_{0.3}N_{0.7}$: Si_3N_4 (2:1) present approximately the same behaviour under nitrogen and argon atmosphere. The formation of new components SiC and TiN induce a mass-gain in both $TiC_{0.3}N_{0.7}$: Si_3N_4 (1:1) and $TiC_{0.3}N_{0.7}$: Si_3N_4 (2:1). However,

the source of the release of NH_3 and water at low temperatures can only be explained by the fact that Si_3N_4 raw powder contains humidity and ammonia.

5.1.7 $TiC_{0.7}N_{0.3}$/SiC (2:1)

DSC results

DSC curves of $TiC_{0.3}N_{0.7}$:SiC (2:1), in nitrogen gas, decreased slowly with increasing temperature, see fig 41, which indicates that mass losses are less. Therefore, there is a loss of weight of 0.21 % at 400°C (stage 1). According to the mass spectrometer, the mass loss is due to the evaporation of water and the release of ammonia and N_2 (see Appendix 7).

In argon atmosphere, TG curve of $TiC_{0.3}N_{0.7}$: SiC (2:1) presents only mass loss of just 0.15 % in first stage which is confirmed by the release of organics CxHy and argon gas (see Appendix 7). Whereas in second stage, a mass loss of 0.23 % is observed due to the decomposition of $TiC_{0.3}N_{0.7}$: SiC (2:1). DSC curve shows a clear exothermic peak at 1359.3 °C that corresponds to the decomposition in stage 3, see fig 42.

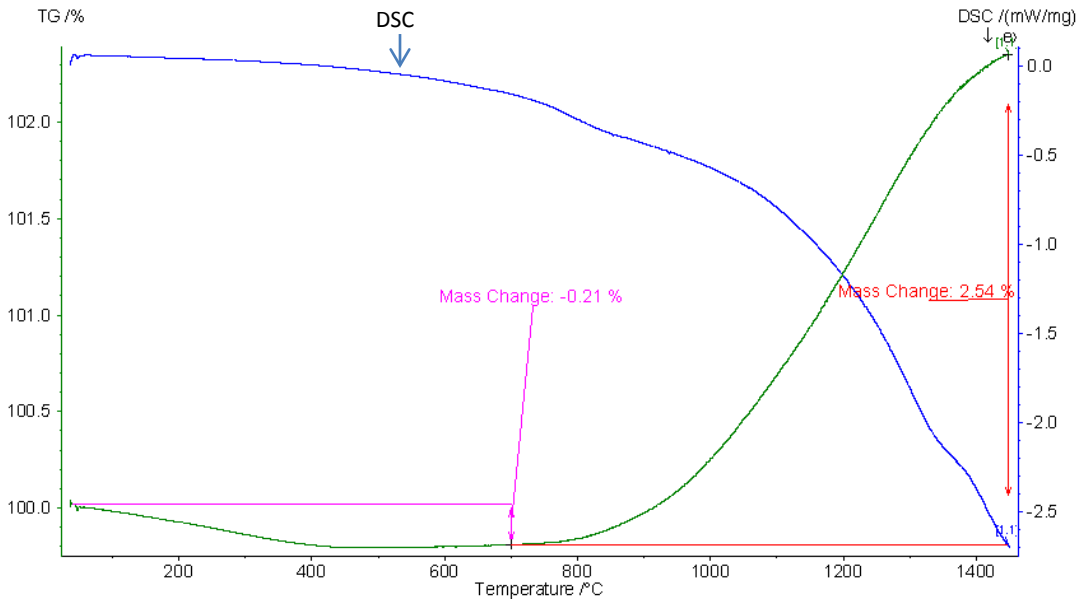

Figure 41: TG/DSC of $TiC_{0.3}N_{0.7}$: SiC (2:1) in nitrogen atmosphere

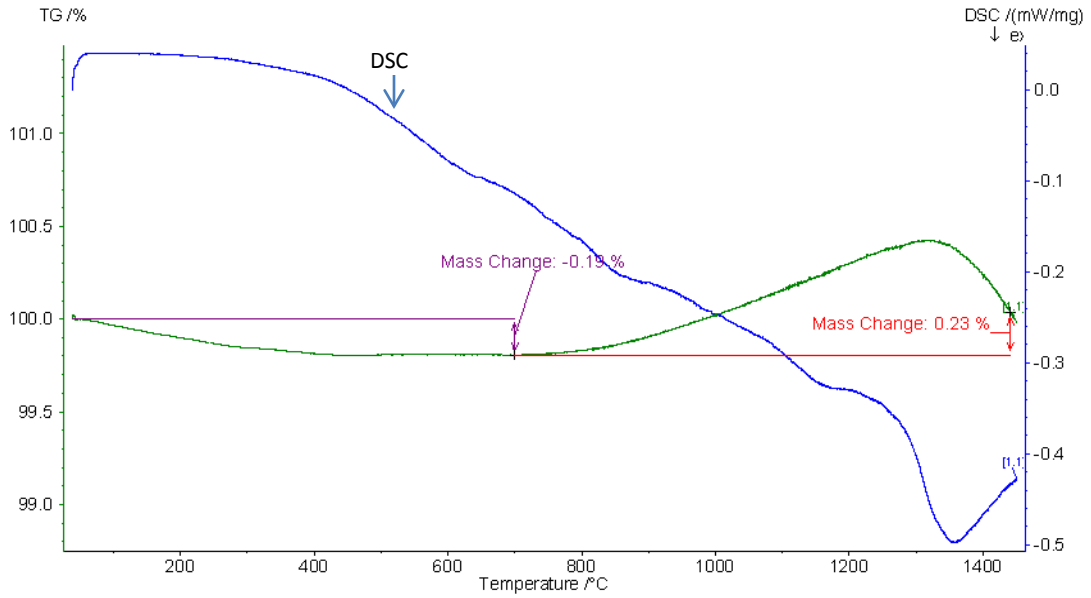

Figure 42: TG/DSC of $TiC_{0.3}N_{0.7}$: SiC (2:1) in argon atmosphere

XRD results

XRD analysis of raw powder shows that only SiC and $TiC_{0.7}N_{0.3}$ are present in the raw powder, see fig 43. However, after DSC run up to 1450 °C with a heating rate of 5°C/min, XRD spectrum showed the formation of a new component which is Si_3N_4 and TiO_2, see figure 44.

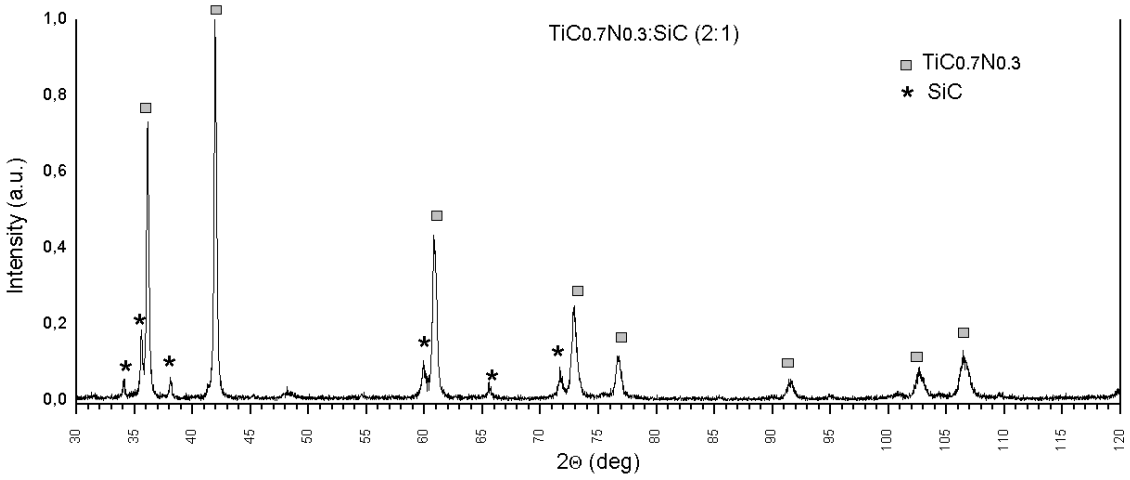

Figure 43: XRD graph of $TiC_{0.3}N_{0.7}$: SiC (2:1)

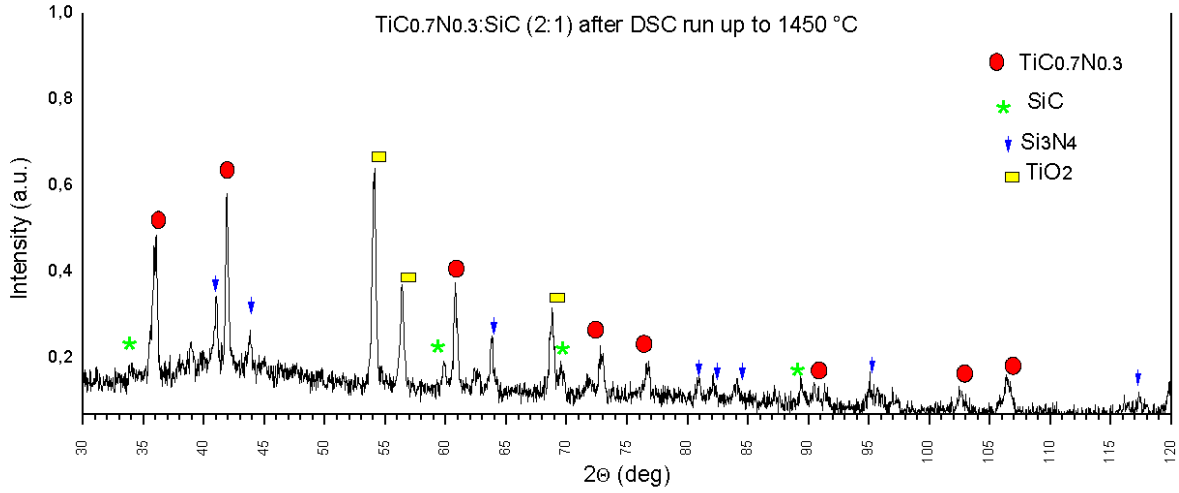

Figure 44: XRD graph of $TiC_{0.3}N_{0.7}$: SiC (2:1) after DSC in nitrogen atmosphere

5.1.8 $TiC_{0.7}N_{0.3}$: SiC (1:1)

DSC results

In nitrogen atmosphere, TG curve of $TiC_{0.7}N_{0.3}$: SiC (1:1) shows a mass loss of 0.27 % in first stage which is confirmed by the release of N_2, H_2O and C_xH_y (see Appendix 8). However, a mass-gain is observed between 1000 °C and 1450 °C (stage 2). DSC curve is decreasing gradually with increasing temperature. However, no peak is observed in this range of temperature, see figure 45.

In argon atmosphere, TG curve of $TiC_{0.7}N_{0.3}$: SiC (1:1) indicates a mass loss of 0.44 % and 0.77 % in first stage and second stage respectively. Mass spectrometer indicates that this loss of weight is due to the release of C_xH_y, H_2O and argon gas (see Appendix 8). DSC curve descended gradually but no obvious reaction peak is observed, see figure 46.

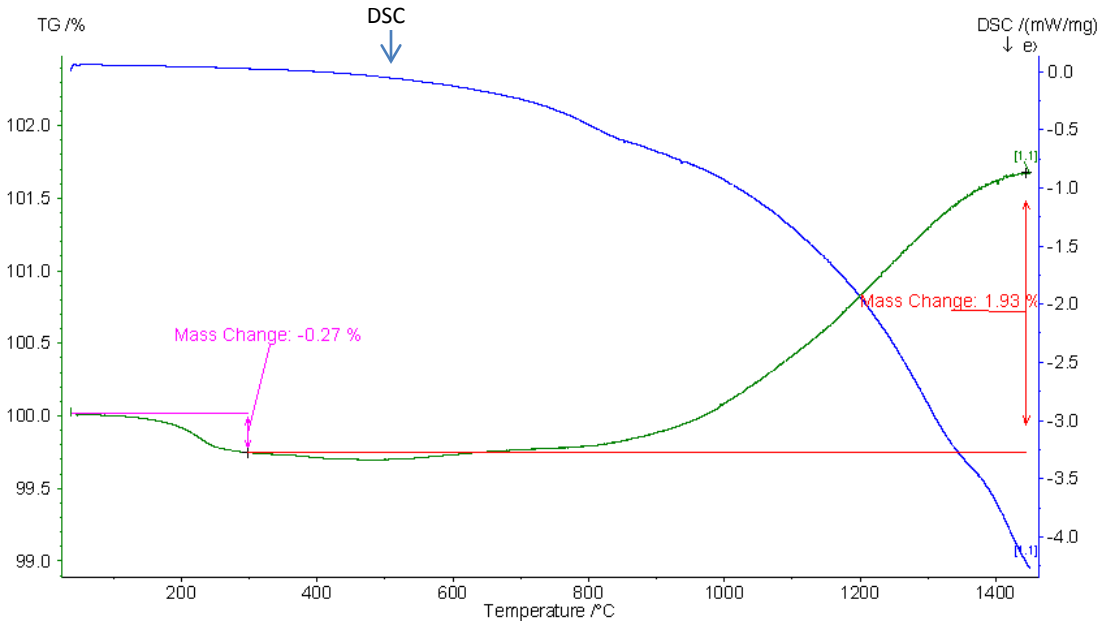

Figure 45: TG/DSC of $TiC_{0.3}N_{0.7}$: SiC (1:1) in nitrogen atmosphere

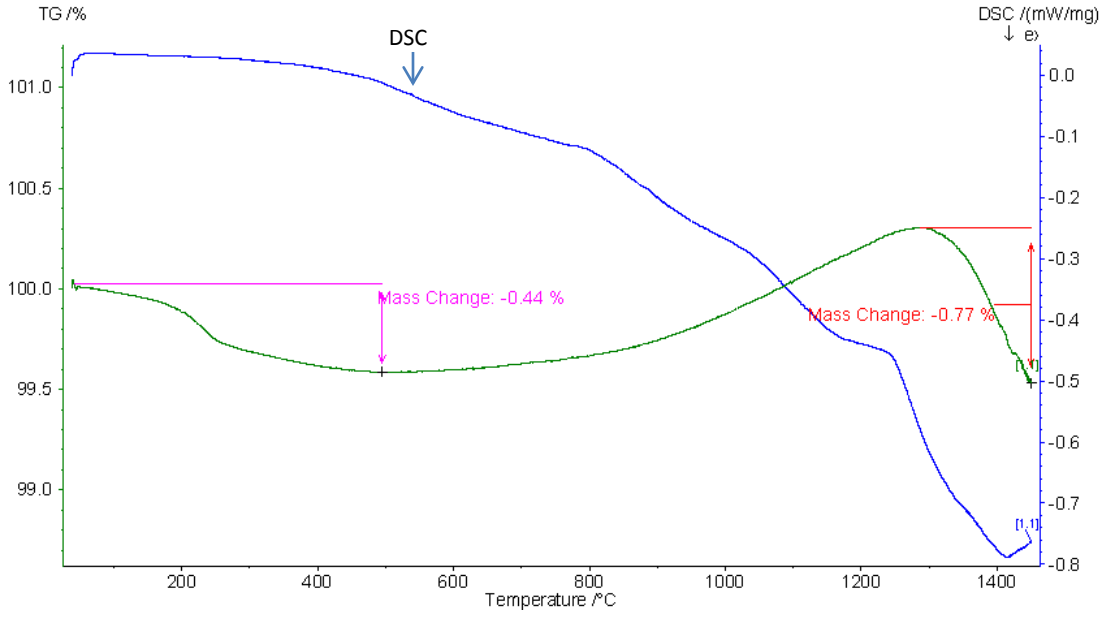

Figure 46: TG/DSC of $TiC_{0.3}N_{0.7}$: SiC (1:1) in argon atmosphere

XRD results

As it is seen in figure 47, XRD analysis of $TiC_{0.7}N_{0.3}$: SiC (1:1) of raw powder shows that only $TiC_{0.7}N_{0.3}$and SiC are present in the raw powder. After DSC run up to 1450 ˚C with a heating rate of 5 °C/min under nitrogen gas, XRD spectrum shows the formation of Ti_2N, TiC and $TiC_{0.7}N_{0.3}$.

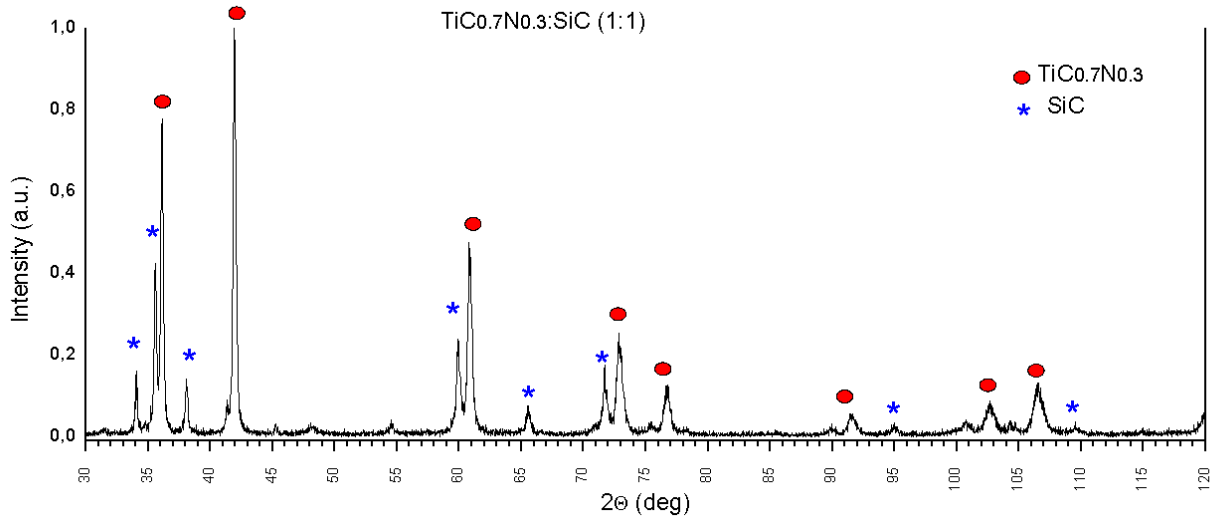

Figure 47: XRD graph of $TiC_{0.3}N_{0.7}$: SiC (1:1)

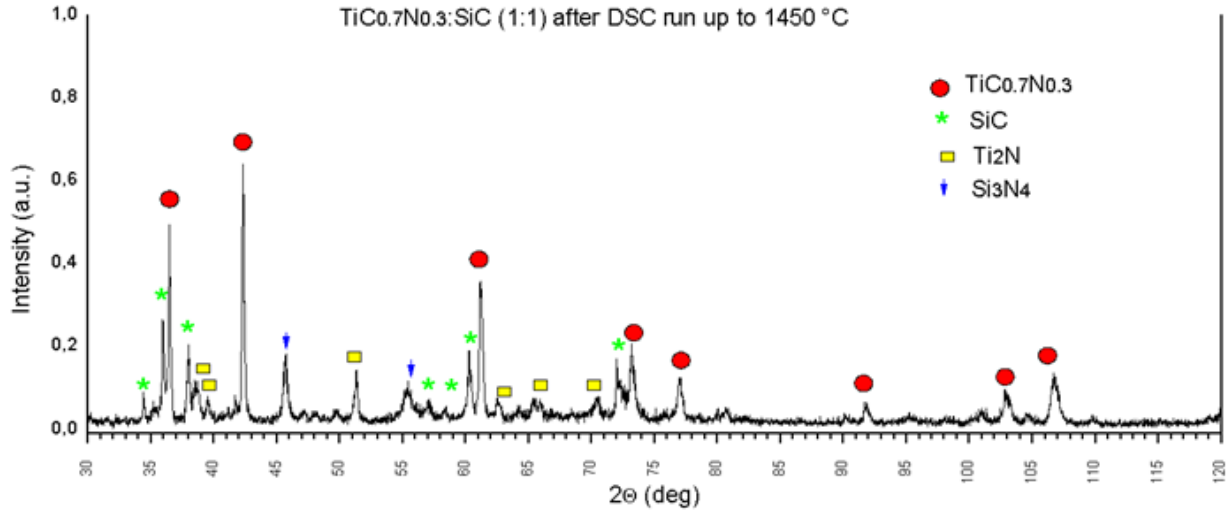

Figure 48: XRD graph of $TiC_{0.3}N_{0.7}$: SiC (1:1) after DSC run

Discussion of results

$TiC_{0.7}N_{0.3}$: SiC (2:1) and $TiC_{0.7}N_{0.3}$: SiC (1:1) have approximately the same DSC and TG curves under argon and nitrogen atmosphere. In nitrogen atmosphere, $TiC_{0.7}N_{0.3}$: SiC with both molar ratio (2:1) and (1:1) present mass-gain in second stage. However, $TiC_{0.7}N_{0.3}$: SiC (2:1) enhanced the formation of Si_3N_4 and TiO_2, while $TiC_{0.7}N_{0.3}$: SiC (1:1) enhanced the formation of Si_3N_4, Ti_2N.

5.2 The in-situ synthesis of a TiC_xN_{1-x}/SiC composite using polycarbomethylsilane (PCS) as a precursor for SiC.

5.2.1 DSC results

The preparation of the in-situ synthesis of TiC_xN_{1-x}/SiC composite using PCS as a precursor for SiC had been done already in our laboratory.

DSC/TG analysis in nitrogen atmosphere has been performed on heat treated powder (1300 ˚C for 1 hour). TG curve shows that a mass loss started at about 1200 ˚C, while at this temperature DSC curve shows an exothermic peak indicating that there is an emitting reaction, which is in our case, the decomposition of the sample, see figure 49.

According to Bouillon (52), see section 2.3, the conversion of PCS to SiC occurs mainly in three steps:

- The pyrolysis temperature of PCS, Tp, is 1000°C<Tp<1200°C interval.
- The thermal degradation of PCS is achieved above 1000°C.
- The grain coarsening of SiC occurred above 1400 °C.

These three steps explain the thermal behaviour of our sample where we have decomposition at 1200 °C.

The gaseous species released during the pyrolysis of PCS are: $(CH_3)_3SiH$, C_2H_6, $(CH_3)_4Si$, CH_4, CO, and $(CH_3)_2SiH_2$, see figure 50. The mass spectrometer results of the in-situ synthesis of TiC_xN_{1-x}/SiC composite show that the same gases were released, see figure 51.
As a result, a crystallization of SiC occurred independently of the other elements ($TiCl_4$, CCl_4).

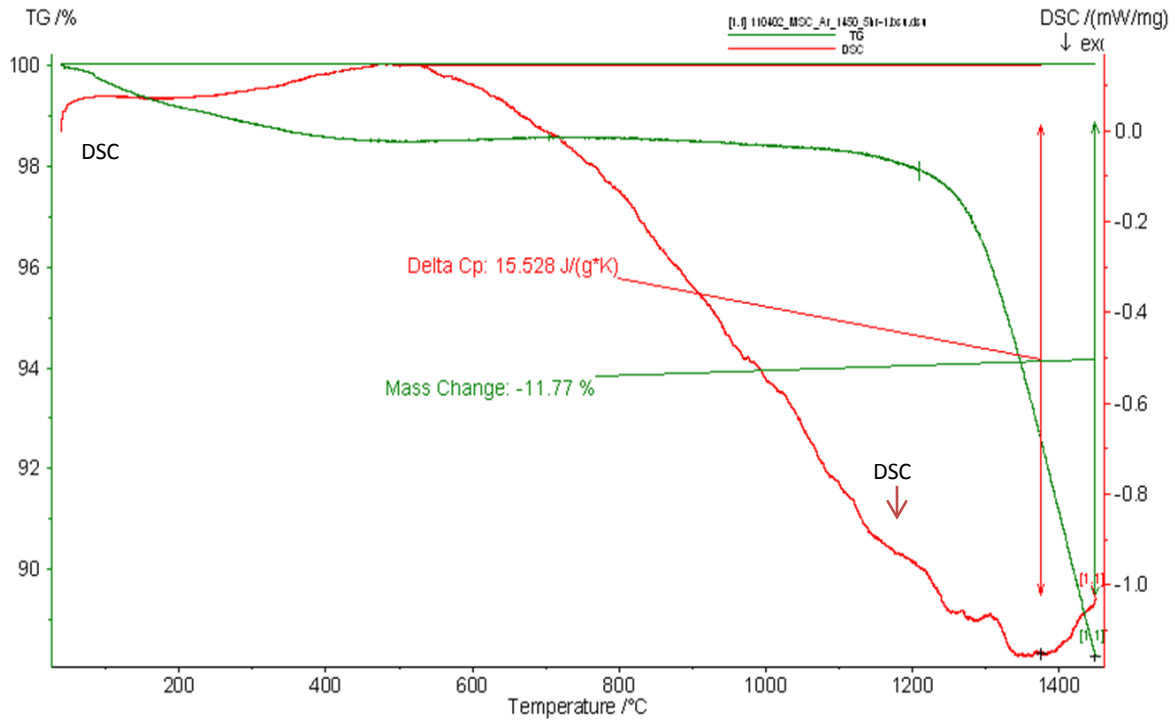

Figure 49: TG/DSC of the in-situ synthesis of a TiC_xN_{1-x}/SiC composite

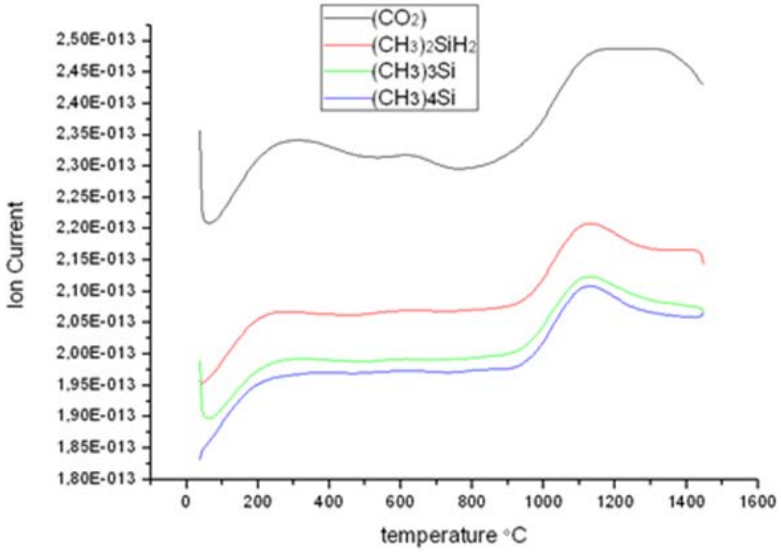

Figure 51: Mass spectrometer curve of the in-situ synthesis of a TiCxN1-x/SiC composite

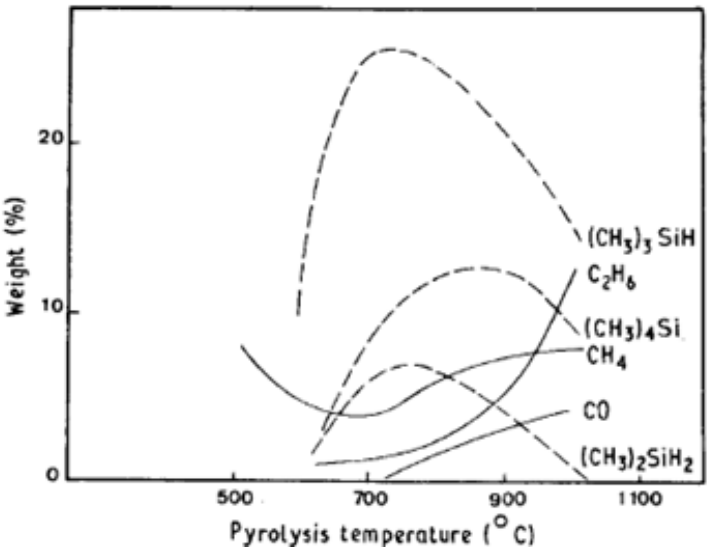

Figure 50: Quantitative analysis of the gaseous species resulting from the pyrolysis of PCS as a function of temperature (52)

6. Conclusions

6.1 Influence of gas atmosphere:

- **In nitrogen atmosphere**

- Si_3N_4 and SiC are stable up to 1450 °C.
- $TiC_{0.3}N_{0.7}$ pick-up nitrogen atoms from 500 °C up to 1450 °C.
- $TiC_{0.3}N_{0.7}$: Si_3N_4 (2:1) has the same thermal behaviour as $TiC_{0.7}N_{0.3}$.
- At 1450 °C, $TiC_{0.3}N_{0.7}$: Si_3N_4 molar ratios (2:1) and (1:1) decompose to SiC and TiN.
- $TiC_{0.7}N_{0.3}$: SiC (2:1) pick-up N_2 from 800 up to 1450 °C.
- At 1450 °C, $TiC_{0.7}N_{0.3}$: SiC molar ratios (2:1) and (1:1) decompose to Si_3N_4 + Ti_2N and Si_3N_4 + TiO_2 respectively.

- **In argon atmosphere**

- Si_3N_4 and SiC decompose to SiO (g) and N_2 at 1370 °C and 1350 °C respectively.
- $TiC_{0.3}N_{0.7}$: Si_3N_4 (2:1) and $TiC_{0.7}N_{0.3}$: SiC (2:1) decompose at 1300 °C.

6.2 Influence of molar ratios

- **In nitrogen and argon atmosphere**

- $TiC_{0.3}N_{0.7}$ and $TiC_{0.7}N_{0.3}$have the same thermal behaviour.
- $TiC_{0.7}N_{0.3}$: SiC molar ratios (2:1) and (1:1) have the same thermal behaviour.
- $TiC_{0.3}N_{0.7}$: Si_3N_4molar ratios (2:1) and (1:1) have the same thermal behaviour.
- $TiC_{0.7}N_{0.3}$: SiC (2:1) in nitrogen atmosphere enhanced the formation of Si_3N_4 and Ti_2N, while $TiC_{0.7}N_{0.3}$: SiC (1:1) enhanced the formation of Si_3N_4 and TiO_2.

6.3 Influence of PCS on the in situ-synthesis of TiC_xN_{1-x}/SiC composite

- SiC nucleus is assumed to form after heating at 1300 °C
- Crystallization of SiC occurs at 1450 °C.
- $TiC_xN_{1-x}$and SiC composite are in-situ synthesized at 1450 °C.

Appendix 1: **Mass Spectrometer curves of $TiC_{0.3}N_{0.7}$**

Nitrogen atmosphere

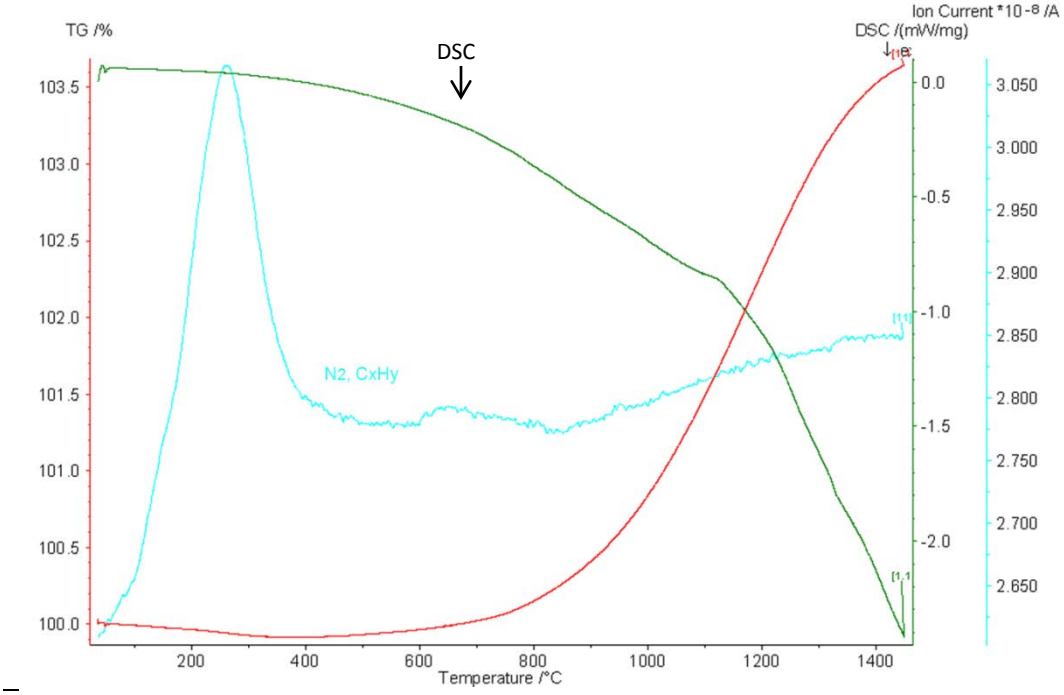

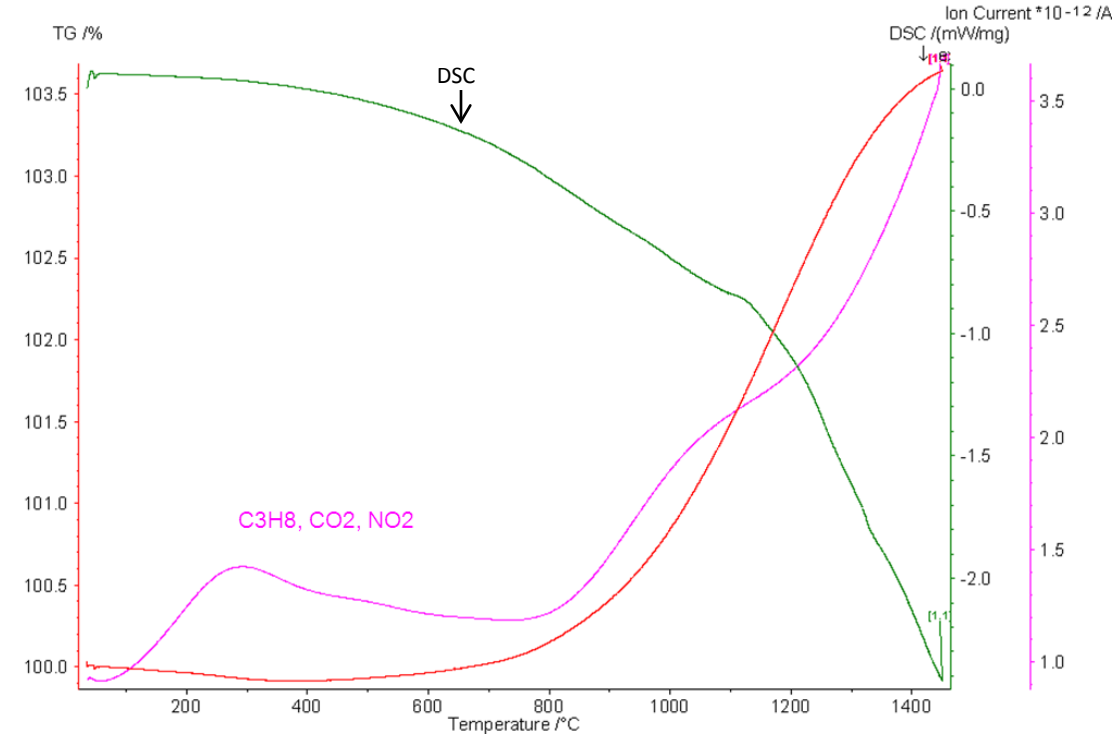

Argon atmosphere

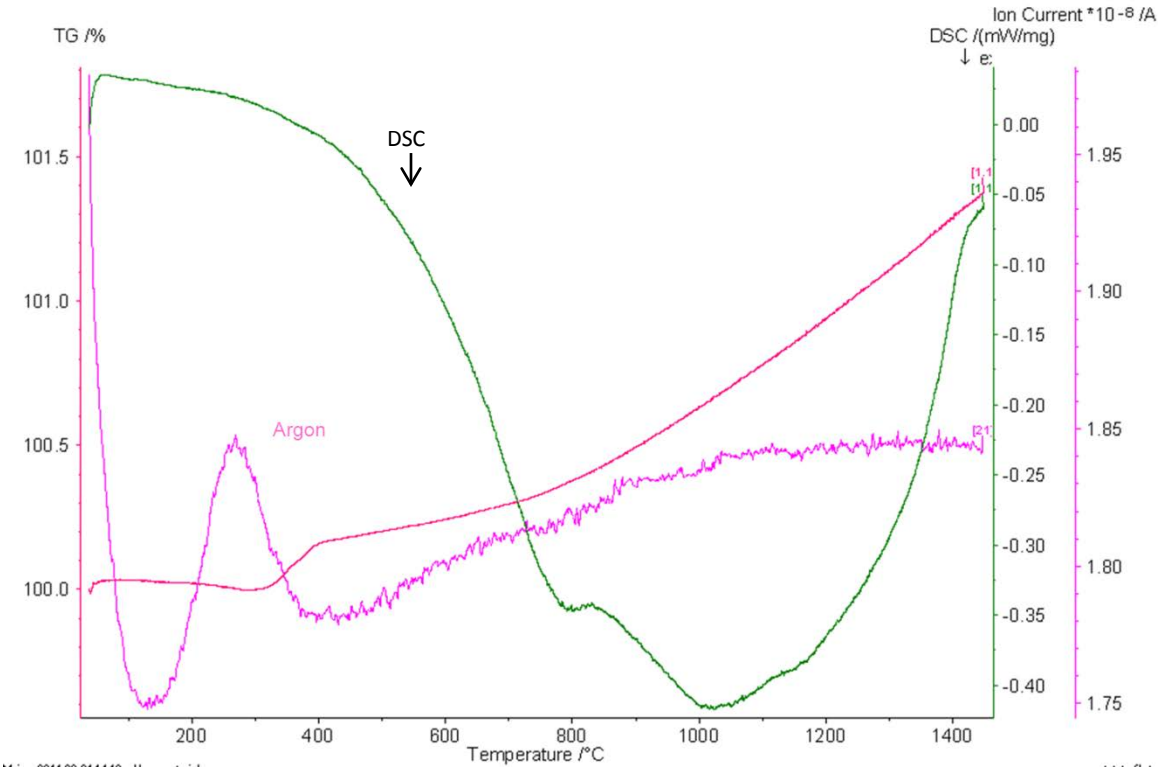

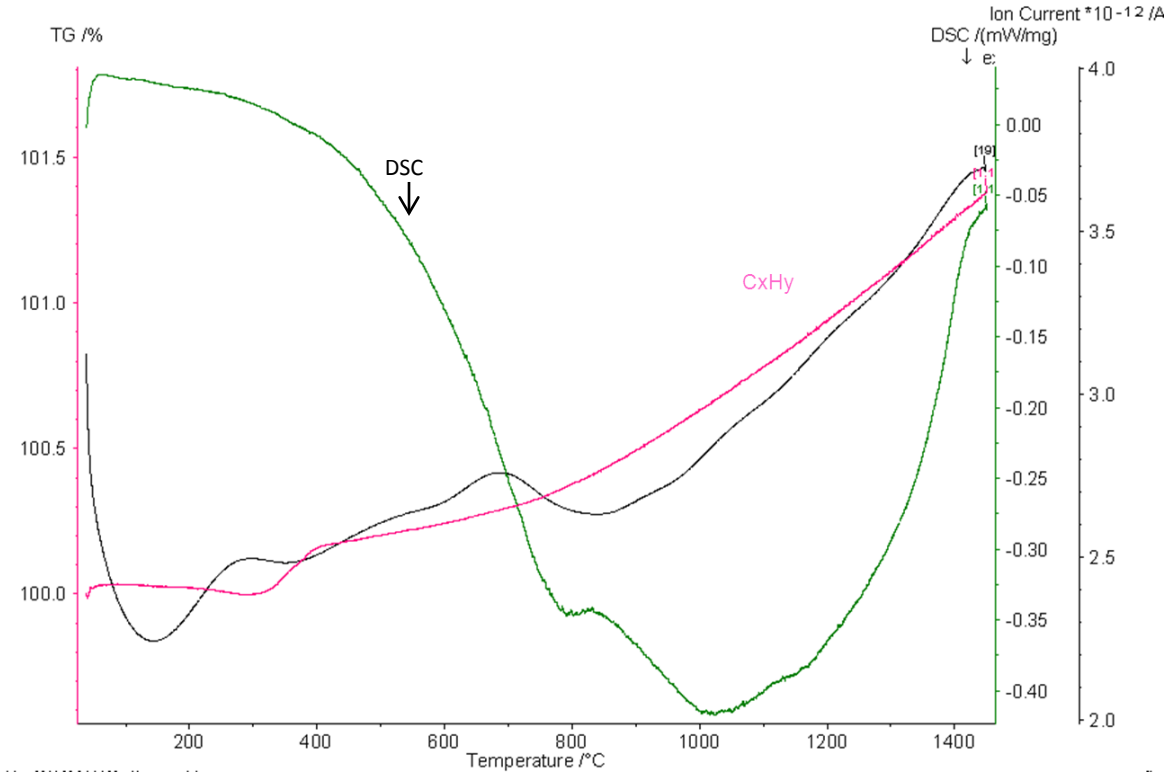

Appendix 2: Mass Spectrometer curves of $TiC_{0.7}N_{0.3}$

Nitrogen atmosphere

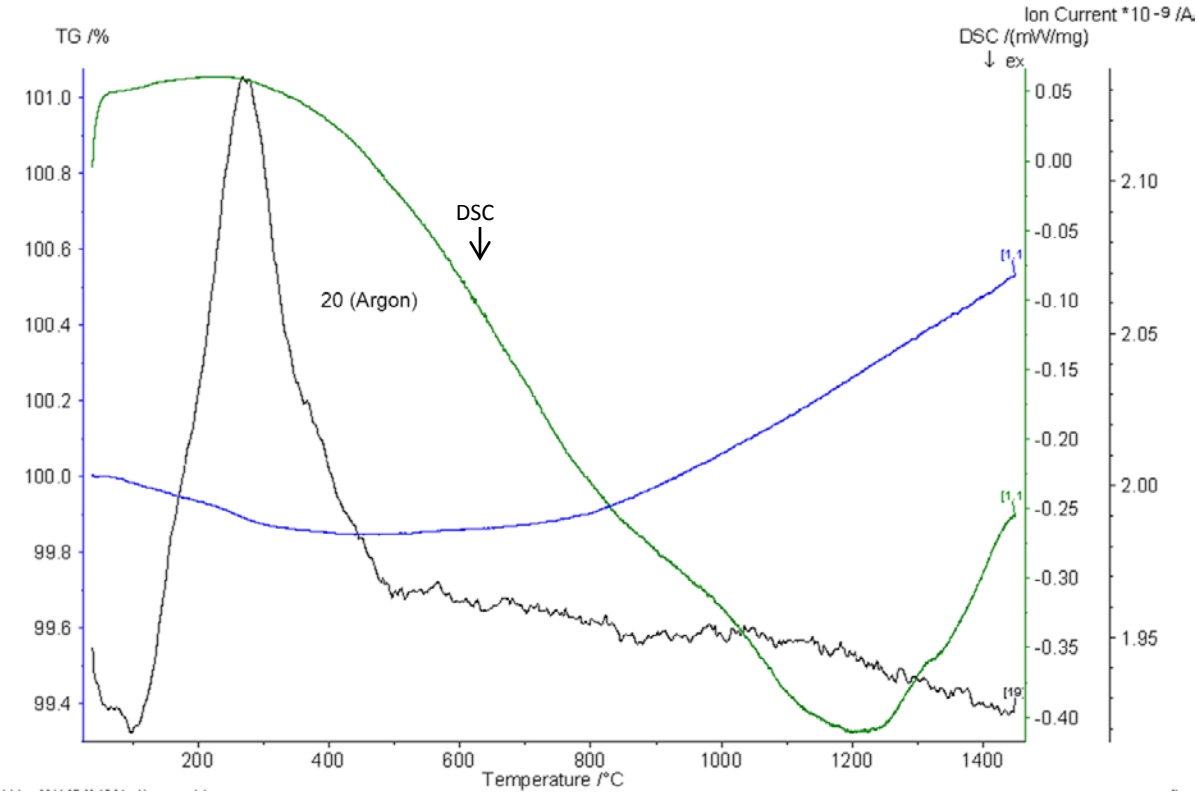

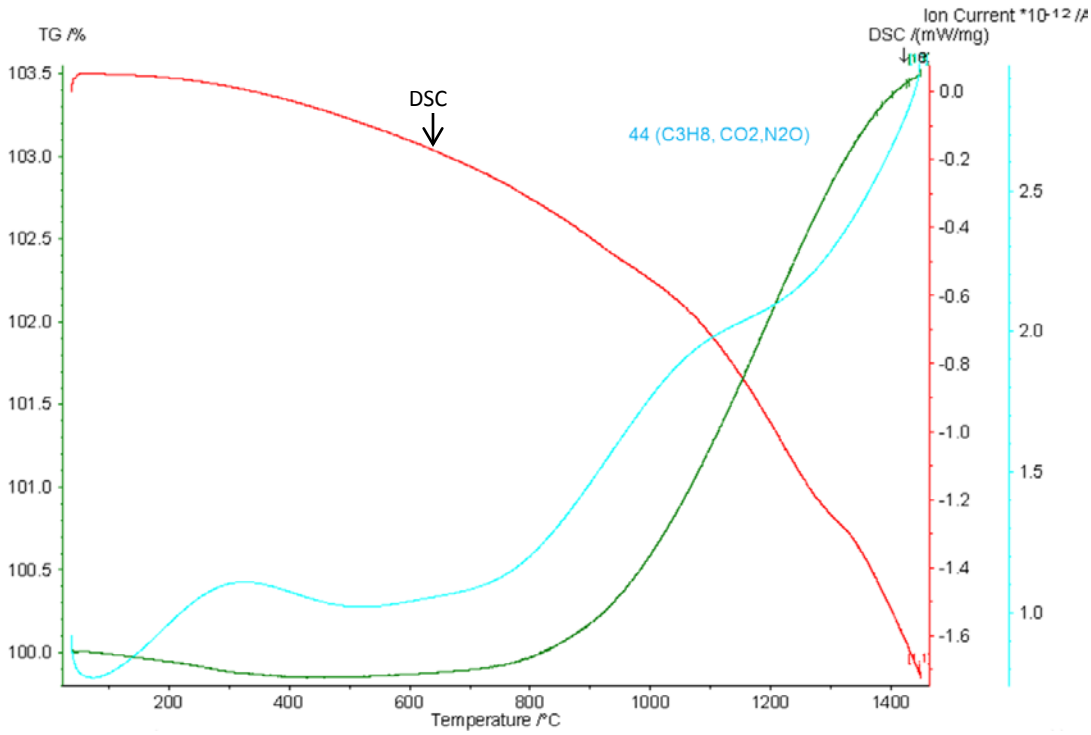

Argon atmosphere

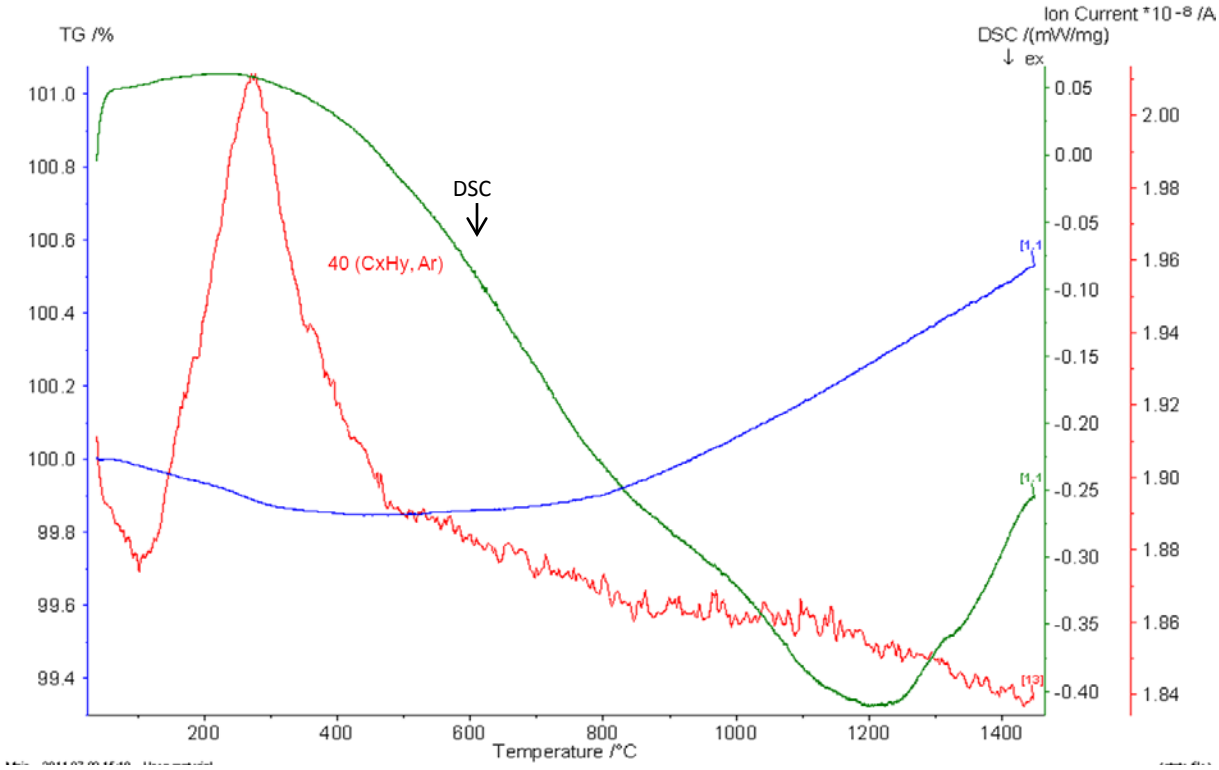

Appendix 3: **Mass Spectrometer curves of Si_3N_4**

Nitrogen atmosphere

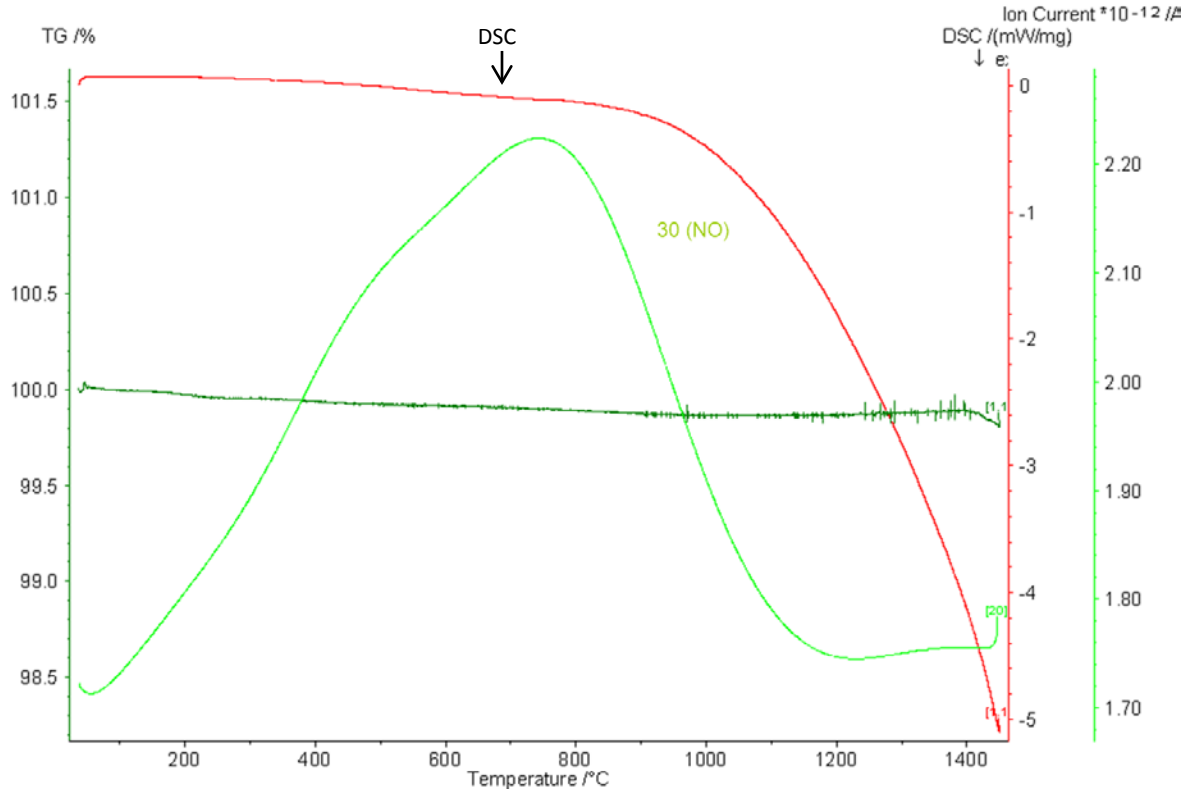

Argon atmosphere

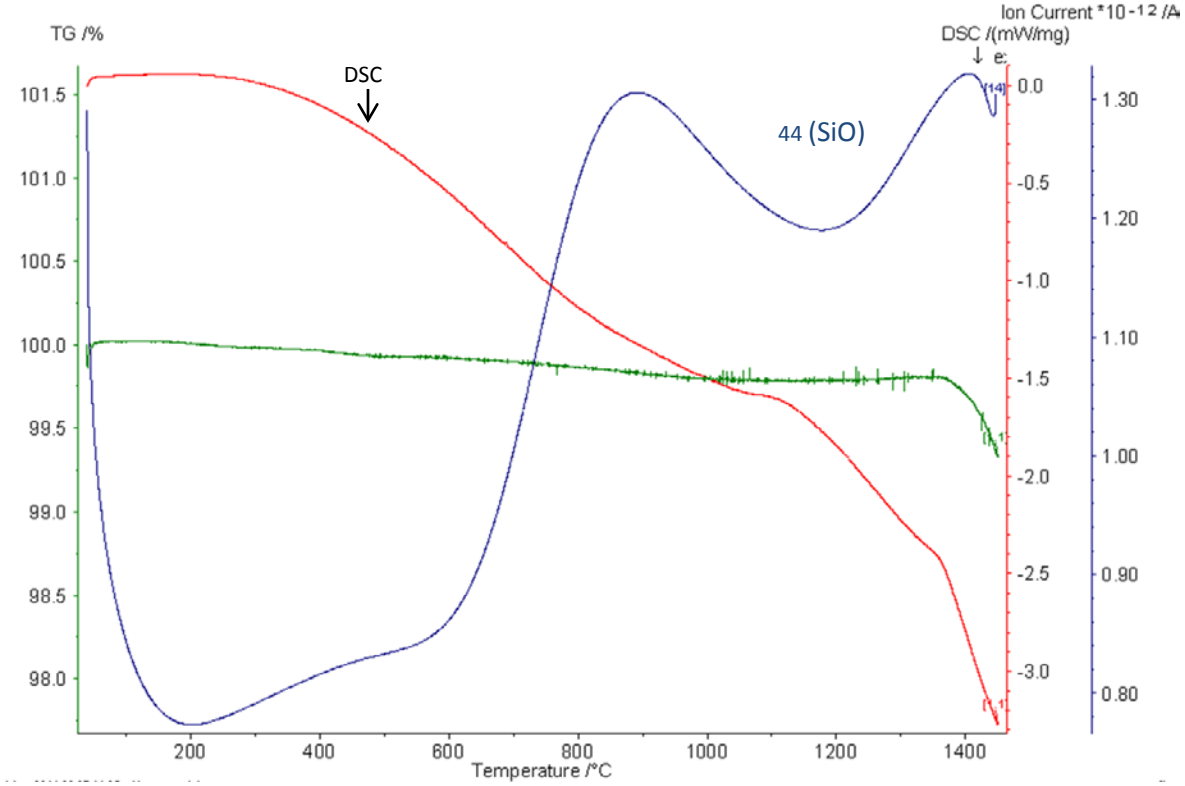

Appendix 4: Mass Spectrometer curves of SiC

Nitrogen atmosphere

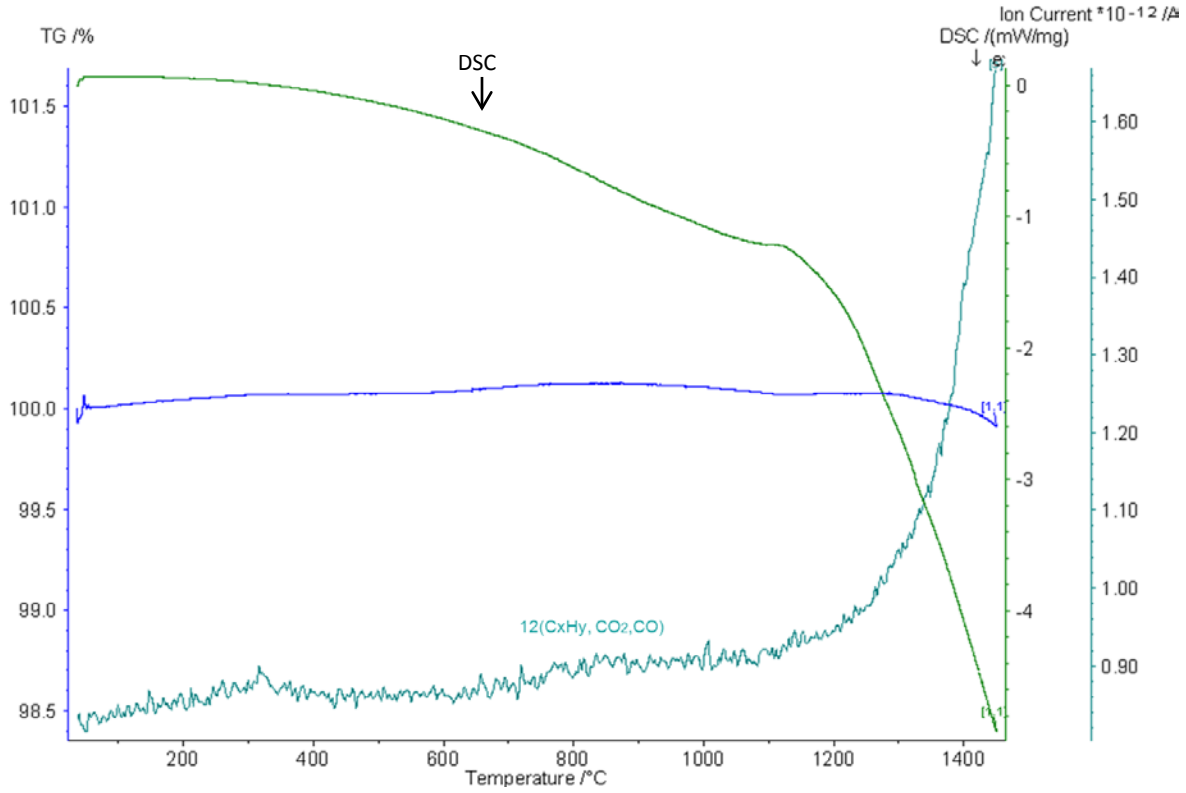

Appendix 5: Mass Spectrometer curves of $TiC_{0.3}N_{0.7}$:Si_3N_4 (2:1)

Nitrogen atmosphere

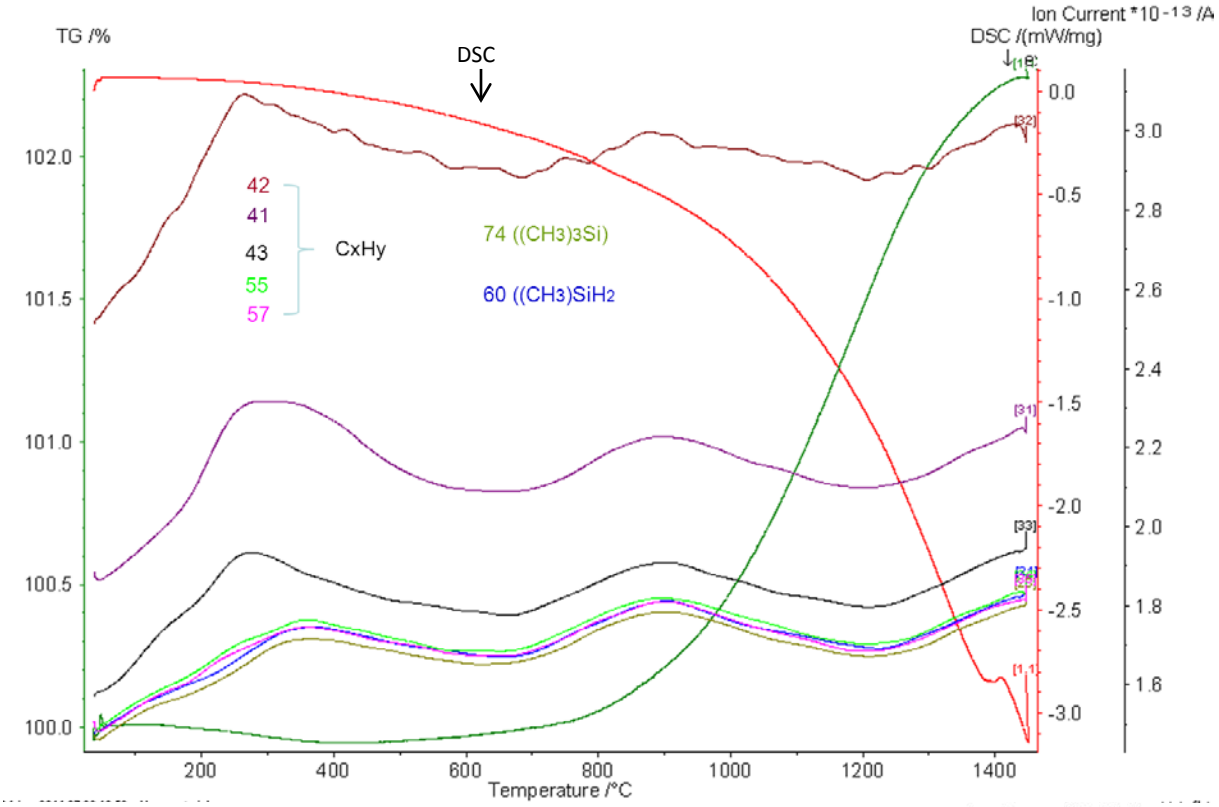

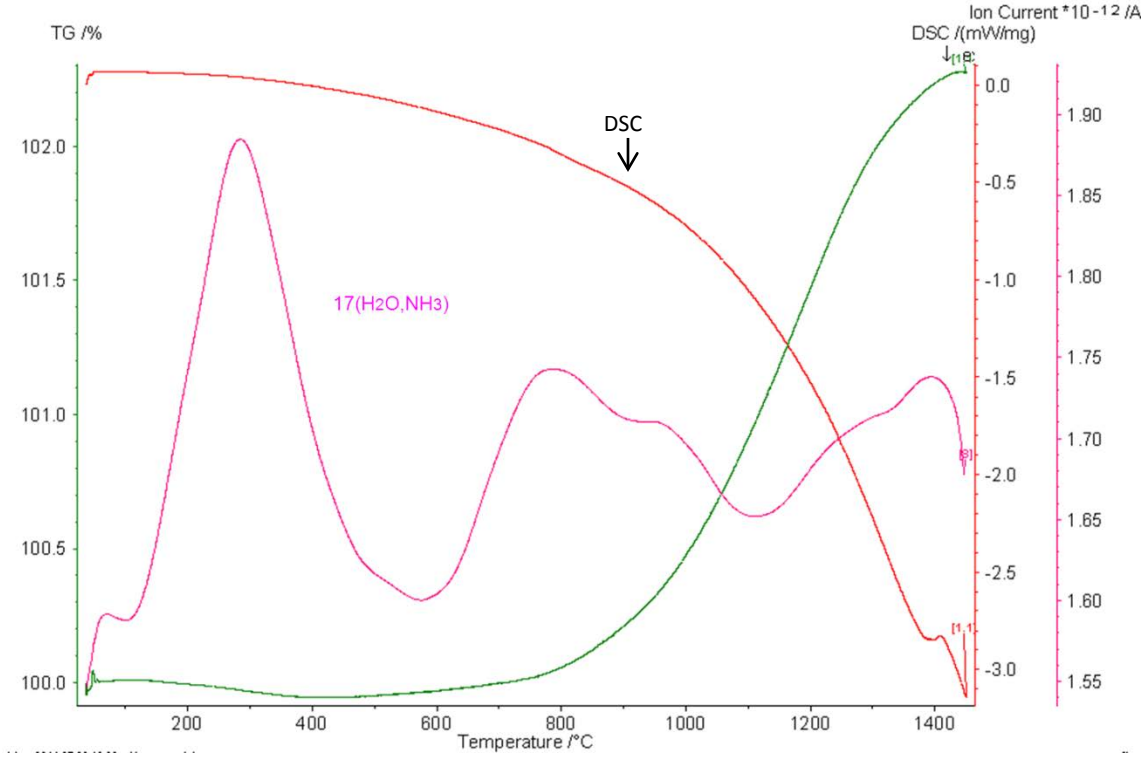

Argon atmosphere

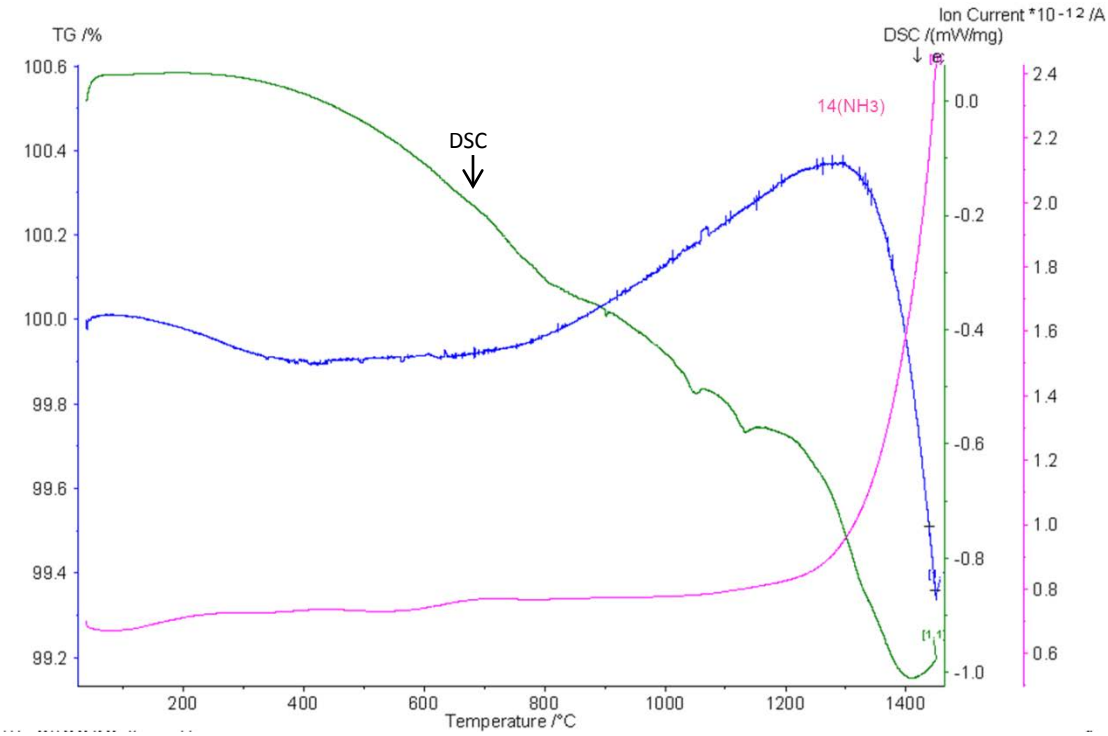

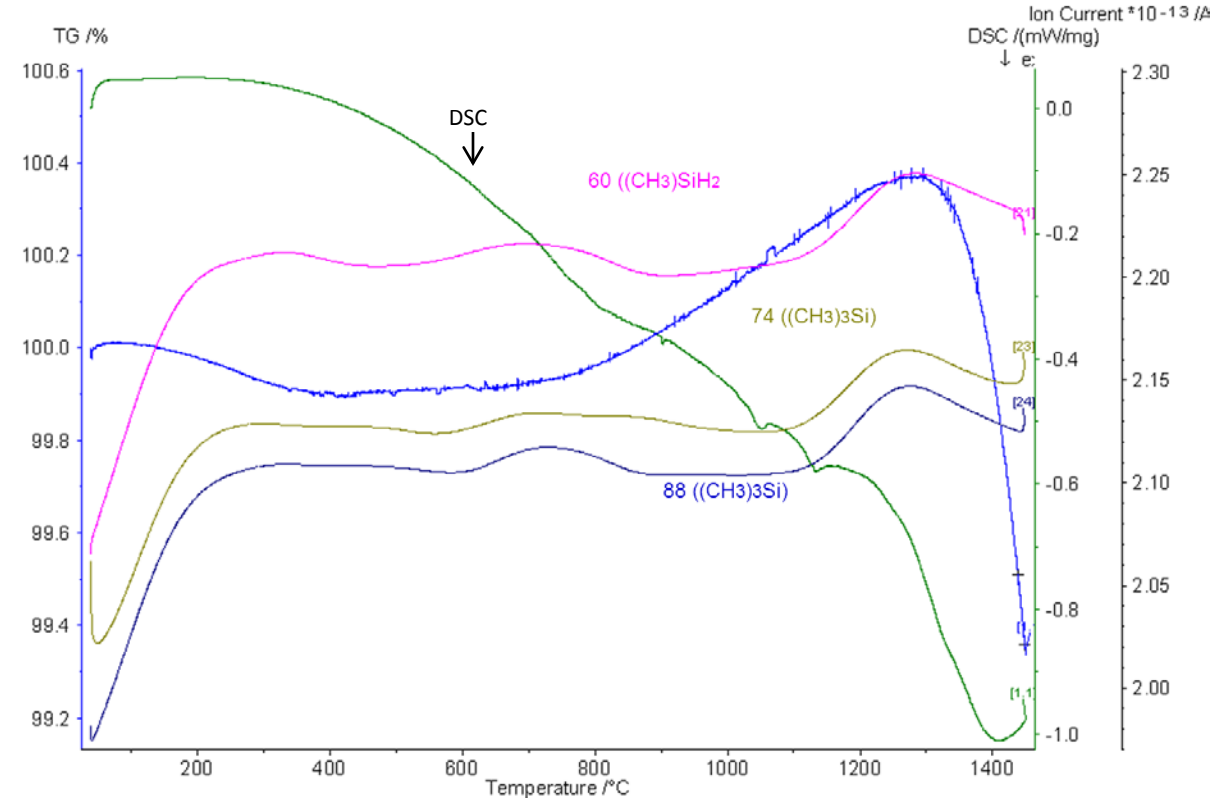

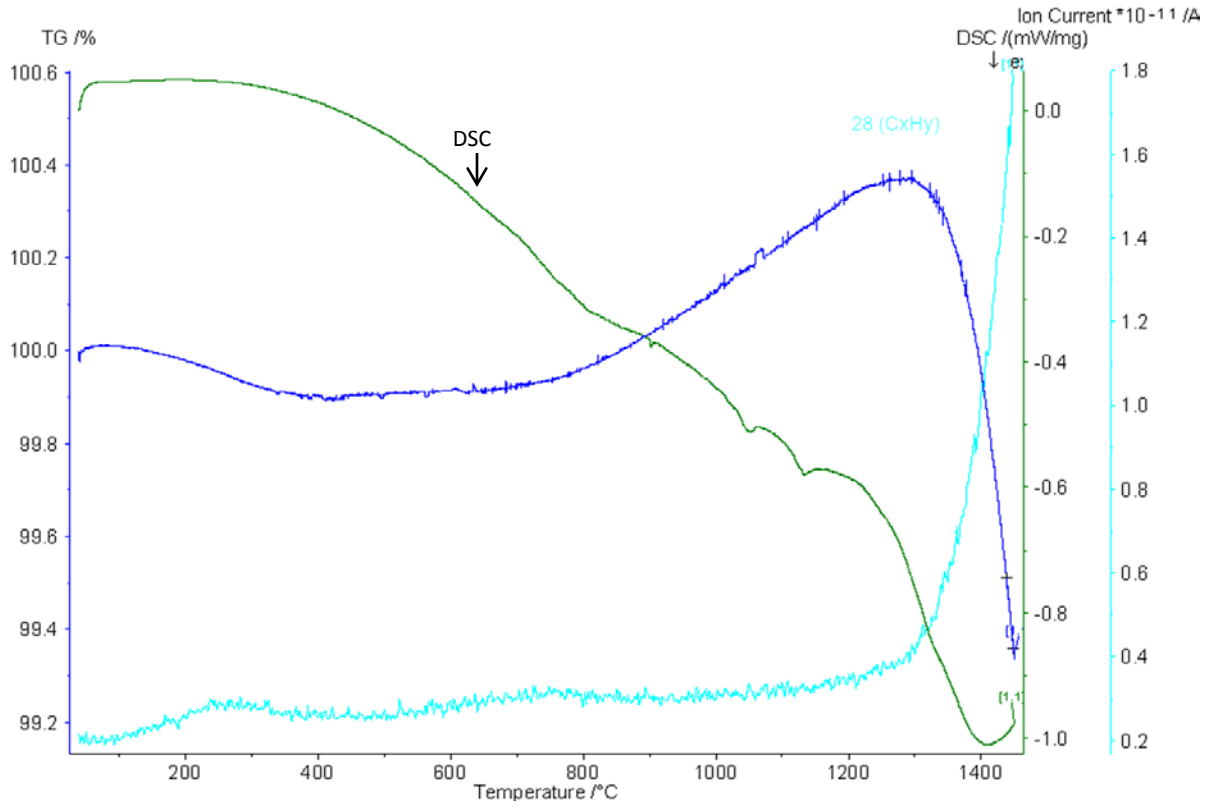
TG /%
DSC /(mW/mg)
Ion Current *10-11 /A
DSC
28 (CxHy)
100.6
100.4
100.2
100.0
99.8
99.6
99.4
99.2
0.0
-0.2
-0.4
-0.6
-0.8
-1.0
1.8
1.6
1.4
1.2
1.0
0.8
0.6
0.4
0.2
200
400
600
800
1000
1200
1400
Temperature /°C

Appendix 6: Mass Spectrometer curves of $TiC_{0.3}N_{0.7}$:Si_3N_4 (1:1)

Nitrogen atmosphere

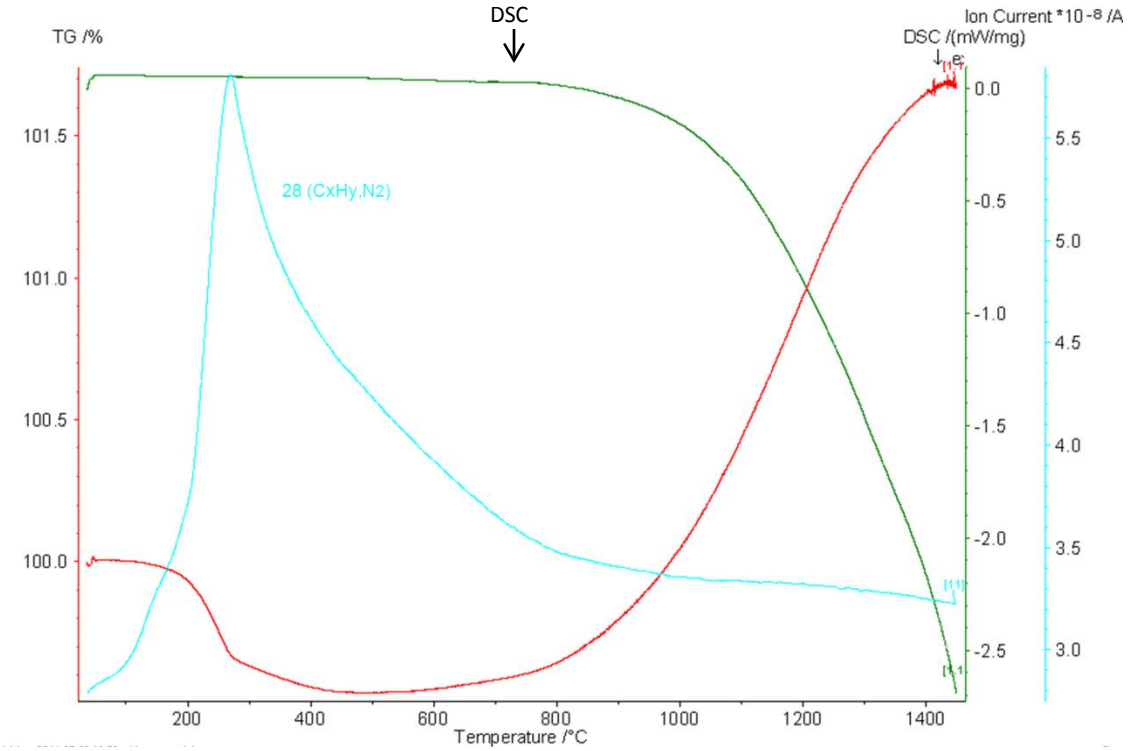

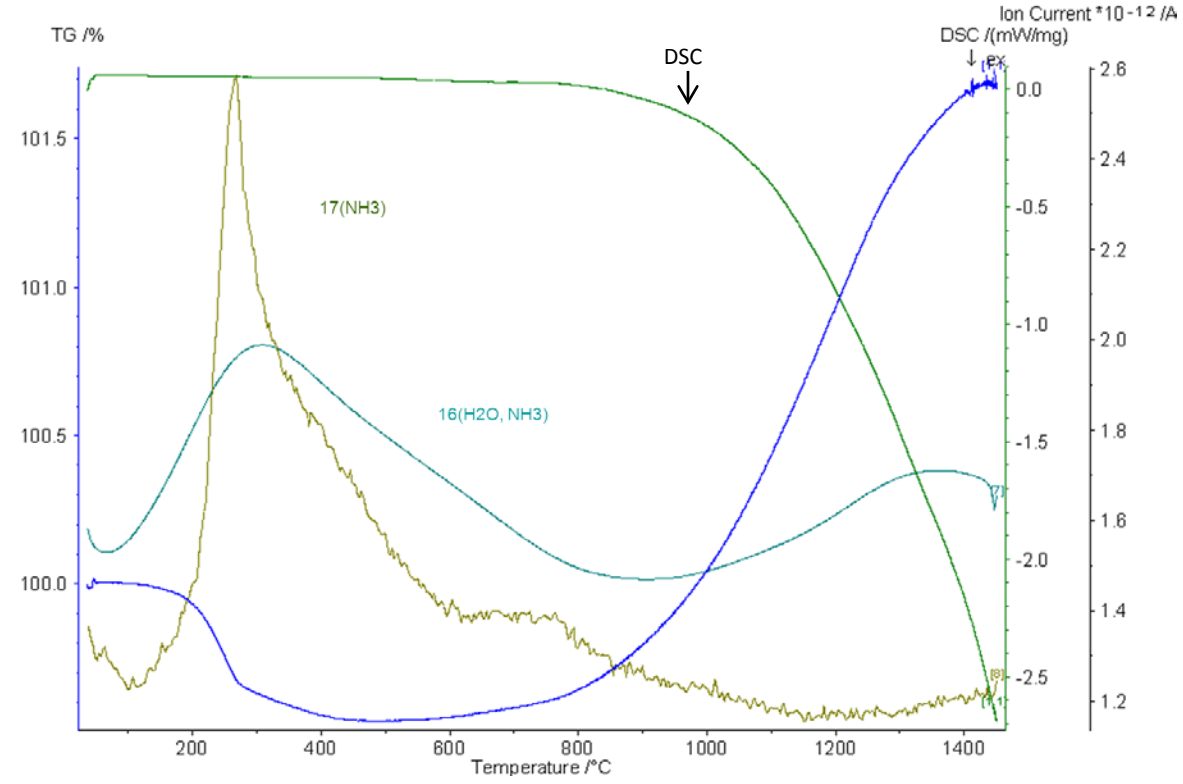

Argon atmosphere

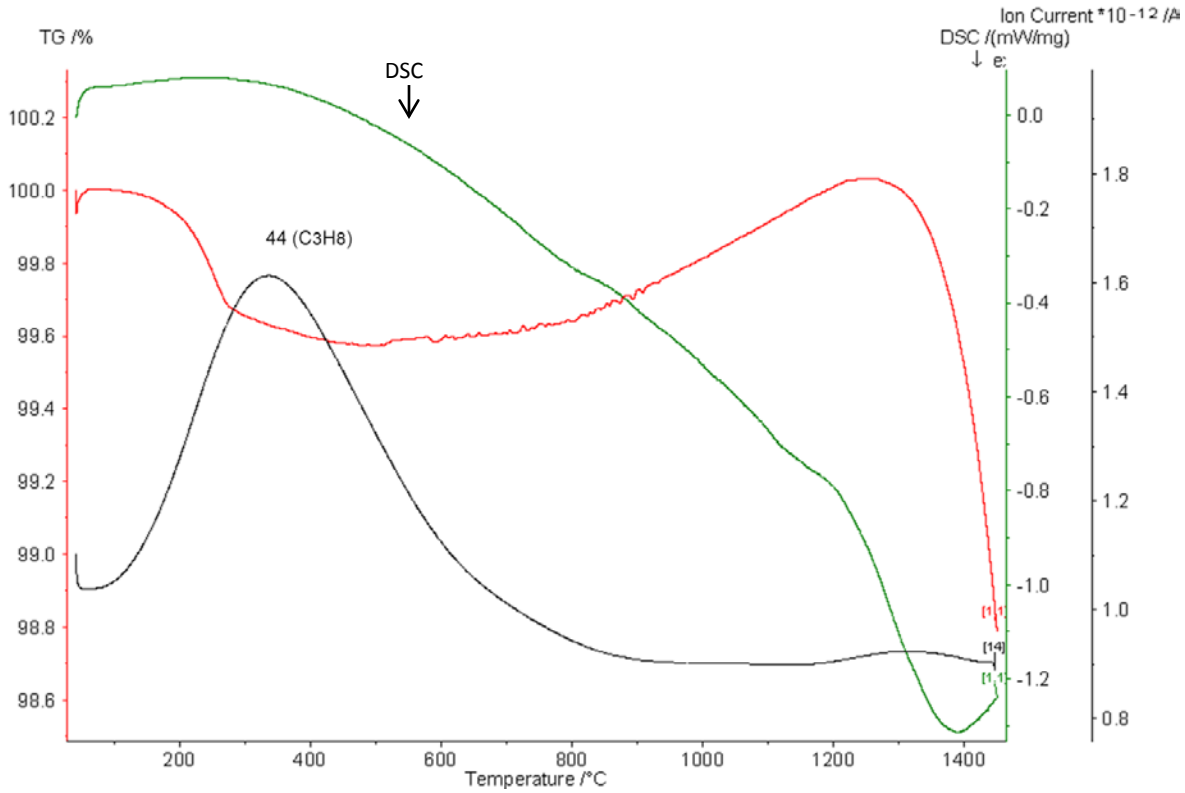

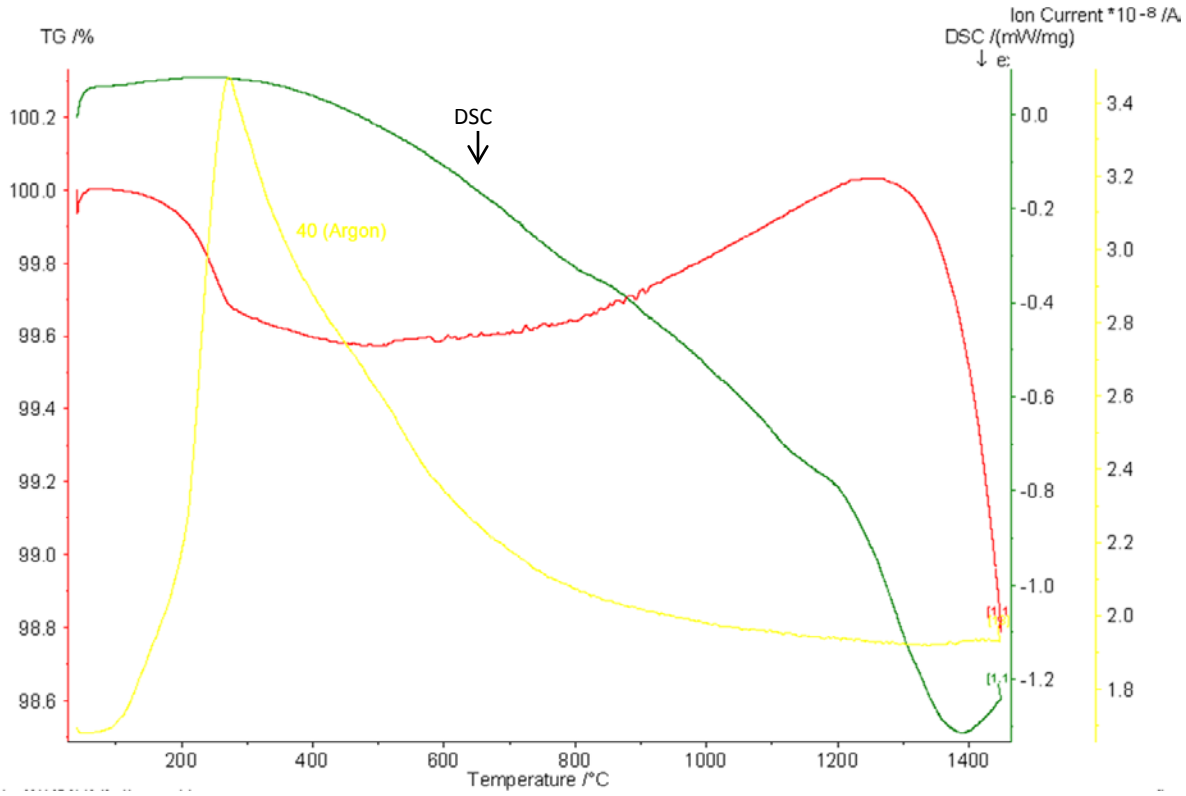

Appendix 7: Mass Spectrometer curves of $TiC_{0.3}N_{0.7}$: SiC (2:1)

Nitrogen atmosphere

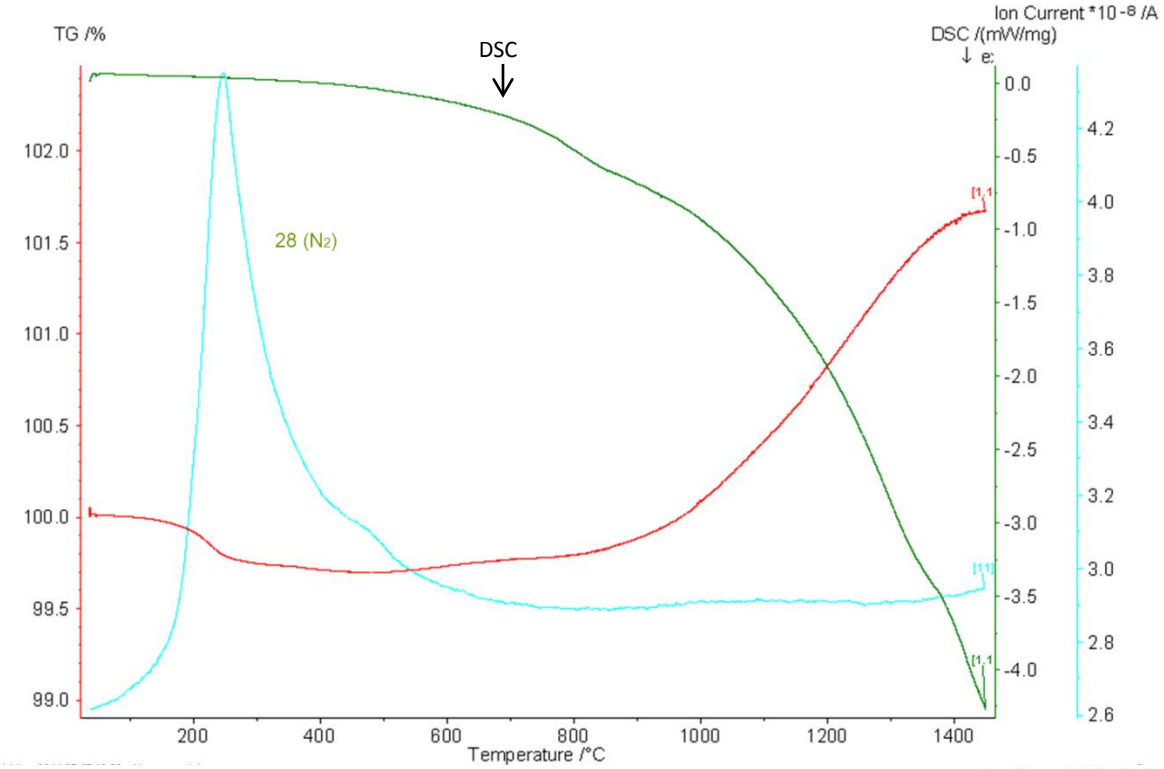

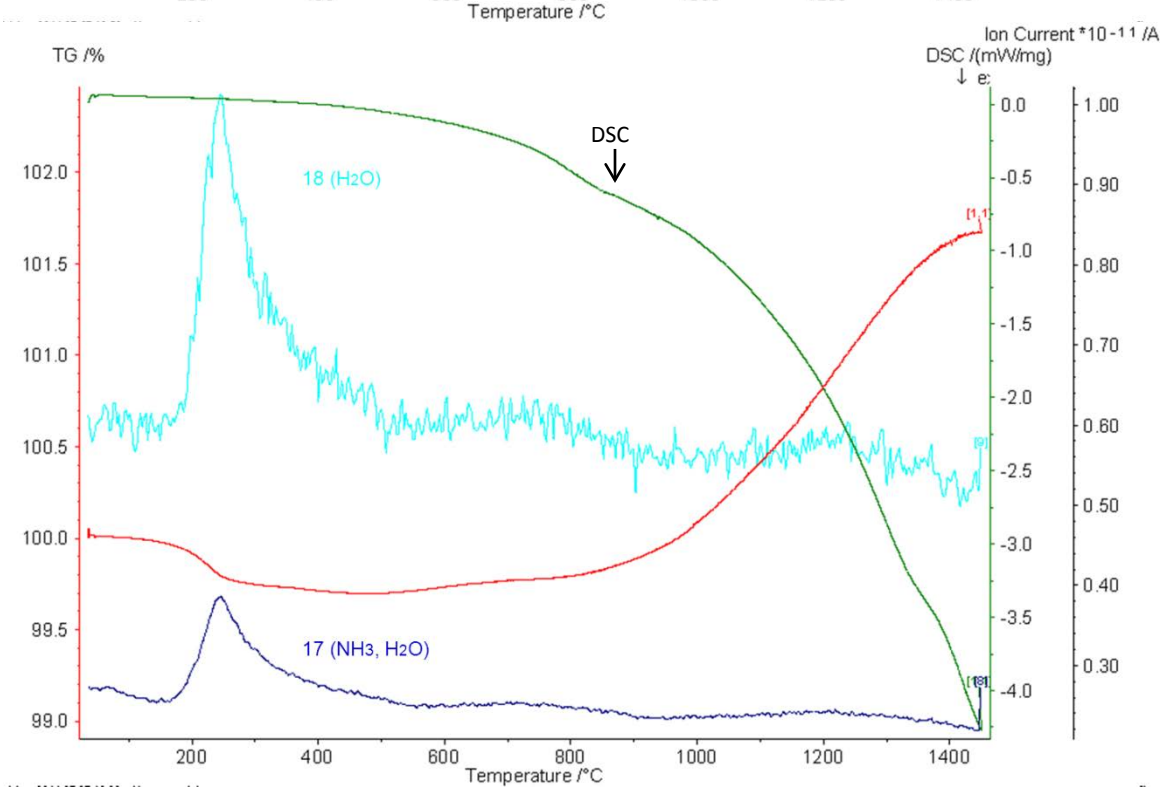

Argon atmosphere

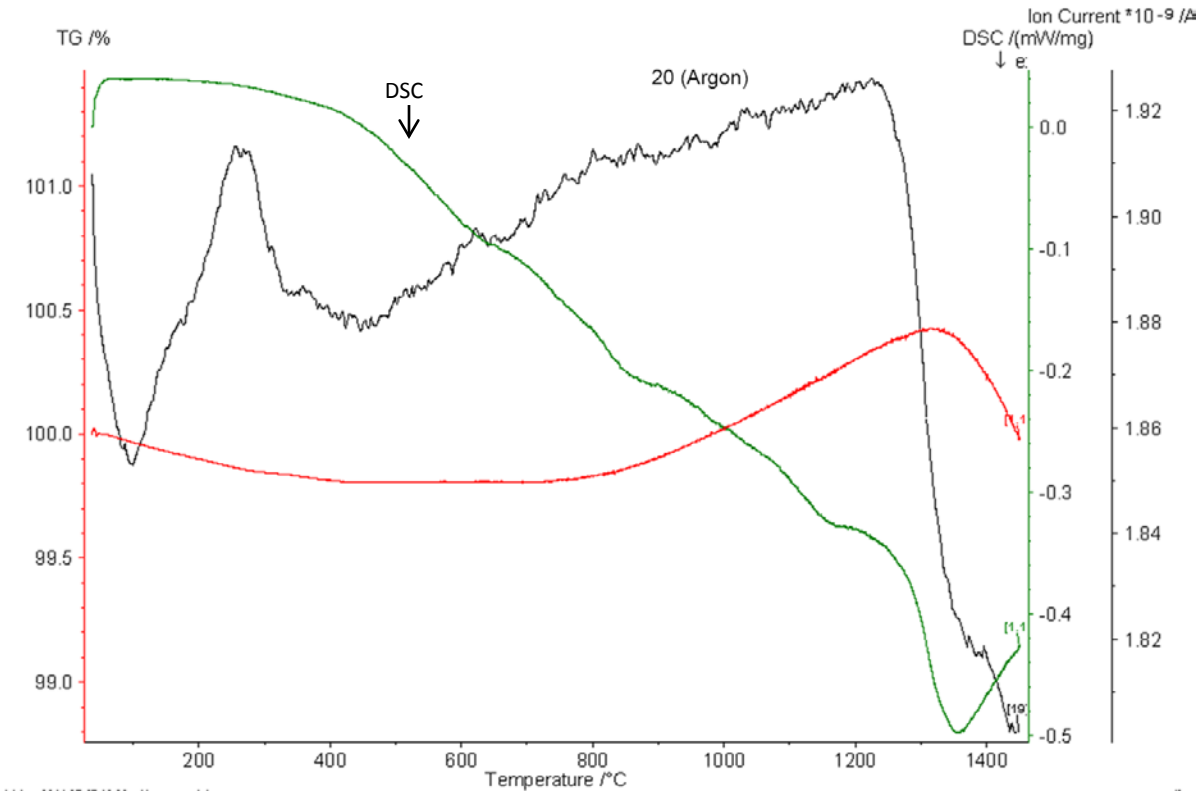

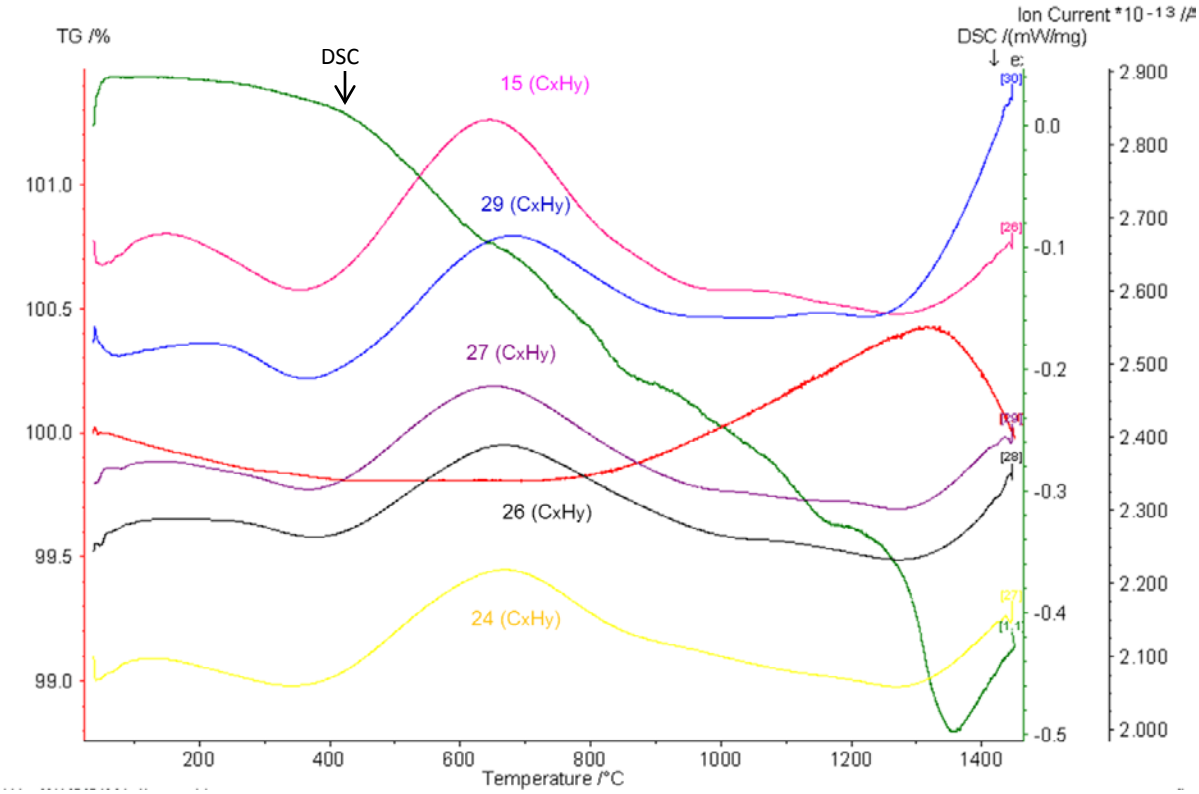

Appendix 8: Mass Spectrometer curves of $TiC_{0.3}N_{0.7}$: SiC (1:1)

Nitrogen atmosphere

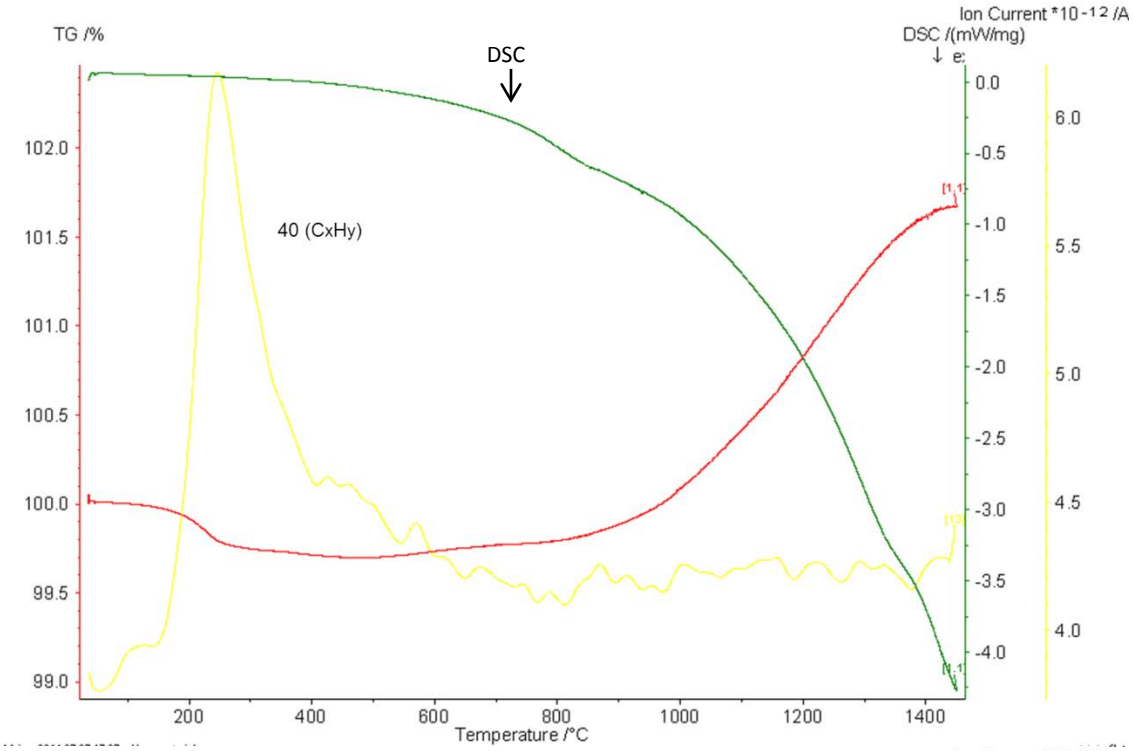

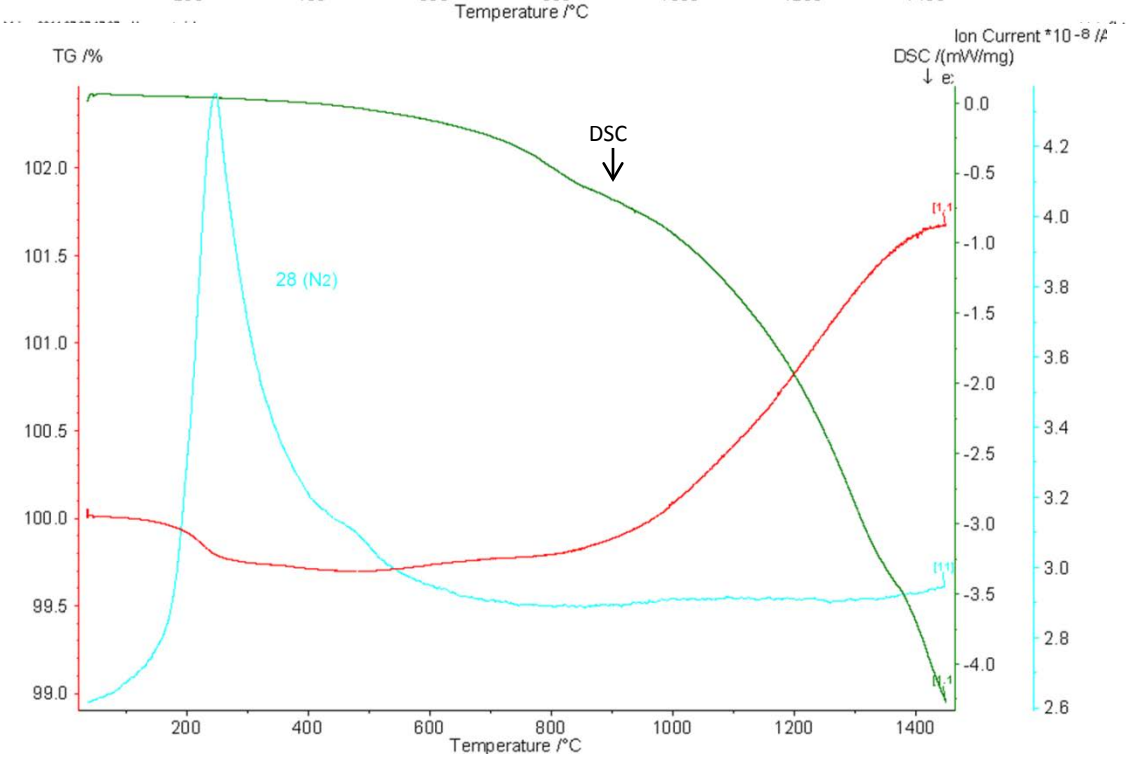

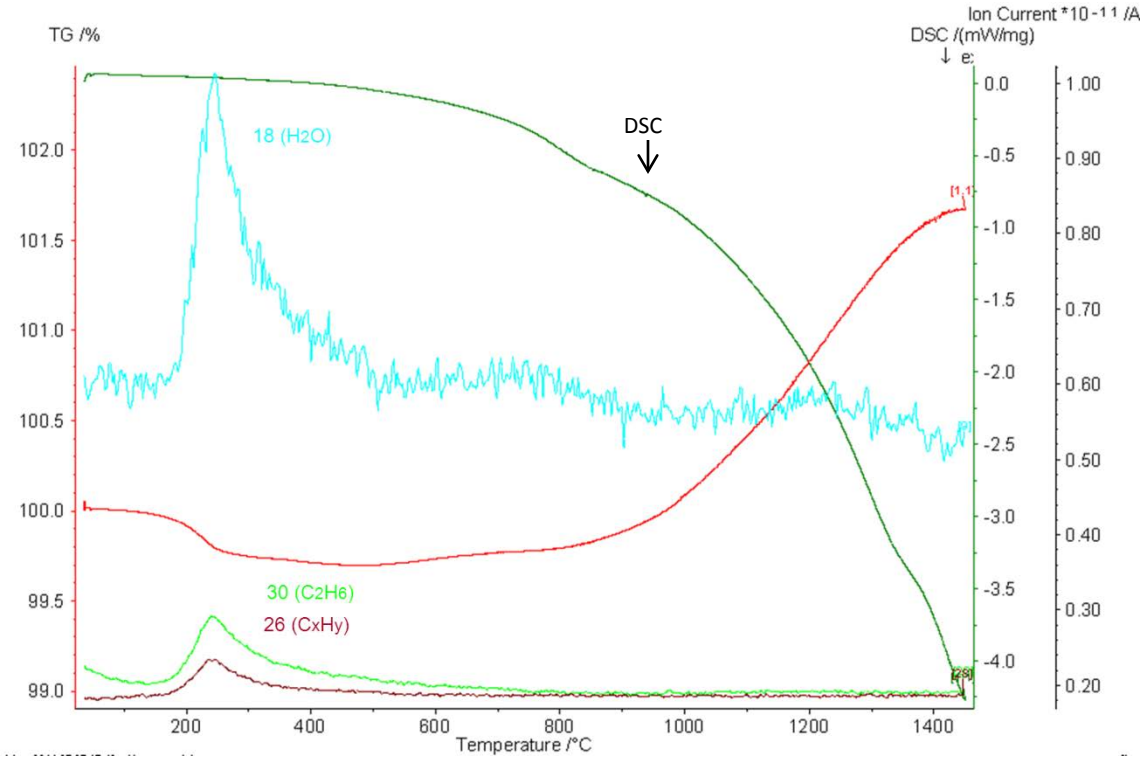
TG /%
Ion Current *10 -11 /A
DSC /(mW/mg)
↓ e:
18 (H2O)
DSC
30 (C2H6)
26 (CxHy)
[1,1]
[28]
102.0
101.5
101.0
100.5
100.0
99.5
99.0
0.0
-0.5
-1.0
-1.5
-2.0
-2.5
-3.0
-3.5
-4.0
1.00
0.90
0.80
0.70
0.60
0.50
0.40
0.30
0.20
200
400
600
800
1000
1200
1400
Temperature /°C

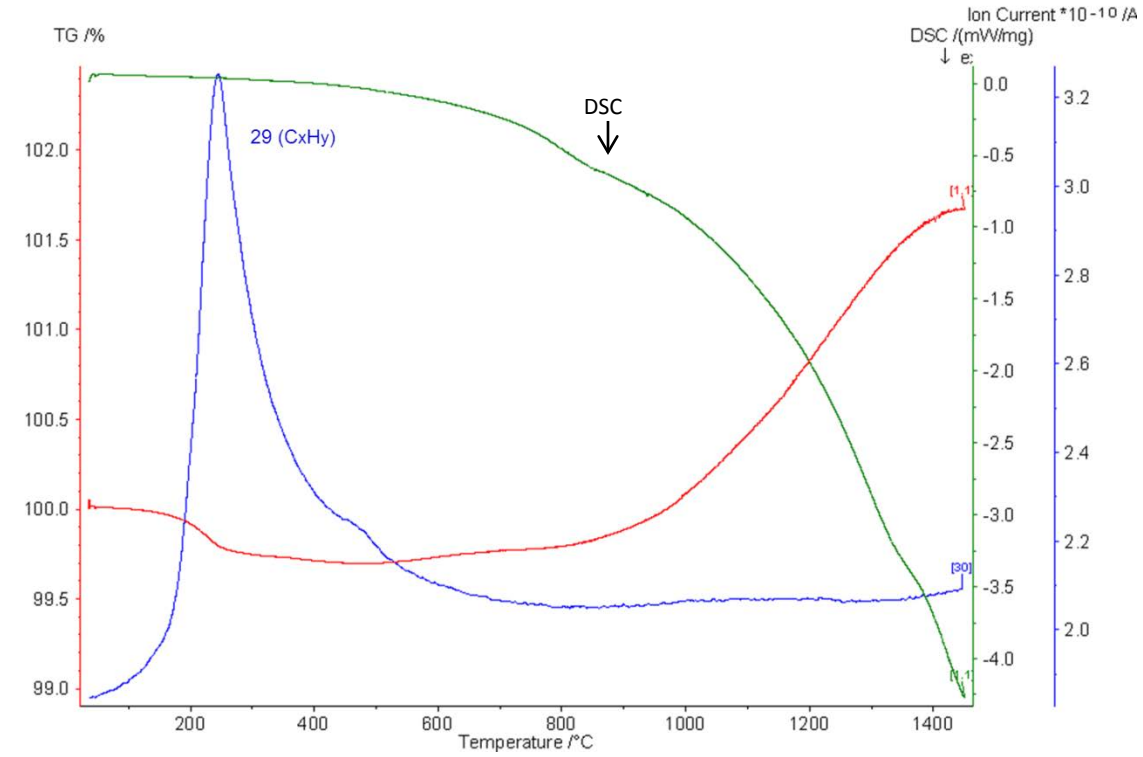
TG /%
Ion Current *10 -10 /A
DSC /(mW/mg)
↓ e:
29 (CxHy)
DSC
[1,1]
[30]
102.0
101.5
101.0
100.5
100.0
99.5
99.0
0.0
-0.5
-1.0
-1.5
-2.0
-2.5
-3.0
-3.5
-4.0
3.2
3.0
2.8
2.6
2.4
2.2
2.0
200
400
600
800
1000
1200
1400
Temperature /°C

Argon atmosphere

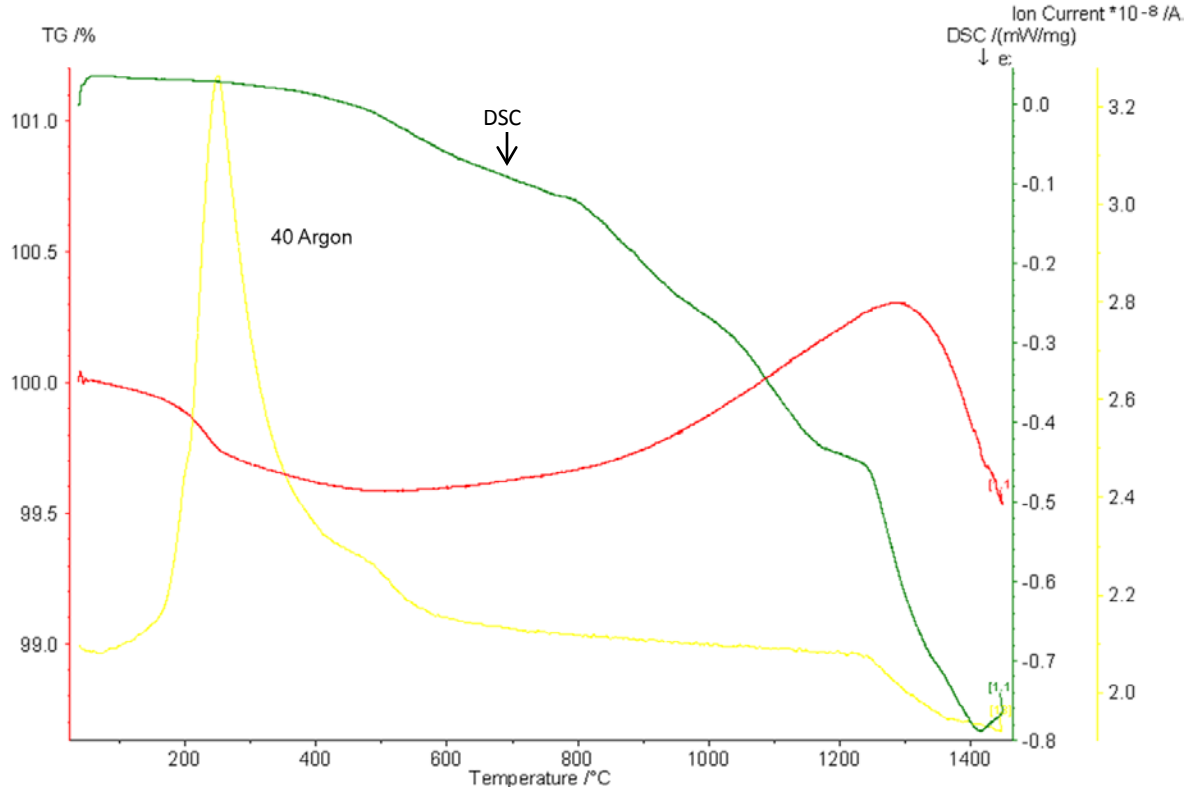

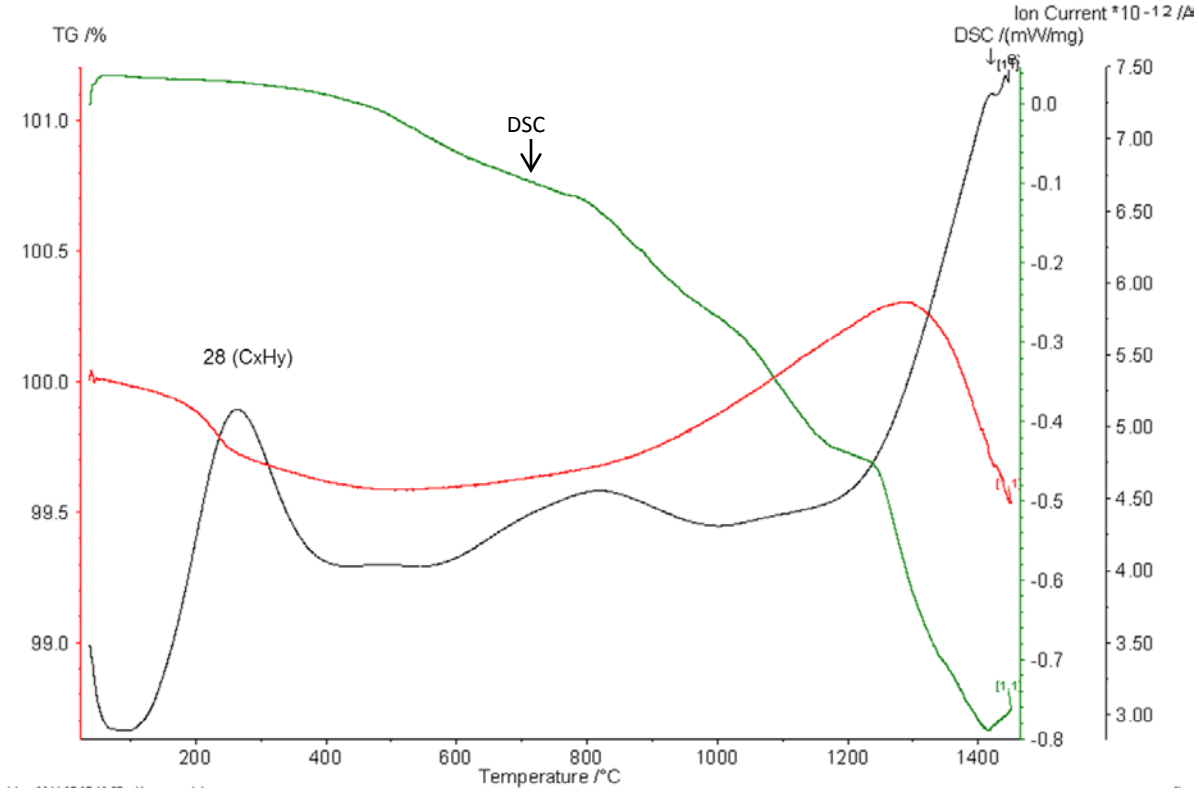

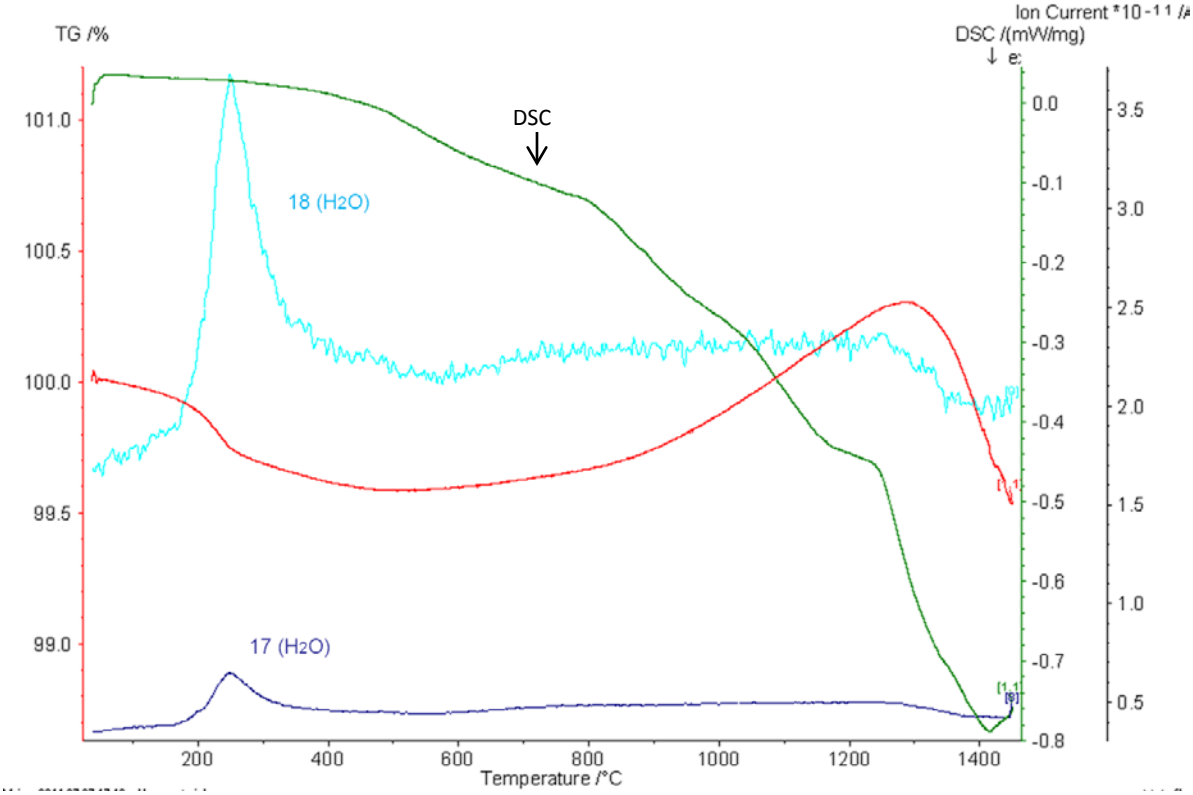
TG /%
DSC /(mW/mg)
Ion Current *10-11 /A
DSC
18 (H2O)
17 (H2O)
101.0
100.5
100.0
99.5
99.0
0.0
-0.1
-0.2
-0.3
-0.4
-0.5
-0.6
-0.7
-0.8
3.5
3.0
2.5
2.0
1.5
1.0
0.5
200
400
600
800
1000
1200
1400
Temperature /°C

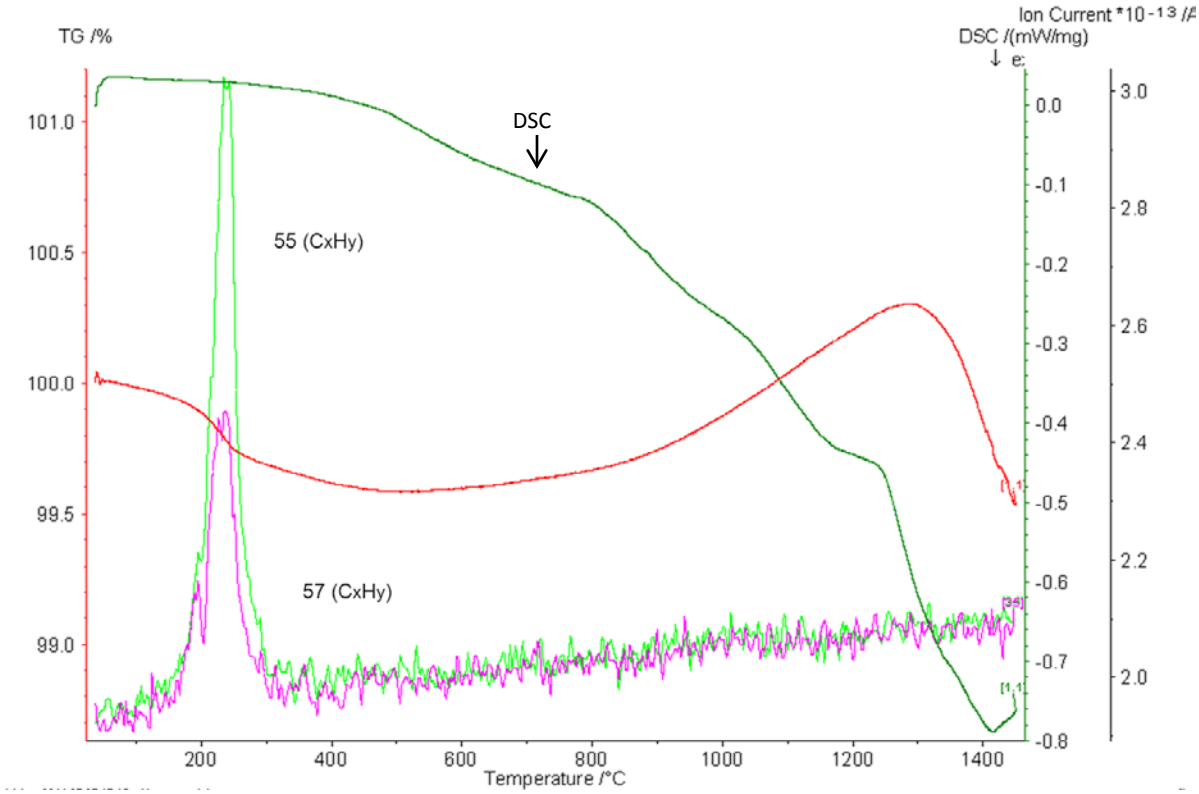
TG /%
DSC /(mW/mg)
Ion Current *10-13 /A
DSC
55 (CxHy)
57 (CxHy)
101.0
100.5
100.0
99.5
99.0
0.0
-0.1
-0.2
-0.3
-0.4
-0.5
-0.6
-0.7
-0.8
3.0
2.8
2.6
2.4
2.2
2.0
200
400
600
800
1000
1200
1400
Temperature /°C

Bibliography

1. **Yongdi Lia, Yadong Yao , Wei Shaoa, Fei Liua, Yunqing Kanga, Guangfu Yina, Zhongbing Huanga and Xiaoming Liaoa.** *Preparation of titanium carbonitride nanoparticles from a novel refluxing-derived precursor.* China : Materials Letters,, 2009.

2. **Jian Suia, Jin-Jun Lu.** *Synthesis of carbon nitride powder by selective etching of $TiC_{0.3}N_{0.7}$ in chlorine-containing atmosphere at moderate temperature.* China : Materials Chemistry and Physics, 2010.

3. **R. Haubner, M. Wilhelm, R. Weissenbacher, B. Lux.** *Boron nitrides- Properties, synthesis and applications.* Vienna : Institue of Chemical Technology of Inorganic Materials, University of Vienna.

4. **Wentorf, R.H. and Bundy,F.P.** *Sintered Superhard Materials.* s.l. : Science.

5. **McKie, Amanda Lynne.** *Mechanical Properties of cBN-Al Composite Materials Dependence on Grain Size of cBN and Binder Content.* s.l. : University of the Witwatersrand, Johannesburg, 2009.

6. **Hao, X.P., Cui, D.L., Shi, G. X.** *synthesis of cBN at low-temperature and low pressure conditions.* s.l. : Chemistry of Materials, 2001.

7. **Nakano, S., Ikawa, H.I,Nakano, S., Ikawa, H.I,.** *Synthesis of cubic Boron Nitride by decomposition of magnesium boron nitride.* s.l. : Journal of American Ceramic Society, 1992.

8. **H. Sachdeva, R. Haubnera,H. Sachdeva, R. Haubnera,.** *Investigation of the c-BN/h-BN phase transformation at normal pressure.* Vienna, Austria : Diamond and Related Materials, 1999.

9. **Fukunaga, Osamu.** *The equilibrium phase boundary between hexagonal and cubic boron nitride.* Japan : Advanced ceramic Technology, 2000.

10. **Riedel, Ralf.** *Handbook of Ceramic Hard Materials.* s.l. : Wiley-VCH Verlag GmbH, 2000. 13.

11. **Osipova, I.I., Shvedkov, E.L.** *Cutting ceramics.* s.l. : Soviet powder mettalurgy and metal ceramics, 1985-1990.

12. **Cho, et al., et al.** *Cemented and cemented/sintered superabrasive polycrystalline bodies and methods of manufacture thereof.* s.l. : Norton Company, 1991.

13. **Vaben, R., Forester, J., Stover, D.** *Toughening of SiC ceramics by a bimoel grain size distribution produced by hipping ultrafine and coarse grained SiC powders.* s.l. : Nanostructured Materials.

14. **Hara, A. Yazu, S.** *Sintered Cutting Tools and Manufacturing Process.* 1979.

15. **Rong, X.Z. Fukunaga.** *Cubic BN-WC-Co composite sintered at high pressures and high temperatures.* s.l. : Diamond Film Technology, 1993.

16. **Bezhenar, B.N.P, Bozhko, S.A., Belyavina, N.N., Markiv, V. Ya.** *Point defects in crystal latices of cubic boron nitride and aluminium nitride depending on conditions of sintering cBN-AlN composite materials.* s.l. : Journal of Superhard Materials.

17. **Benko, E., Morgiel, J. Czeppe, T.** *BN sintered with Al: Microstructure and hardness.* s.l. : ceramics international.

18. **Ewa Benko, , a, Jan Skrzypek Stanis awb, Bogna Królickaa, A. Wyczesanyc and Tery L.Barrd.** *cBN–TiN, cBN–TiC composites: chemical equilibria, microstructure and hardness mechanical investigations.* s.l. : Diamond and Related Materials, 1999.

19. **E. Benko, , a, T. L. Barrb, S. Hardcastlec, E. Hoppeb, A. Bernasikd and J. Morgiel.** *XPS study of the cBN–TiC system.* s.l. : Ceramics International, 2001.

20. **P. Klimczyka, E. Benkoa, b, K. Lawniczak-Jablonska, , c, E. Piskorskac, M. Heinonend, A. Ormaniecb, W.Gorczynska–Zawislana and V. S. Urbanoviche.** *Cubic boron nitride—Ti/TiN composites: hardness and phase equilibrium as function of temperature.* s.l. : Journal of Alloys and Compounds.

21. **L. Eusterbrock, J. Lehmann, G. Ziegler.** *Analysis of pyrolysis products during thermal decomposition of organic components in ceramic green bodies.* s.l. : ceramic forum international, 2003.

22. **W S. Rees Jr, D. Seyferth.** *Non-polymeric binders for ceramic powders: utilization of neutral and ionic species derived from decaborane.* s.l. : Journal of materials science, 1989.

23. **S. Baklouti, J. Bouaziz, T. Chartier, J-F Baumard.** *binder burnout and evolution of mechanical strength of dry-pressed ceramics containing poly(vinyl alcohol).* s.l. : journal of the european cermaic society,, 2001.

24. **N. Grassie, G.A Perdomo Mendoza.** *thermal Degradation of Polyether-Urethanes: Part1 Thermal Degradation of Poly(Ethylene Glycols) Used in the preparation of Polyyurethanes.* s.l. : Polymer Degradation and Stability, 1984.

25. **M.M. Fares, J. Hacaloglu, S. Suzer.** *Characterization of degradation products of polyethylene oxide by pyrolysis mass spectrometry.* s.l. : Journal of European Polymer, 1994.

26. **Laurence Vel, G~rard Demazeau and.** *Cubic boron nitride: synthesis, physicochemical properties.* France : Materials Science and Engineering, 1991.

27. **Rield, Ralf.** *handbook of ceramic Hard Materials 2.* Germany : Wiley-VCH, 2000.

28. **Murray, H. A. Wriedt and J. L.** *The N-Ti (Nitrogen-Titanium) system.* s.l. : Journal of Phase Equilibria. 4.

29. **Feng-shi Yina, c, Li Zhoub, Zhi-feng Xuc, Bing Xuea, Xue-bo Jianga.** *Synthesis of nanocrystalline titanium carbonitride during milling.* s.l. : Journal of Alloys and Compounds, 2008.

30. **Xin Fenga, Li-Yi Shia.** *Novel chemical metathesis route to prepare TiCN nanocrystallites at low temperature.* China : Materials Chemistry and Physics, 2005.

31. **Guozhen Shen, Kaibin Tang Changhua An, Qing Yang, Chunrui Wang and Yitai Qian.** *A simple route to prepare nanocrystalline titanium carbonitride.* China : Materials Research Bulletin, 2002.

32. **O. Lichtenberger, E. Pippel, J. Woltersdorf, R.Riedel.** *Formation of nanocrystalline titanium carbonitride.* Germany : Materials Chemistry and Physics, 2003.

33. **H. Montigauda, b, B.Tanguya, G. Demazeau, I. Alvesa, M. Birotc and J. Dunogues.** *Solvothermal synthesis of the graphitic form of C_3N_4 as macroscopic sample.* France : Diamond and Related Materials, 1999.

34. **Hemley, David M. Teter and Russell J.** *Low-Compressibility Carbon Nitrides.* s.l. : Science, 1996.

35. **H. Montigaud, B. Tanguy, G. Demazeau, I. Alves and S. Courjault.** *C_3N_4: Dream or reality? Solvothermal synthesis as macroscopic samples of the C_3N_4 graphitic form.* France : JOURNAL OF MATERIALS SCIENCE, 2000.

36. **Yan Cheny, Liping Guoz, Feng Cheny and E G Wangyx.** *Synthesis and characterization of C3N4 crystalline films on silicon.* China : J. Phys.: Condens. Matter,, 1996,.

37. **H AMa1, X P Jia1, L X Chen1, PWZhu1, W L.Guo1, X B Guo1.** *High-pressure pyrolysis study of C3N6H6: a route to.* China : JOURNAL OF PHYSICS: CONDENSED MATTER, 2002.

38. **Jian Suia, Jin-Jun Lu.** *Synthesis of carbon nitride powder by selective etching of $TiC_{0.3}N_{0.7}$ in chlorine-containing atmosphere at moderate temperature.* China : Materials Chemistry and Physics,, 2010.

39. **Riley, Frank L.** *Silicon Nitride and Related Materials.* United Kingdom : American Ceramic Society, 1999.

40. **Terwilliger, G. R.** *Properties of Sintered Silicon Nitride.* s.l. : Journal of American Ceramic Society, 1975.

41. **A. Giachello, P. C. Martinengo, G. Tommasini, and P.Popper.** *Sintering of Silicon Nitride in a Powder Bed.* s.l. : Journal of Material Science, 1979.

42. *http://www.railwaypro.com/wp/?p=871.*

43. **Bandyopadhyay, Debashis.** *The Ti-Si-C System (Titanium-Silicon-Carbon).* s.l. : Basic and Applied.

44. **Brukl, C. E.** *Ternary Phase Equilibria in Transition Metal–Boron–Carbon–Silicon Systems.* s.l. : Air Force Materials Laboratory,Wright-Patterson Air Force Base, 1966.

45. **W. J. J. Wakelkamp, F. J. J. van Loo, and R. Metselaar.** *Phase Relations in the.* s.l. : Journal of, 1991.

46. **Seifert, H. J.** *Thermodynamics and Phase Equilibria in the System Ti–Si–C–N. Stuttgart.* s.l. : Max-Planck-Institut fu¨r Metallforschung, 1993.

47. **Aldinger, Yong Du and Julius C. Schuster Hans J. Seifert and Fritz.** *Experimental Investigation and Thermodynamic Calculation of the.* Germany : Journal of American Ceramic Society, 1999.

48. **Ren-Guan Duan, Javier E. Garay, Joshua D. Kuntz, and Amiya K.Mukherjeew.** *Electrically Conductive In Situ Formed Nano-Si_3N_4/SiC/TiCxN1-x Ceramic Composite Consolidated by Pulse Electric Current Sintering (PECS).* California : Journal of American Ceramic Society, 2005.

49. **Seifert, Hans Jürgen.** *REFRACTORY AND HARD MATERIALS IN THE Ti-Si-B-C-N SYSTEM –PHASE EQUILIBRIA, PHASE REACTIONS AND THERMAL STABILITIES.* Gainesville : Materials Sciences, 2004.

50. **Qiao, W.M., Yoon, S.H.** 2007. 4467-4471.

51. google.com. *http://www.cpeo.org/techtree/ttdescript/pyrols.htm.* [Online]

52. **E. BOUILLON, F. LANGLAIS, R. PAILLER, R. NASLAIN, F. CRUEGE.** *Conversion mechanisms of a polycarbosilane precursor into an SiC-based ceramic material.* s.l. : JOURNAL OF MATERIALS SCIENCE, 1991.

53. **Stephen B. Warrington, Günther W. H. Höhne.** *Ullmann's Encyclopedia of Industrial Chemistry.* s.l. : Wiley-VCH Verlag GmbH & Co. KGaA, 2002.

54. http://www.netzsch-thermal-analysis.com/en/products/dilatometer. [Online]

55. **Gabbott, Paul.** *Principles and Applications of Thermal Analysis.* USA : Blackwell publishing, 2008.

56. *Basics of X-ray Diffraction.* s.l. : Scintag Inc, 1999.

57. **C. Suryanarayana, M. Grant Norton.** *X-Ray diffraction: a practical approach.* s.l. : Science, 1998.